Master's thesis

NTNU
Norwegian University of Science and Technology
Faculty of Engineering
Department of Mechanical and Industrial Engineering

Tommy Tollin

Linear and Nonlinear Control-Solutions to Mitigate Slugging in Wells, a Modeling and Simulation Study

Master's thesis in Subsea Control Systems
Supervisor: Christian Holden
June 2019

NTNU
Norwegian University of
Science and Technology

Tommy Tollin

Linear and Nonlinear Control-Solutions to Mitigate Slugging in Wells, a Modeling and Simulation Study

Master's thesis in Subsea Control Systems
Supervisor: Christian Holden
June 2019

Norwegian University of Science and Technology
Faculty of Engineering
Department of Mechanical and Industrial Engineering

NTNU
Norwegian University of
Science and Technology

Abstract

Unstable flow in wells, pipelines and risers may cause a lot of problems in oil and gas production systems. Severe slugging is one of them. This unwanted phenomenon may cause large flow and pressure fluctuations, which may result in wear and tear on equipment and unstable production. This can be costly if not dealt with effectively. Active-slug control may address this problem by actuating the topside- or downhole-choke valves, using measurements both down-hole and topside, to eliminate these instabilities.

After a quantitative description of the physical characteristics of slugging, several different models, describing severe slugging in horizontal extended reach-wells, are developed in Dymola. Anti-slug solutions with PI-controllers, using both bottom-hole- and topside- actuators and measurements, are implemented. To handle plant-changes in the reservoir a cascade control system using one PI-controller and a gain-scheduling PI-controller is implemented down-hole to cover a wider range of operating conditions.

The conclusion from the modeling and simulation study is that both bottom-hole- and topside- actuators and measurements can mitigate terrain-induced riser slugging in wells in this modeling environment. The gain-scheduling PI-controller implemented bottom-hole are able to stabilize both the flow and pressure at this location, when plant-changes are introduced to one of the implemented systems.

Aknowledgement

I would like to express my deep appreciation and thanks to my supervisors at NTNU, associate professor Christian Holden and PhD candidate Sveinung Johan Ohrem for their support throughout this semester with my master thesis. They have helped me through tough times in this process and I couldn't have done this job without them. I will also like to thank Esmaeil Jahanshahi, PhD and Key Expert Digitalization, Data Science at Siemens for providing dynamics of the model that i ended up implementing. At last, i would like to thank Pål Kittelsen at Equinor and PhD student Torstein Thode Kristoffersen for the help with my modeling work.

Contents

List of Tables

List of Figures

Chapter 1

Introduction

1.1 Motivation and Background

Offshore oil and gas multi-phase production and the transportation of hydrocarbons in pipeline-riser systems face huge challenges due to unstable flow regimes, like slugging. These instabilities, often occurring at low temperatures, pressures and flow-rates, have an oscillatory behavior which may result in production losses and damage on equipment and facilities. The origin of the severe slugging phenomenon is often found to be in pipeline-riser systems or production wells, where the geometry is described as a declining horizontal section followed by a vertical section.

There are many consequences in the upstream production process due to unstable flow and slugging. The unwanted pressure and flow oscillations provide a risk of shutdown of operation and the total production is decreased. Large production variations due to these instabilities may also result in a much more complicated separation process, as well as costly consequences like wear-and-tear on the equipment and facilities.

Well geometry and fluid composition have shown to be important factors in characterizing instability in an oil well. In horizontal extended reach-wells[40], or in mature wells, with reduced reservoir pressures and increased gas-oil-ratio, the hydrocarbon phases travel at a lower velocities, yielding a huge potential for unstable flow regimes. Unstable wells are often difficult to operate efficiently due to these severe pressure and flow fluctuations, but these instabilities are still not entirely understood.

The ability to detect slug-regimes and model the behavior of this phenomenon has been important in order to create efficient anti-slug control strategies to mitigate slugging. Several criteria for slug-detection and models to reproduce the slugging behavior have been provided in the literature study, prior to this work[60].

Existing anti-slug control systems are often not operating in practise because of robustness problems, for example because of inflow disturbances or plant changes. The operators turn off the controller and, instead, use manual choking strategies when the control system becomes unstable.

The purpose of this thesis is to find robust anti-slug control solutions to mitigate the unstable flow in wells, as well as nonlinearity caused by plant-changes. The software used in this work is the modeling and simulation environment, Dymola[16]. The licence with all the necessary components used in this thesis is provided by Equinor through the Subpro library in Dymola. The riser-slug model, used as a basis for this work, is also from the Subpro library and based on Jahanshahi's model[32]. Based on Malekzadeh numerical work[40], the riser-slug model is turned into several well-slug model for anti-slug control.

This chapter will provide the problem formulation, objectives, research questions, limitations, contributions and structure of this thesis.

1.2 Problem Formulation

The main focus of this thesis is to create a realistic well-slug model as well as an expanded system, including important elements in an offshore oil and gas production facility, relevant for Slug-control in Dymola. Also, do reseach on different controllers and find the suitable controller, actuator and measurement that fits the slug model with the ability to stabilize the pressure, resulting in a high, stable mass flow towards topside.

1.2.1 Objectives

The objectives of this thesis are:

- Investigate unstable flow in horizontal extended-reach wells
- Identify a model able to recreate slugging in horizontal extended-reach wells

- Design and implement 3 well-slug models with different geometries, inflow- and reservoir conditions in Dymola
- Connect the different well-slug models to an integrated 3-well system
- Investigate and apply anti-slug control solutions to mitigate slugging in the implemented systems
- Introduce non-linearity, i.e plant-changes, and mitigate it using an adaptive control strategy
- Draw conclusions based on the theory, modeling and simulation results

1.2.2 Research Questions

The main research question of this thesis can be formulated as follows:

- Which parameters and conditions, characterizing slugging, have to be manipulated in order to create terrain induced slugging in wells, in Dymola?
- How do the dynamics of the system change when different wells are connected in this modeling environment?
- Which anti-slug control solutions could be applied to mitigate unstable flow in different implemented slug-models in Dymola?

1.3 Limitations

The modeling in this thesis is based on the riser-slug model, provided by Jahanshahi[32]. Jahanshahi used a reference slug-model provided by OLGA to compare his model in the simulations. Because we did not use OLGA, it was challenging to identify our model with his reference model. By changing specific parameters, the riser-slug model is then converted into well-slug models, yielding specific geometries and properties. The anti-slug control focuses on terrain-induced riser-slugging in horizontal extended-reach wells, which is a limitation. The applied control solutions in this thesis work only for a specific type of slugging occuring in horizontal wells. The previous work done to recreate this kind of unstable flow[40] is done with the multi-phase simulator OLGA,

and since all the modeling and simulations in this work are done in Dymola, the results are restricted to the dynamics provided by this modeling environment. In Dymola, we used a specific three-phase fluid model, which represents the oil, gas and water flowing through our systems. This fluid model, as well as most of the implemented components, are provided by the Subpro library for the modeling and simulation work.

1.4 Contributions

To my knowledge, based on my research, this kind of model-implementation in Dymola has not been done before. Therefore, the contributions of this thesis are:

- A riser-slug model was turned into several well-slug models with different geometry, reservoir properties and inflow-conditions.
- The well-slug models were connected into a larger, integrated 3-well system with a complex system dynamics.
- Linear PI-controllers were designed and implemented to mitigate well-slugging using both topside and bottom-hole measurements and actuators in the implemented systems.
- A cascade gain-scheduling PI-control structure was implemented to handle nonlinearity introduced by plant-changes.

1.5 Structure of the thesis

- Chapter 1: (this chapter) introduces the motivation and background for this work. A problem formulation is provided as well as the objectives, research questions, limitations and contributions
- Chapter 2: focuses on the theory and literature surrounding the problem formulation. Offshore oil production is described as well as flow assurance, multi-phase slugging and anti-slug control approaches
- Chapter 3: focuses on the modeling part, and covers the system dynamics used in the implemented models in Dymola

- Chapter 4: describes the anti-slug control solutions designed and implemented in the different models in Dymola as well as simulation results of the different control structures
- Chapter 5: conclusions drawn and recommendations for future work

Chapter 2

Theory

2.1 Offshore Oil Production

In this Section the most relevant parts of offshore oil production will be described to provide a better understanding of the fundamentals, that create the conditions for unstable flow, introduced in Section 2.2. Most of this theory is taken from the literature study[60], prior to this work.

2.1.1 Petroleum Reservoir

Crude oil is a mixture of hydrocarbons and other organic compounds (usually containing liquid and/or gas), found in rock formations known as reservoirs. The reservoir rock is porous and permeable and the structure is bounded by impermeable geological traps, keeping the hydrocarbons in place. Gravitational forces arrange the vertical structure of the fluids and Figure 2.1 shows a cross-section of a typical reservoir, containing hydrocarbons [10]. The amount of oil and gas in a reservoir is dependent on initial reservoir pressure, temperature and hydrocarbon mixture composition, i.e. the composition of oil and gas. Some reservoirs are rich in oil, while others are rich in gas [1].

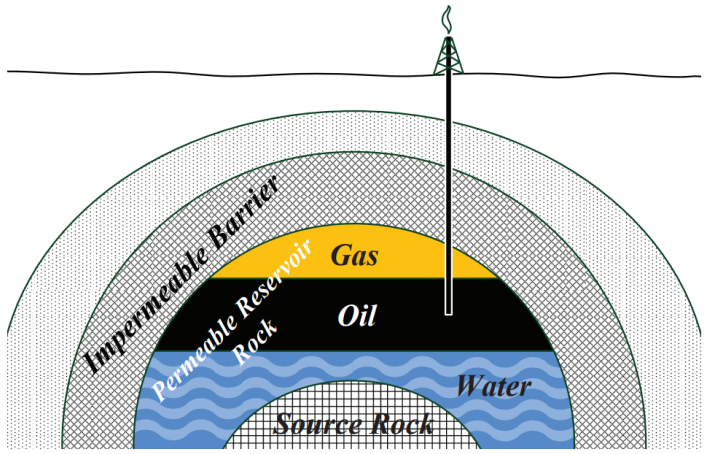

Figure 2.1: Cross-Section of a typical reservoir [10]

2.1.2 Subsea Oil Wells

An oil well is generally referred to as a hole drilled or dug in the earth from which petroleum flows or is pumped from a reservoir. A producing well most often has oil as its primary connercial product. Oil wells almost always produce some gas and frequently produce water. Most oil wells eventually produce mostly gas or water[59].

Subsea oil wells may yield different geometries through the hydrocarbon reservoirs, but are often long vertical pipes or long horizontal pipes followed by a vertical inclination, connecting the reservoirs to the wellhead. The wellhead can be located either on the seabed(offshore fields) or on land (onshore fields). The most common wells are drilled vertically, but the trajectories may also deviate from the conventional well-configurations, such as horizontal or multi-branched (side-tracked) wells[42]. The length of the well may also vary from hundreds to thousands of meters.

Initially, most hydrocarbon reservoirs have pressures high enough to allow a natural well production. However, if the reservoir pressure is low, or in mature fields, the subsea wells will need to compensate for the resulting low reservoir pressure. An artificial lift is then provided by either pumps, heating or gas lift. During gas lift, a casing is built around the well filled with gas which is injected at the bottom of the well [35]. Most wells are equipped with a production choke valve at the wellhead as illustrated in

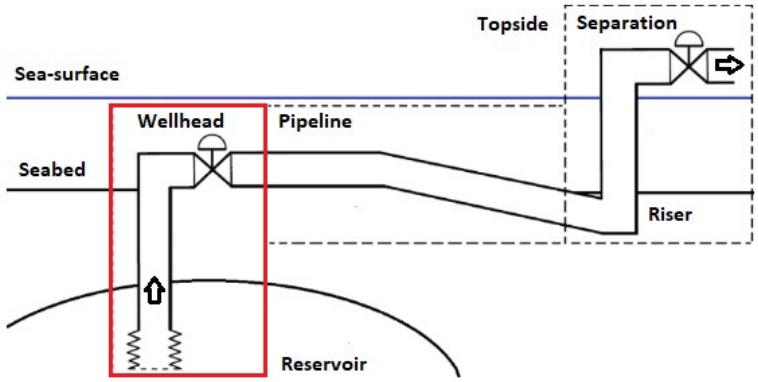

Figure 2.2: Illustration of an oil well in an oil field

Figure 2.2, which enables control of the outflow[12]. The reservoir pressure typically decreases over time, resulting in decreased fluid velocities and an increased gas-liquid ratio (GLR). The amount of water produced (water cut) also increases over time. This increases the liquid density and reduces the velocity of the fluids, which may yield a potential for unstable flow in wells [37]. One of the major concerns and challenges here is slugging, which will be covered in detail in Section 2.3. The red rectangle in Figure 2.2 shows a schematic overview of an oil-well connecting the reservoir to topside, separated by a typical pipeline and riser model.

2.1.2.1 Horizontal Wells

Horizontal drilling of wells has become a popular technological innovation in the oil industry over the last decades. Starting with drilling attempts in the 1950s in the Soviet Union, the technology has today become mainstream all over the world. There are several benefits from horizontal drilling compared to conventionally drilled wells(pure vertical, illustrated in Figure 2.2), like increased oil recovery, lower production costs and a reduced number of platforms and wells per field. Another motivation for horizontal drilling is to reduce water and gas coning, where gas or water infiltrates the perforation zone in the near-wellbore, reducing oil production. Figure 2.3 shows 3 different types of horizontal wells: long-, medium- and short- radius, where the difference between them is the radius of curvature from the horizontal to vertical Section[7].

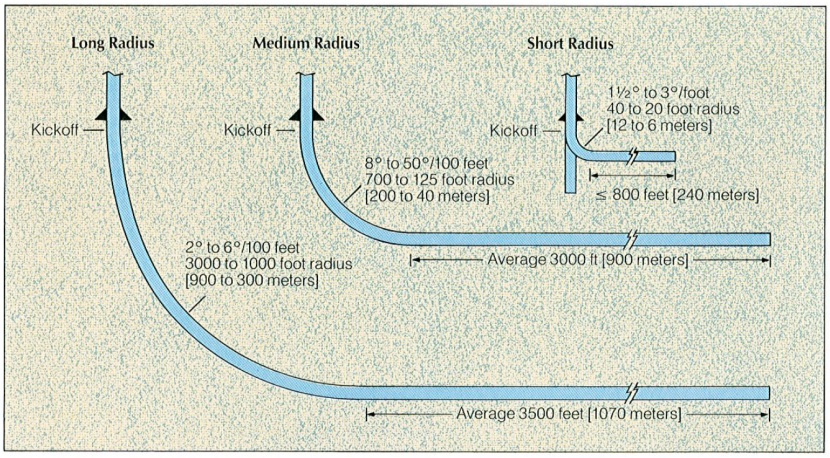

Figure 2.3: Long-, medium- and short-radius horizontal wells [7]

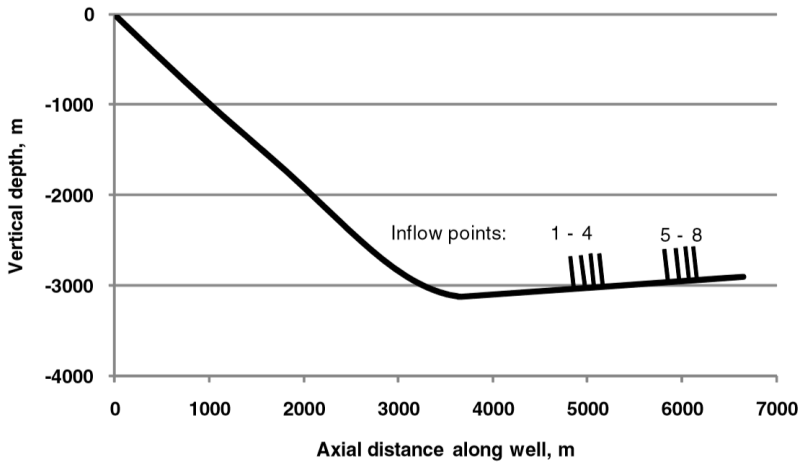

Figure 2.4: Extended reach well [40]

Extended reach drilling and completion technologies in horizontal wells allow the oil companies to find oil in smaller hydrocarbon pockets, enabling possibilities for maximized recovery from these fields. Horizontal wells may also have some kind of undulation, with deviation of some degrees form the horizontal part (Figure 2.4). This

inclination angle could either be designed on purpose in, for example, fish-hook wells, snake wells and undulating wells, or as a result of insufficient drilling control[40].

The optimal well trajectory of horizontal wells is based on their geological setting. Fish-hook wells has a geometry shaped as a fish-hook, drilling the deepest reservoirs first, followed by the shallowest reservoirs at the end of the wellbore. It could also be a snake well, characterized as a horizontal sinusoidal pattern cutting through layers of shale and sands , reaching a number of different reservoir pockets on it's way. [40].

As a horizontal well gets longer and follows a more complicated and undulating trajectory, wellbore hydrodynamics plays an important role in well performance, especially when involving two-phase gas liquid flow. Geometry and inflow conditions may yield a potential for unstable flow, which will be further described in Section 2.3.3.

2.1.3 Subsea Pipelines and Risers

Pipelines and risers are used for several purposes in the development of hydrocarbon resources (oil and gas), see Figure 2.5. These includes [2]:

- Export(transportation) pipelines;
- Flowlines to transfer product from platforms to export lines;
- Water injection or chemical injection flowlines;
- Flowlines to transfer product between platforms, subsea manifolds and satellite wells;
- Pipeline bundles.

As shown in Figure 2.5, risers are vertical sections of the pipeline. They connect the topside facilities to the seabed installations. The horizontal pipelines are placed on the seabed, yielding a geometry which could be subjected to terrain irregularities. Subsea pipelines and risers yield different geometries and conditions like pressure and mass flow rate of the different phases (oil, gas and water), which could result in unstable flow. The riser may also be subjected to the slugging phenomenon, which will be described in Section 2.3. The multi-phase flow coming out of the pipeline is regulated by the topside choke valve, and a separator is usually installed downstream to the right of this valve (Figure 2.5).

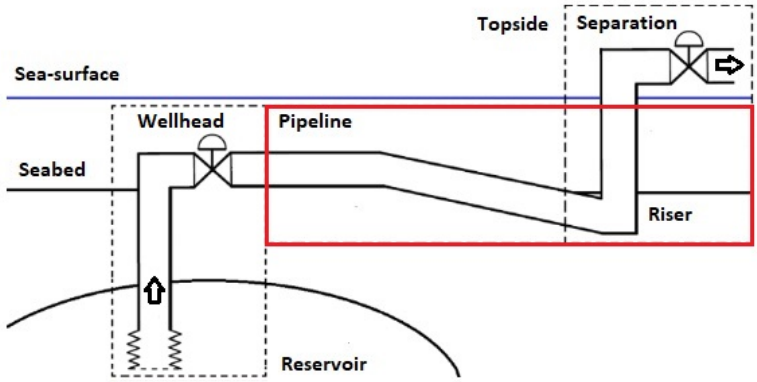

Figure 2.5: illustration of pipeline and riser in an oil field

2.1.4 The Separation Process

One of the functions of an oil production facility is to separate the components of the produced fluids. The oil and gas are then processed into saleable products. The separation process can be utilized either topside as illustrated in Figure 2.5, or subsea. This technology is used in mature fields (brownfields) where reservoirs produce more water than oil [34], but also in green fields with high gas oil ratios (GOR), facing risks of blocked flowlines due to hydrate formation [30]. Separators are based on either two- or three-phase separation. Two-phase separators separate a mixture of two-phases (gas-oil, gas-water, gas-condensate or oil-water). Three-phase separators are used to separate the gas from liquid and water from oil [47].

A simple three-phase gravity separator is shown in Figure 2.6. Here, two level controllers regulate the oil and water levels and one pressure controller, on the outlet gas valve, keeps the separator pressure constant [47]. Unstable flow, like slugging, could severely complicate the separation process [12], resulting in a poor oil and water separation [44].

2.1.5 Subsea Processing

Subsea processing is the definition of any active fluid treatment at or below seabed, before reaching the topside receiving facility. New technological challenges arise when

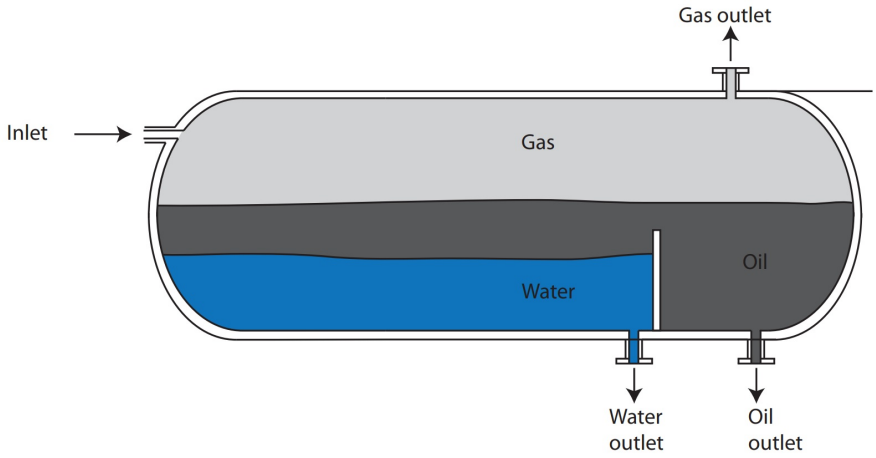

Figure 2.6: Typical Three-phase Gravity separator[47]

companies move into deeper waters, exploring more complex oilfield. They are met head-to-head with subsea processing technology. Drivers of subsea processing are either to increase, maintain or accelerate oil production, justifying large investments, and/or to handle the produced products down-hole[34].

The main components of a subsea processing system are shown in Figure 2.7. Subsea separation seperates the water from the produced crude multi-phase composition and injects the water back to a disposal reservoir. In addition, subsea boosting using pumps helps the separated oil and gas phases to reach the topside facility faster by increasing the the back-pressure. Water removal reduces the back pressure in oil wells, increasing the recovery from low-pressure reservoirs.

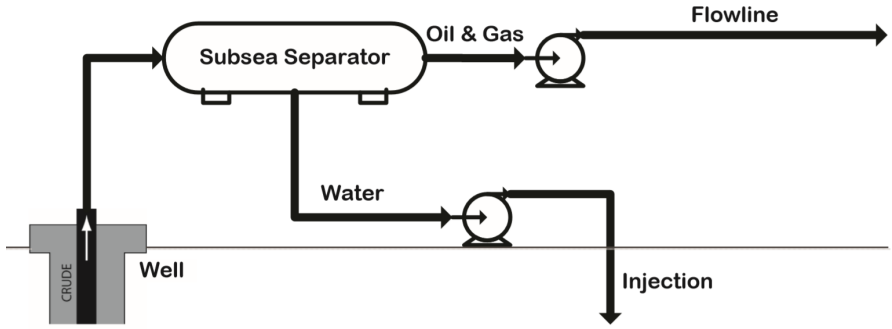

Figure 2.7: Schematic presentation of a subsea processing system[30]

2.2 Flow Assurance

2.2.1 Multiphase Transport

The combined transport of hydrocarbon liquids and gases may offer significant economical savings compared to platform-based separation, but multi-phase flow is more complex than single-phase flow and involves complex interactions. Multi-phase flow is the definition of liquids, gases and/or solid particles, flowing together as a mixture, without being completely dissolved in each other. Since wells produce oil, gas and water simultaneously ([3] p.517), multi-phase flow occurs on pipes all the way from the reservoir to the topside receiving facility. Multi-phase transport of fluids in offshore production systems comes with a lot of challenges that could possibly result in wear and tear of equipment, and of changes in the design requirements of subsea equipment [30, 58] . Multi-phase flow of gas and liquid appears in both vertical and horizontal pipes and the flow regime varies based on the flow rate of the phases, fluid properties and pipe geometry. Typical flow patterns in vertical pipes (Figure 2.8) are bubbly flow, slug flow, churn flow and annular flow, while horizontal pipes (Figure 2.9) have patterns such as bubble flow, slug flow, plug flow, annular flow, stratified /sprayed flow and wavy flow ([3] p.371).

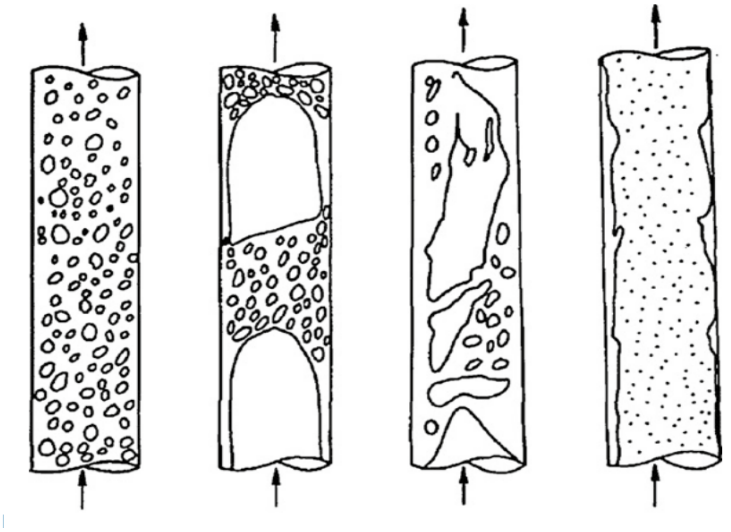

Figure 2.8: Typical flow patterns in a vertical pipeline (from left to right): Bubbly flow, slug flow, churn flow, and annular flow [3]

2.2.2 Flow Assurance Challenges

Flow assurance refers to ensuring safe and economically viable flow of hydrocarbons from the reservoir to topside and is closely linked to multi-phase flow technology ([3] p.331). Flow assurance has been a very important focus point in the industry to provide safe, reliable and efficient operation throughout the life of the production system. This term involves handling solid deposits, such as gas hydrates, wax deposition on walls, asphaltene, scales, corrosion, emulsions and severe slugging, among others [30]. The focus is mainly preventing and controlling solid deposits that could potentially block the fluid flow [3]. Handling these challenges is the key for a stable operation. As oil production moves into deeper waters, flow assurance becomes a major issue, since traditional approaches for handling these challenges suddenly becomes infeasible [62].

Flow assurance is critical during deep-water production because of the high pressures and low temperatures involved. The financial loss from production interruption or equipment damage due to an unlucky accident can be enormous. What complicates the flow assurance task even further is that these solid deposits can interact with each other and cause blockage of the pipeline, resulting in flow assurance failure [30].

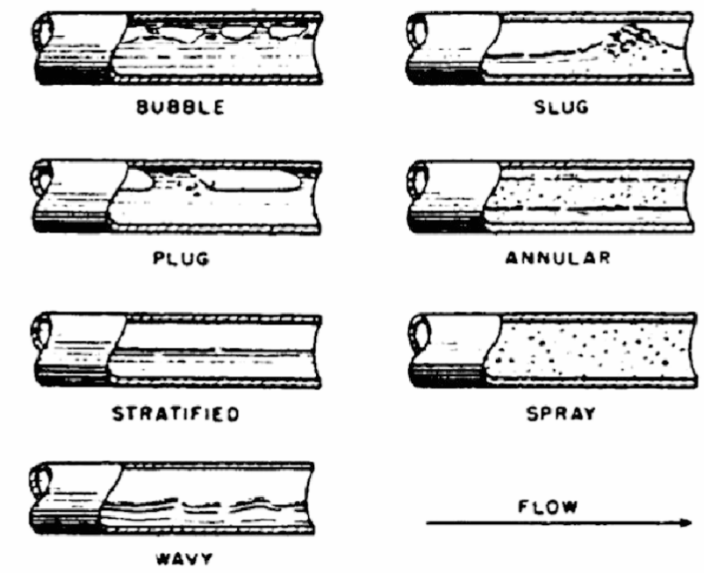

Figure 2.9: Multiphase flow pattern in horizontal pipelines [3]

2.3 Multiphase Slugging

2.3.1 Physical Description

The slugging phenomenon is a common multi-phase flow pattern consisting of an inhomogeneous distribution of gas, hydrocarbon liquids, water and sand. Slugging appears in wells, pipelines and risers in upstream gas/oil production systems. The gas and liquid phases usually have different velocities when flowing in pipelines due to viscosity and density differences. In upward flow, there is normally a less dense and viscous gas phase, flowing at a higher velocity than the liquid. The opposite can be said in terrains with downward slopes, where the liquid flows with higher velocities than the gas [30].

Slug-flow is usually characterized by the formation of elongated gas bubbles, flowing through a pipe, periodically separated by liquid plugs (slugs) [58, 45, 26]. This may occur at different geometric locations within an upstream production process. The slug-size may vary significantly from one system to another [12]. The degree of slugging also depends on important factors such as pressure, liquid- and gas- flowrates, and flowline topography [23]. The occurrence of slugging is typically classified based on slug size and cause of birth [12]. This Section will cover the most frequent types of slugging, that occur in well-pipeline-riser systems.

2.3.1.1 Hydrodynamic Slugging

This type of slugging appears in the horizontal parts of the flowline subjected to a gas-liquid flow regime but may also occur in risers and wells. The occurrence is due to velocity differences of the different phases. The liquid slugs are usually not severe, often short in length, but high in frequency. Hydrodynamic slugging does not negatively influence the oil recovery process and is normally considered unavoidable [30].

2.3.1.2 Terrain-Induced Slugging

Terrain-induced slugging appears in flowlines and wells as a result of the irregular surface of the seabed (Figure 2.10). The accumulation of liquid at the lower elevations in the pipe causes a pressure buildup. When the pressure is high enough, the liquid is

pushed down and block the gas flow in the pipe. Severe slugging is a typical case of terrain-induced slugging.

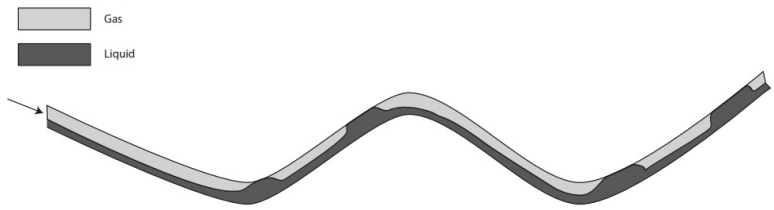

Figure 2.10: Terrain-induced Slugging [12]

2.3.1.3 Casing-heading Slugs in Gas-Lifted Wells

This is a well-known phenomenon occurring in gas-lifted wells. To use gas lift, an annulus is built around the well and filled with gas. The gas is then injected through a check-valve at the bottom of the well. Casing-heading is a periodic phenomenon, which consist of several pressure buildup phases in the casing without production and high flow-rate phases. These oscillations reduce the overall oil production and may damage equipment and facilities. Casing-heading is well reported in the literature [35, 17, 49, 27, 28].

2.3.1.4 Density-Wave in Gas-Lifted wells

Density-wave slugging may happen in long risers and wells. During gas lift, when critical flow is obtained through the gas injection, the annulus is decoupled from the tubing and the casing -heading instability is eliminated. However, some wells may still produce in a cyclic manner. Gas may accumulate at the bottom of the riser (well), creating variations in mixture density, resulting in a region with low density. This region will travel upward as a density wave[19].

2.3.1.5 Severe Slugging

Riser slugging is the most common form of severe slugging, where a downward inclination of the pipeline ending to the riser may enable liquid to accumulate in the bottom of

the riser and cause a blockage in the pipeline. The gas in the pipeline is compressed and when the gas pressure exceeds the hydrostatic pressure in the riser, the gas is expanding, pushing the liquid column out of the riser and into the separator. [36]. Low gas and liquid velocities may trigger the severe slugging cyclic process.

During severe slugging, the slug length varies, but in worst case scenarios it can fill the whole riser, and only one slug is present in the riser. The flow pattern in risers is not always severe slugging. It depends on different factors such as inflow conditions, pipeline-riser geometry, the topside choke valve as well as the separator pressure.

Severe slugging is not restricted to pipeline-riser systems. Horizontal wells may have a similar geometry, where a pipeline segment with a downward inclination angle is followed by another segment/riser with an upward inclination angle. As a result, unstable flow in production wells can be as severe as terrain-induced slugging in pipeline-riser systems, but the underlaying instability is not fully understood [37]. The severe slugging phenomenon has been the most researched slugging phenomenon over the last four decades [36, 57, 41, 30]. The mechanism of riser slug formation is shown in Figure 2.11 (adapted from [45]) and can be described by the following four steps:

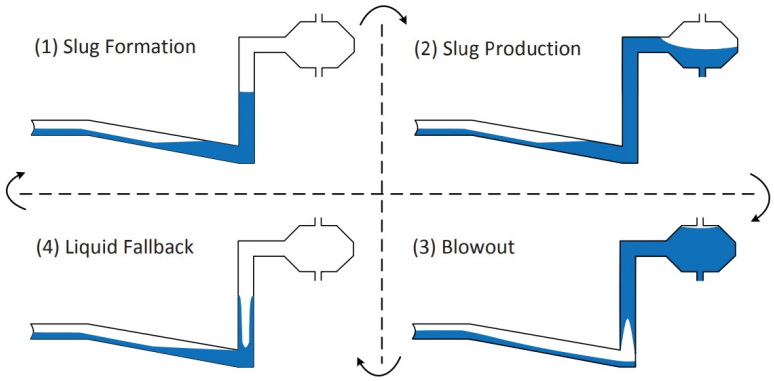

Figure 2.11: schematic overview of riser slugging in a flowline-riser system [30]

- Step 1: If the gas and liquid velocities are low enough, the process starts, liquid accumulates and blocks the low point of the pipeline-riser system due to gravity, preventing gas-flow. The slug will continue to grow and start to fill the riser.
- Step 2: The pressure will continue to increase as long as the pressure drop over

the riser is below the hydrostatic head of the liquid and the slug continues to accumulate. The liquid slugs will reach the top of the riser and flow into the separator. This is called the "slug production phase."

- Step 3: When the pressure-drop over the riser exceeds the hydrostatic head, the liquid is pushed out of the riser. The pressure drops due to the reduced static head of the liquid, causing the gas to propagate and accelerating the "blow out phase."
- Step 4: When all the liquid has been pushed out of the top of the riser, the velocities are now so small that the liquid falls back and starts to accumulate again. This is called the "liquid fallback phase."

2.3.2 Industrial Consequences of Unstable Flow

Unstable flow regimes have been a major operational problem in subsea oil-gas production systems over the last decades and might cause severe flow-rate and pressure fluctuations at all parts of the production process, including wells. Some of the problems due to well-instabilities might be: [35]:

- Fluctuations contrary to a smooth production might imply shutdown risks and safety aspects
- The total peak production of oil and gas is often smaller than the capacity of what the systems design allows
- During an unstable operating mode in gas lifted wells, the gas lift efficiency is often dramatically reduced
- Instabilities provide difficulties to compute the optimal gas lift allocation
- Wear and tear on equipment and other drawbacks on facilities during well operations

Slugging is an undesirable phenomenon in all situations, because it will always result in production losses. The mechanisms leading to these losses can be illustrated in Figure 2.12. Here, the open loop(natural) oil production is plotted as a function of the opening of the outlet valve. A fixed, large choke-opening causes slugging, resulting

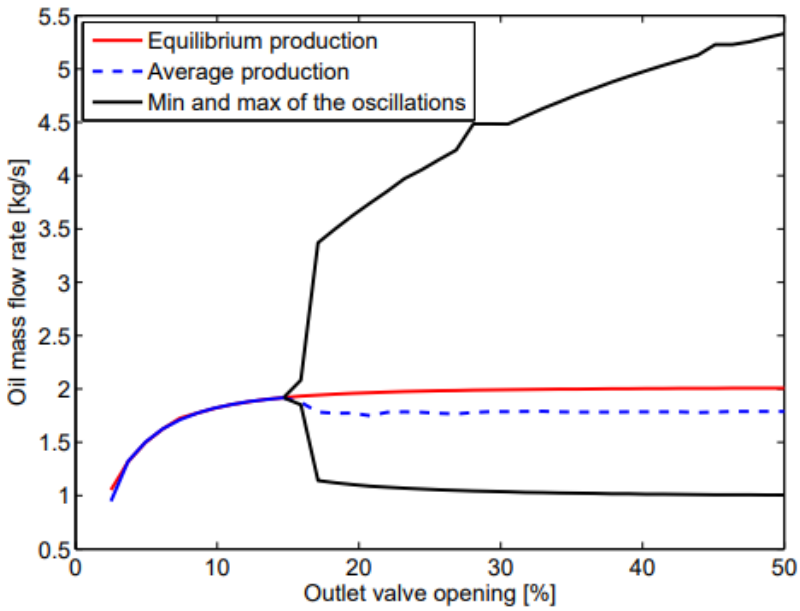

Figure 2.12: Bifurcation diagram of a test well [12]

in unstable production. Black lines illustrate the magnitudes of the oscillations, and the blue dotted line shows the average. The red line shows the "nominal" equilibrium production and, since the average is lower, this is a direct cause for production losses [12].

2.3.3 Unstable Wells

Well geometry and fluid composition have shown to be important factors in characterizing instability in oil wells [37]. Often, due to drilling, wells have a horizontal Section slowly transitioning into a vertical one, much like the pipeline-riser from wellhead to topside. Under certain operating conditions, oil wells with long horizontal bores and gas lifted wells, tend to have erratical behavior, resulting in pressure and flow fluctuations causing unstable production. With low gas and liquid velocities this might trigger the severe slugging mechanism and could be as critical for the production as terrain induced slugging in pipeline-riser systems [37]. Unstable flow in wells may also be due to well

instability, which characterizes slugging in wells not activated by gas-lift [12]

In mature wells when the reservoir pressure decreases, the increased gas-oil ratio (GOR) in addition to the increased water cut(fraction), results in lower velocities and a denser liquid phase. This might also yield a potential for unstable flow in production wells [37].

Unstable wells are often difficult to operate efficiently due to the potentially large pressure and flow fluctuations, causing unstable production. There is a lot of uncertainty to the exact reasons of the occurrence of the well instability, because most of the focus has mainly been on the outlet performance, i.e. the results of the slugging control [12, 30, 35], rather than the dynamics down in the well, which might be the real cause of the problem [50]. Therefore, the underlaying instabilities are not fully understood.

2.3.3.1 Terrain-Induced Oil/Water Slugging in Wytch Farm

There have also been reports of unstable flow and slugging behavior in oil/water reservoirs. In 1998, a maturing BP oilfield called Wytch Farm experienced operating problems with its ESP wells [4]. Large fluctuations were seen in flow-rate, pressure and supply current of the ESP-pumps. The slugging in well M5, consisting of oil and water seemed to originate at the foot of the well, where water (the heaviest component) seemed to accumulate. This resulted in a terrain-induced slugging flow in the well. Experiments using a test model of the production liner, tubing Section and the casing were performed. The slugs were generated in the production liner. At low flow rates slugs survived longer, were longer in size and were more frequent on their travel through the three Sections of the experiment (liner, tubing and casing). At higher volumetric flow-rates, the results showed that the slugs decayed at a higher rate over the tubing Section. No slugs were seen to survive and see the casing, and discrete slugs were barely formed.

2.3.3.2 Terrain-Slugging from the Brage Field

Another special case was reported in 2002 from the Brage field, operated by Norsk Hydro in the North-sea [11]. They experienced instability caused by an erratic flow manner from the oil producing gas-lifted wells. The instabilities were not due to the casing-heading mechanism. Low gas and liquid flow-rates in the well below the gas lift entry point resulted in a separation of the different phases. In the well, this caused a

back-flow of water and slugs were formed. The U-shape of the well was believed to have an impact on setting up terrain slugs with liquid blocking the flow when low flow-rates were discovered.

2.3.3.3 Severe Slugging in Extended Reach Wells

A modeling study done by R. Malekzadeh and R.F. Mudde in 2012 [40], numerically proved that the severe slugging phenomenon may occur at the bottom of the wellbore of an extended reach well-geometry. Figure 2.13 shows the geometry of the well under consideration in their test case.

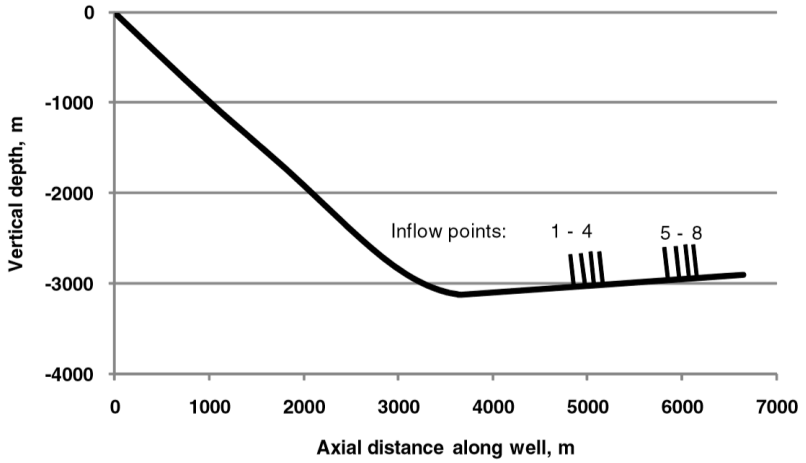

Figure 2.13: Geometry description of the well. x=0 corresponds to the wellhead. [40]

The test well (Figure 2.13) consisted of eight inflow points which were distributed along the slightly downward-inclined Section of the well. The flow from all inflow points enters the tubing. The total lenght of the well was 6670m. The downward-inclined Section of the well was approximately 3000m long with 1.3 degree downward inclination. The inner diameter of the tubing was 0.089m. At the top side of the vertical Section of the well a separator was located with a constant back-pressure of 20barg. The transient wellbore flow model, OLGA, used a PI calculated by Cheng's method[8] for each inflow point, which represented the reservoir.

Accumulation of a sufficient amount of oil at the lowest point in the well (axial

distance along the well equals to 3670m) created a blockage. Then the slug grew mainly in the slightly downward-inclined Section and also partly in the vertical Section of the well and eventually was blown out via the vertical section of the well into the separator. Figure 2.14 shows the pressure at the lowest point in the wellbore, corresponding to 3670m axial distance along the well.

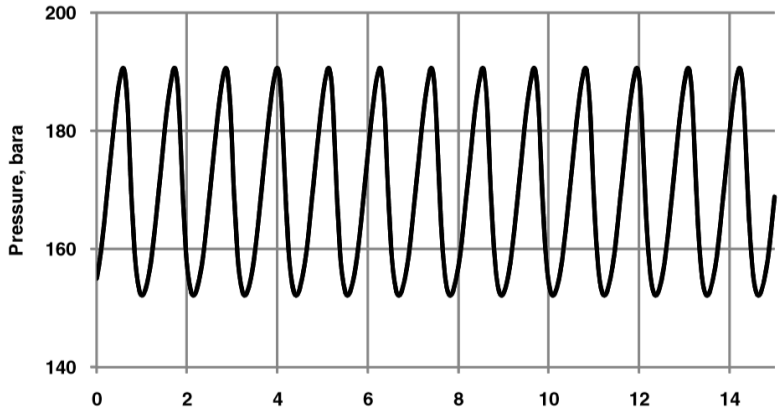

Figure 2.14: Transient behaviour of pressure at the bottom of the wellbore, x=3670m. [40]

2.4 Slug Modeling

To gain insight of the slugging mechanism and to design an efficient control strategy to mitigate slugging in a pipeline-riser system, modeling of the flow behaviour is necessary. These dynamic models will be able to reproduce slugging, which may result in flow-rate- and pressure- fluctuations. There are several ways to model these systems. Storkaas[55], Di-Meglio[13] and Jahanshahi[30] among others, have provided models using mass balance equations based on Ordinary Differential Equations (ODEs). In addition to other equations, these models describe all the dynamics of the preferred system. The different models are compared with multi-phase flow-simulators like OLGA[5] to prove their accuracy[30] before used in control-laws. This has shown to provide effective and accurate anti-slug control solutions for the pipeline-riser systems during severe slugging[30].

2.4.1 Modeling of Well Instability

One of the main issues of slug modeling is that most models are based on the mass-balance principle, which requires liquid and gas phases to be known, but this is often not possible [44]. Predicting and modeling unstable flow in production wells is complex and the multi-phase flow simulator OLGA might not be capable to reproduce the instabilities occurring in wells. Though, it has still been shown numerically in OLGA using Cheng's method[8] for inflow-conditions, that severe slugging may happen in horizontal gas wells with a specific geometry and properties[40]. In addition, the dynamics down-hole are not entirely understood, which further complicates modeling [37]. In wells, transmitters and sensors acquiring the required data for dynamic modeling might also be limited or unavailable [44].

There has been some interesting research regarding the terms "Smart wells" or "intelligent wells" [22]. These wells are equipped with down-hole transmitters that may monitor the well and reservoir conditions, which could solve problems related to sensor measurements, but they are not widely used to date.

2.5 Anti-slug Control

The slugging behavior, especially the severe slugging mechanism, is undesired in any oil and gas production system, because of the negative impact it brings with an unstable flow regime. Severe pressure and flow fluctuations in wells-pipelines-risers may result in significant production losses and wear and tear on equipment (as explained in Section 2.3.2).

Anti-slug control provides solutions to these problems, handling the complex nature of severe slugging, hence reducing its oscillatory behavior. This Section will cover the most common anti-slug solutions, used to date.

2.5.1 Topside Choking

A traditional approach to handling slugging behavior in the pipeline-riser Section, has been to manually choke the flow using the topside choke valve. Manual topside choking, i.e. closing the topside choke valve, was one of the first methods to prevent the severe slugging phenomenon, introduced in 1973 [64]. Results proved that the increased

back pressure would eliminate the oscillatory behavior, but would also reduce the flow capacity, resulting in a lower production.

2.5.2 Gas Injection during Gas-Lift

Another traditional, but costly approach has been to increase the gas-lift flow during gas-lift [17]. Increasing the pressure drop caused by friction, hence eliminating the highly oscillating flow.

2.5.3 Passive Anti-slug Solutions

Passive approaches to anti-slug control have also been used conventionally. These methods focus on system/design changes to the process to eliminate slugging. Passive slug elimination techniques are "self-acting" methods without any external influence [63]. In 1973, Yocum introduced different solutions to mitigate severe slugging in pipeline-riser systems by creating a process change to the system [64], leading it into a stable region without slug-flow. These solutions can be split into three groups:

- Reducing the line diameter near the riser;
- Using dual multiple risers;
- Mixing the fluids at the riser base to avoid accumulation, hence preventing severe slugging

Other passive approaches can also be mentioned, like Flow conditioners. In 2013, Xing introduced the concept of "Wavy Pipes," [63], installed in pipeline-riser systems to accelerate the gas movement compared to the liquid accumulation, hence avoiding severe slugging. Slug Catchers have also been conventionally used [21] . These buffer tanks are located either after the riser or topside of the well with the ability to store the largest slugs formed in a system. A slug-catcher is a simple, effective solution, but represents a heavy investment cost [30].

2.5.4 Active Slug-Control

Control systems using feedback control strategies are widely used in the oil and gas industry. By taking the system output into consideration, it is able to adjust the system

performance in order meet a desired output response. Active slug elimination approaches involve automatic feedback control mechanisms, manipulating some actuators, installed in the process system, subjected to some sensor feedback signals. These signals can come from pressure, temperature and/or flow transmitters, depending on the specific system. The selections of actuators and sensors can be guided by some fundamental system property analysis [31]. Active feedback control to mitigate slugging is well provided in the literature[23, 11, 56]. Many existing anti-slug solutions may not be operating properly because of robustness problems [31].

The closed-loop dynamics of a system, i.e. the dynamics of the feedback control system may become unstable after some time during operation. This may be due to process changes or inflow disturbances. Non-linearity is another source of process change, because the gain of the system (i.e. the closed loop gain from the controller) may change drastically in different operating conditions. Measurements or valves may also cause a time delay, which may be another problematic factor for stabilization [30]. In addition, measurements from sensors, especially down-hole, might not be available or working properly [11]. This may as well lead to robustness and/or stabilization problems at locations where maintenance could be more difficult or in worst case- impossible.

Automatic feedback control has proved to have the ability to change the boundaries between different flow regimes, by changing the dynamics of a given steady-state operating point from unstable to stable[30] . A robust controller must be able to stabilize the unstable system in a wide range of operating conditions: hence the system should not deviate from the design operating performance or set-point.

2.5.4.1 PI-Control

Active feedback control of the production choke using a PI controller has been a favored solution for anti-slug control for a long time [23, 11, 49]. It can be used to stabilize or reduce well instabilities. Conventionally, the down-hole pressure has been measured variably to stabilize this pressure at a specific set-point. However, a PI-controller on the bottom-pressure can be sensitive to the movement where the controller is triggered. The controller must be turned on when the oscillations of the bottom pressure are increasing to ensure its efficiency [15]. When using a PI-controller on the bottom pressure, it is reliant on the availability of the bottom-hole pressure sensor, hence when it fails, slugging will start to occur again [11].

For well-pipeline-riser systems with an emphasis on riser-slugging, Jahanshahi[30] performed a controllability analysis, including the selection of suitable control variables (CVs) for stability control. He also performed a robustness and performance analysis on a well-pipeline-riser system. He concluded that the bottom-hole pressure and the riser-base pressure were the best CVs for SISO (Single-Input-Single -Output, described in Chapter 4) control of these systems.

2.5.4.2 Nonlinear Control Strategies

During severe slugging in pipeline-riser systems, model-based control laws linearizing the dynamics of mass and liquid in the riser, have been proven to perform better than many considered PI strategies [12, 14]. The most common anti-slug control strategies uses measurements of the down-hole pressure as the controlled variable (CV) of a PID controller and the choke opening as the manipulated variable [23, 55]. If measurements are not available, we can use an observer to get an estimate of the down-hole sensor data based on other measurements. Models have been used to provide an estimate of the Bottom-Hole Pressure, stabilized by a PI-controller[49]. Eikrem and Aamo [18] also proved experimentally that a reduced order nonlinear observer, by using an estimated down-hole pressure based on topside measurements and a PI-controller, could stabilize a gas-lifted well.

The nonlinearity at different operating conditions or other plant-changes in oil-production system may require nonlinear control solutions to stabilize the system [30, 37, 28, 49]. In 2008, Kaasa [37] provided a nonlinear model-based control for stabilization of unstable flow in oil wells. He developed a simple empirical model, describing the behavior of the down-hole pressure in case of severe slugging. That model were implemented into an integrator using Backstepping approach, which stabilized at lower pressure set-points, corresponding to higher flow-rates.

Chapter 3

Modeling

Based on the work done in the project thesis prior to this work[60], the goal of this master thesis is to recreate severe terrain-induced riser-slugging in wells, similar to Malekzadeh's work[40], in Dymola, and mitigate it using some kind of suitable controller dynamics in Chapter 4. To recreate well-slugging, we implemented Jahanshahi's and Skogestad's riser-slug model (implemented from [32]) from the Subpro Library in Dymola, and turned the pipeline-riser geometry into different well-geometries. 3 well-systems were created with different properties and geometries, connected to a reservoir, choke valves, sensors, a pipeline-riser system and a topside facility.

The different separate well-systems were connected together, resulting in an integrated 3-well system (explained in Section 3.3.3), by connecting them to a manifold. This Chapter will cover all the dynamics and the behaviours of the different implemented systems, leading up to the anti-slug control in Chapter 4.

Figure 3.1 shows an example of an oil and gas production system, from the Subpro library in Dymola, consisting of several blocks representing a reservoir, productivity index, a well, chokes, sensors, a pipeline and a topside boundary.

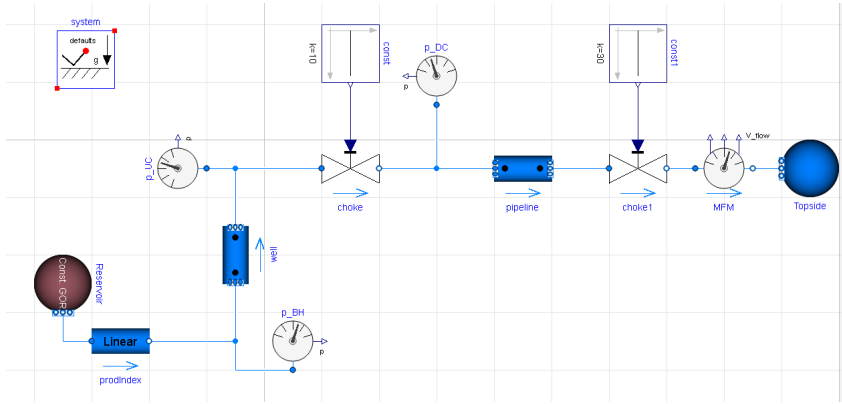

Figure 3.1: Example of an oil and gas production system in Dymola (Subpro Library)

3.1 Modeling in Dymola

Dymola is a commercial, multi-engineering modeling and simulation environment, based on the open Modelica modeling language[16]. Large and complex systems are derived from component models, based on mathematical equations to describe the dynamic behavior of the given system with a wide range of provided toolkits. Subsystems are represented by interconnected components, and connection between these components form additional equations. Dymola then processes the complete system of equations in order to generate efficient simulation code.

3.1.1 Modeling an Offshore Oil and Gas Production System

To create an offshore oil and gas production system in Dymola, it is necessary to have blocks for several components like the reservoir, productivity index, the well, sensors, chokes, pipeline, riser and a topside component. When connected, this results in a complex system dynamics with pipes that could be several thousands of meters long/high. This implicates that it takes a significant time to simulate and analyze the system behaviour.

It is also important to choose a suitable equation-based-solver to fit such a stiff system like this one. We chose the the **Esdirk45a - order 5 stiff**-solver, because it gave us the desired system responses in our simulations. The goal with this model is to

create suitable conditions that fit a real oil and gas production system, trying to identify properties and flow-conditions, similar to Jahahnshahi's [32] and Malekzadeh's[40] work.

Because our system is developed in a modeling environment, we wanted to make sure that the down-hole conditions caused by slugging were as extreme as possible in order to make the anti-slug control in Chapter 4 more challenging

An offshore production system like the one shown in Figure 3.1, which consists of multiple components from the reservoir to the receiving topside facility, is considered as an online application. Because these models in Dymola are based on physics, it can naturally describe nonlinear processes and potentially a wide range of operating conditions. Implementing adaptivity is essential for online use to ensure robustness over time. That is why we introduced a control strategy to mitigate plant changes in Section 4.2.4.3.

3.1.2 Modeling Challenges

It might not be possible to describe well-slugging with a riser-slug model in a real environment, but the research has not shown any available well-slug models, representing the severe slugging phenomenon in wells. We ended up using most components from the Subpro library in Dymola, including a riser-slug model[32], with the possibilities of changing the geometry, properties and inflow-conditions to try to describe a slugging well. Because we did not have any working slug-model from simulation (i.e OLGA), we had to identify the different parameters by a systematic trial and error approach in Dymola that would create a working slug-model.

Because of the nature of Dymola, all the components affect each other and result in complex dynamics where one tiny change to one of the parameters in the model would drastically change the system behaviour. As a result of this, we had to be cautious identifying the correct parameters in order to make progress.

Because of the lack of previous works regarding modeling of severe slugging in wells, we may consider questioning the reliability of the modeling and simulation results in Dymola.

3.2 System Dynamics

This Section will explain the dynamics of all the systems implemented in Dymola for this thesis. The ones that will be covered in this thesis is the riser-slug system, which has created the foundation of the three well-slug systems, and then the resulting 3-well system, which connects all three wells to a pipeline-riser system in a more integrated, complicated oil and gas production system.

3.2.1 Oil Reservoir Model

The oil reservoir model is the same for all the implemented system, and is modelled as a well source, specifying the gas-oil-ratio (GOR) as a linear function of oil rate from a nominal point:

$$GOR = GOR_0 + (w_o - w_{o,0})(\frac{GOR_n - GOR_0}{w_{o,n} - w_{o,0}}) \tag{3.1}$$

Where GOR_0 is the 0-production GOR, w_o is the oil production, $w_{o,0}$ is the 0-production limit of oil, GOR_n is the nominal GOR and $w_{o,n}$ is the nominal oil production.

In our models we specify that the nominal GOR is equal to the production GOR ($GOR_n = GOR_0$). In 3.1 the effective GOR is then equal to the production GOR (($GOR = GOR_0$), for simplicity.

The gas-oil-ratio (GOR) is then defined as the standard gas volume to the oil volume:

$$GOR = \frac{\frac{X_G}{\rho_{STP}}}{\frac{X_O}{\rho_O}} \tag{3.2}$$

Where X_G is the mass fraction of gas, ρ_{STP} is the molar density at standard conditions, given to be 42.295 mol/m3 (at 15$\circ c$, 1.01 bar). X_O is the mass fraction of oil and ρ_O the density of oil.

The reservoir model provides a pressure, which generates a mass flow consisting of a specified medium (which in our case is a Three-phase fluid model, explained in Section 3.2.2), which flows through the system. In the model, it is possible to specify parameters such as boundary pressure, temperature, molecular mass of both gas and oil, fixed water cut (volume H2O/volume liquid), GOR as well as nominal oil production.

3.2.2 Three-Phase Fluid Model

The flow model and medium, which flows through all the implemented systems, is the three-phase medium provided by the Subpro library in Dymola, a package containing 5 different components:

- 1. Light gas with molecular weight MM1 (=16g/mol)
- 2. Heavy gas with molecular weight MM2 (=600g/mol)
- 3. Light hydrocarbon liquid with molecular weight MM1 (=16g/mol)
- 4. Heavy hydrocarbon liquid with molecular weight MM2 (=600g/mol)
- 5. Water

The mass fractions of these 5 components (4 of them being independent) together with the pressure and temperature defines the state of the medium (p,T,X). That means there must be specified 6 variables to uniquely define the state of the fluid.

The relative distribution between the light and heavy gas component determines the molecular mass of the gas. The molar mass can vary between 16 and 600 by varying the distribution. Typically, there will be much more of the light component in the gas. The same goes for the liquid, where it is natural that the heavy component dominates.

3.2.2.1 Molar ;asses

The molar mass of gas is calculated as:

$$MM_{gas} = \frac{X_{G1} + X_{G2}}{\frac{X_{G1}}{MM_1} + \frac{X_{G2}}{MM_2}} \tag{3.3}$$

Where X_{G1} and X_{G2} are the mass fractions of the light and heavy gas, and MM_1 and MM_2 are the molecular weights. The molar mass of liquid (oil) is calculated in the same way.

3.2.2.2 Density Calculations

The density of gas is calculated as:

$$\rho_G = \frac{MM_G}{V} \tag{3.4}$$

and

$$p * V = z * R * T \tag{3.5}$$

where MM is the molar mass (kg/mol), p is the pressure, V is the volume, z is the compressibility, R is the gas constant and T is the temperature.

The density of oil is either set to a constant value, or calculated as:

$$\rho_O = A + \frac{B}{MM_O} + C * T_C \tag{3.6}$$

where A,B and C are constants, MM_O is molar mass of oil and T is the temperature. The water density is constant and the total density is calculated as:

$$\rho = \frac{1}{\frac{X_G}{\rho_G} + \frac{X_O}{\rho_O} + \frac{X_W}{\rho_W}} \tag{3.7}$$

where X represents the mass fractions of the gas, oil and water phases.

3.2.2.3 Volume Fractions

The water cut, defined as the ratio of water volume to the liquid volume is calculated as:

$$WC = \frac{\frac{X_W}{\rho_W}}{\frac{X_W}{\rho_W} + \frac{X_O}{\rho_O}} \tag{3.8}$$

3.2.3 Productivity Index Model

The productivity index is the model that gives the inflow performance to the well. It is represented as a static linear, pipe model, transporting fluids between its two ports, without storing mass or energy. This static pipe sets the medium of the whole system, which is a three-phase fluid model (oil + gas + water) provided by the Subpro library. This segment is adiabatic, which means that no heat is gained or lost, neglecting changes in kinetic energy from inlet to outlet. This pipe element is set to use a nominal volume flow-rate, with mass flow given by:

$$\dot{m}_{flow} = k_m * \rho * \mathrm{d}p^n \tag{3.9}$$

where k_m is a mass flow constant, ρ the density and $\mathrm{d}p^n$ is the pressure drop. Setting

n=1 gives a mass flow rate which is proportional of the pressure drop, giving a linear relation (default).

3.2.4 Production Choke- and Topside Choke Valve Model

Both the production choke valves and the topside choke valves used in all the implemented models have the same dynamics, for simplicity. The choke valve model is designed according to the IEC 60534-2-1/ISA S.75 standards[29] for valve sizing, compressible fluid, and no phase change, also covering choked-flow conditions. The medium flowing through the valve is the three-phase fluid flow (oil + gas + water)(Section 3.2.2), provided by the Subpro library. This model assumes adiabatic operation (no heat losses to the ambient) and changes in kinetic energy from inlet to outlet are neglected in the energy balance. For simplicity, the valve characteristics are set to a linear, inherent flow characteristic.

3.2.4.1 Model Equations

The IEC valve equation for compressible flow is:

$$\dot{m}_{flow} = N_6 * F_p * C_v * Y * \sqrt{x_s * p_1 * \rho} \tag{3.10}$$

where N_6 is a numerical constant, F_p is the piping geometry factor, C_v the flow coefficient (US), Y the expansion factor, x_s a pressure differential ratio, p_1 the inlet absolute static pressure measured at point A and ρ the fluid density.

3.2.4.2 Model Type for the Flowing Density

The model type for the flowing density in this model supports stratified flow, mixed two-phase flow and mixed compressible flow. The latter is used in this thesis, and the flowing density for mixed compressible flow is calculated as:

$$\rho_{flow} = Y^2 \rho_{mix} \tag{3.11}$$

where ρ_{mix} is the mixed fluid density.

3.2.5 Riser Slug Model

The Slug model used in this thesis is a Riser slug model based on Jahanshahi and Skogestad's paper [32], adapted to modelica fluid where pipe flow friction has been neglected. The dynamics of this model is taken from directly from this paper[32].

The model is represented by four state equations, which are the mass conservation laws for the individual phases in the pipeline and riser Sections:

$$\dot{m}_{G1} = w_{G,in} - w_{G,lp} \tag{3.12}$$

$$\dot{m}_{L1} = w_{L,in} - w_{L,lp} \tag{3.13}$$

$$\dot{m}_{G2} = w_{G,lp} - w_{G,out} \tag{3.14}$$

$$\dot{m}_{L2} = w_{L,lp} - w_{L,out} \tag{3.15}$$

Where m_{G1} is the mass of gas in the pipeline, m_{L1} is the mass of liquid in the pipeline, m_{G2} is the mass of gas in the riser and m_{L2} is the mass of liquid in the riser.

In Dymola, Three tuning parameters are used to fit the model to the desired pipeline-riser system.

- K_h: correction factor for level of liquid in pipeline
- K_G: orifice coefficient for gas flow through low point
- K_L: orifice coefficient for liquid flow through low point

In our systems, because we did not have any reference model from OLGA[32], representing a working slug-model, we used the default values provided by the riser-slug model in Dymola. K_h was set to 0.7 and K_G, K_L, as shown in Section 3.3, table 3.1.

3.2.5.1 Boundary Conditions

In Dymola, the Riser-slug model is extended from the partial component model with two ports to fit the modelica environment. This model defines an interface for components with two ports, where the treatment of the design-flow direction and flow reversal are predefined based on the parameter **allowFLowReversal**. The component may transport fluid and may have internal storage for a given fluid **Medium**. This means

that In- and outflow relations in Dymola are specified by the sum of medium mass fractions of the different components between port a and b in the model.

a) Inflow Conditions:

In the equations 3.12 and 3.13, $w_{G,in}$ and $w_{L,in}$ are inlet gas and liquid mass flow rates, assumed constant, but the boundary inlet conditions might change easily.

The inflow conditions of gas in the riser-slug model in Dymola becomes the sum of mass of individual components of gas flowing through port a (eq 3.16). For liquid, it's the total mass flow minus the mass flow of gas flowing through port a (eq: 3.17):

$$w_{G,in} = \sum w_{G,a} \tag{3.16}$$

$$w_{L,in} = w_{tot,a} - w_{G,a} \tag{3.17}$$

The liquid volume fraction in the pipeline can be written based on the liquid mass fraction and densities of the two phases [6]:

$$\alpha_L = \frac{\alpha_{Lm}/\rho_L}{\alpha_{Lm}/\rho_L + (1-\alpha_{Lm})/\rho_G} \tag{3.18}$$

Where α_{Lm} is the liquid mass fraction, ρ_L is the liquid density and ρ_G is the gas density. The average liquid mass fraction in the pipeline Section can be fairly well approximated using the inflow boundary condition:

$$\overline{\alpha}_{Lm1} \cong \frac{w_{L,in}}{w_{G,in} + w_{L,in}} \tag{3.19}$$

Where $w_{L,in}$ and $w_{G,in}$ are the inlet mass flow-rates of liquid and gas respectively. Combining eq: 3.19 and eq: 3.18 gives the average liquid volume fraction in the pipeline:

$$\overline{\alpha}_{L1} \cong \frac{\overline{\rho}_{G1} w_{L,in}}{\overline{\rho}_{G1} w_{L,in} + \rho_L w_{G,in}} \tag{3.20}$$

In equation 3.20, the gas density $\overline{\rho}_{G1}$ can be calculated based on the nominal pressure

(steady-state) of the pipeline:

$$\overline{\rho}_{G1} = \frac{P_{1,nom} M_G}{R T_1} \tag{3.21}$$

b) Outflow Conditions:

in Jahanshahi's and Skogestad's model[32], a constant separator pressure condition and a choke valve model for the outflow of two-phase mixture are assumed as the boundary conditions at the riser outlet.

$w_{L,out}$ and $w_{G,out}$, the outlet mass flow rates of liquid and gas, are calculated as follows [32]:

$$w_{L,out} = \alpha_{Lm,t} w_{mix,out} \tag{3.22}$$

$$w_{G,out} = (1 - \alpha_{Lm,t}) w_{mix,out} \tag{3.23}$$

where $w_{mix,out}$ contains the characteristic valve equation of the topside choke valve, relative valve opening, density and pressure difference upstream and downstream the choke, which is not present in the Dymola representation of this model.

The outflow conditions of gas in Dymola is the sum of the mass of individual components of gas flowing through port a (eq 3.24). For liquid, it's the total mass flow minus the mass flow of gas through port a (eq 3.25): Because the flow direction is chosen from port a to port b in Dymola, the outflow conditions is given by:

$$w_{G,out} = -(\sum w_{G,b}) \tag{3.24}$$

$$w_{L,out} = -(w_{tot,a} - w_{G,b}) \tag{3.25}$$

Liquid mass fraction at top of the riser, $\alpha_{Lm,t}$, is given by eq:3.44.

3.2.5.2 Pipeline Model

Consider the steady-state conditions in which gas and liquid are distributed homogeneously along the pipeline. In this situation the mass of liquid in the pipeline is given

by $\overline{m}_{L1} = \rho_L V_1 \overline{\alpha}_{L1}$, where V_1 is the pipeline volume, and the level of liquid in pipeline at the low-point is approximately $\overline{h}_1 \cong h_c \overline{\alpha}_{L1}$. As shown in Figure3.2, h_c is the height of the pipeline in the low-point. If liquid content(kg) of pipeline increases by Δm_{L1}, it starts to fill up the pipeline from the low-point. A length of pipeline equal to ΔL will be occupied by only liquid and level of liquid increases by $\Delta h_1 = \Delta L sin(\theta)$.

$$\begin{aligned} \Delta m_{L1} &= \Delta L \pi r_1^2 (1 - \overline{\alpha}_{L1}) \rho_L \\ h_1 &= \overline{h}_1 + \Delta L sin(\theta) \\ h_1 &= \overline{h}_1 + \frac{\Delta m_{L1}}{\pi r_1^2 (1 - \overline{\alpha}_{L1}) \rho_L} \\ \overline{h}_1 &= K_h h_c \overline{\alpha}_{L1} \end{aligned} \tag{3.26}$$

Where K_h is a correction factor around unity which can be used for fine-tuning of the model.

$$h_1 = \overline{h}_1 + (\frac{m_{L1} - \rho_L V_1 \overline{\alpha}_{L1}}{\pi r_1^2 (1 - \overline{\alpha}_{L1}) \rho_L}) sin(\theta) \tag{3.27}$$

Therefore, level of liquid in the pipeline h_1 can be written as a function of liquid mass in pipeline m_{L1} which is a state variable of the model. All of the other parameters are constant. Figure 3.2 and Figure 3.3 gives the schematic representation of the model parameters. When implemented in Dymola, the riser-slug model doesn't take into account the Topside Choke valve, which is implemented separately in the model.

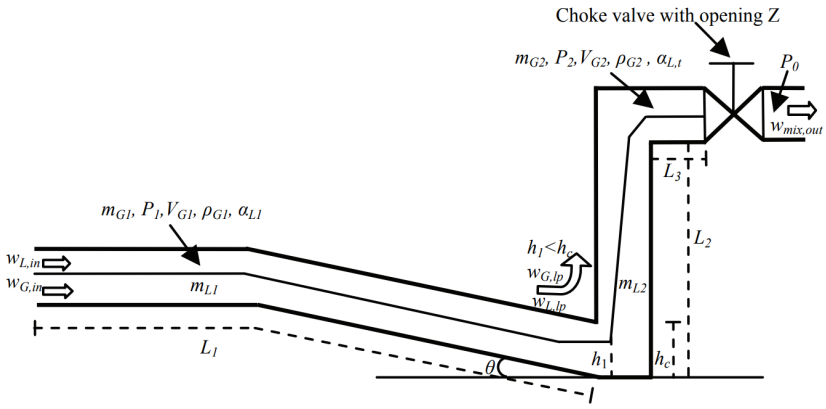

Figure 3.2: Simplified representation of desired flow regime [32]

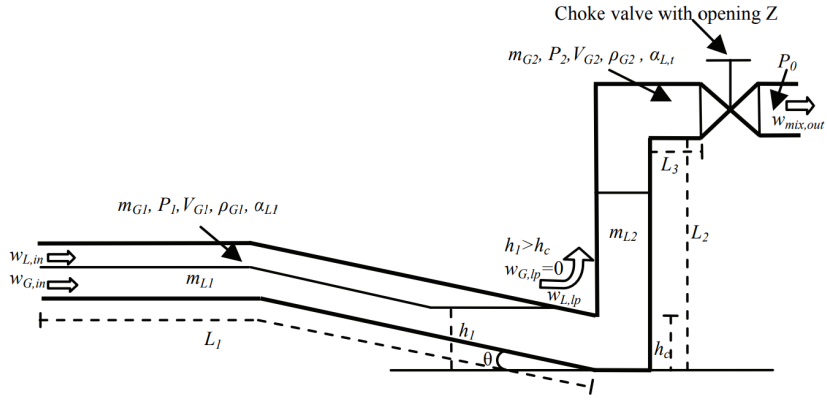

Figure 3.3: Simplified representation of liquid blocking leading to riser slugging [32]

Volume occupied by gas in the pipeline:

$$V_{G1} = V_1 - m_{L1}/\rho_L \tag{3.28}$$

Gas density in pipeline:

$$\rho_{G1} = \frac{m_{G1}}{V_{G1}} \tag{3.29}$$

Pressure in pipeline assuming ideal gas:

$$P_1 = \frac{\rho_{G1} R T_1}{M_G} \tag{3.30}$$

3.2.5.3 Riser Model

As shown from Figure 3.2 and Figure 3.3, the total volume of riser:

$$V_2 = \pi r_2^2 (L_2 + L_3) \tag{3.31}$$

Volume occupied by gas in riser:

$$V_{G2} = V_2 - m_{L2}/\rho_L \tag{3.32}$$

Density of gas at top of the riser:

$$\rho_{G2} = \frac{m_{G2}}{V_{G2}} \tag{3.33}$$

Pressure at top of riser form ideal gas law:

$$P_2 = \frac{\rho_{G2} R T_2}{M_G} \tag{3.34}$$

Average liquid volume fraction in riser:

$$\overline{\alpha}_{L2} = \frac{m_{L2}}{V_2 \rho_L} \tag{3.35}$$

Average density of mixture inside riser:

$$\overline{\rho}_m = \frac{m_{G2} + m_{L2}}{V_2} \tag{3.36}$$

3.2.5.4 Gas Flow at the Low-Point

As shown in Fig. 3.3, when the liquid level in the pipeline Section is above the critical level ($h_1 > h_c$), liquid blocks the low-point and the gas flow rate $w_{G,lp}$ at the low-point is zero.

$$w_{G,lp} = 0, h_1 \geq h_c \tag{3.37}$$

When the liquid is not blocking at the low-point ($h_1 < h_c$ in Figure 3.2), the gas will flow from volume V_{G1} to V_{G2} with a mass rate $w_{G,lp}$ [kg/s]. From physical insight, the two most important parameters determining the gas rate are the pressure drop over the low-point and the opening area. This suggests that the gas transport could be described by a "orifice equation", where the pressure drop is driving the gas through a "orifice" with opening area of A_G [52]:

$$w_{G,lp} = K_G A_G \sqrt{\rho_{G1} \Delta P_G}, h_1 < h_c \tag{3.38}$$

Since there's no pipe friction in Dymola, ΔP_G becomes:

$$\Delta P_G = P_1 - P_2 - \overline{\rho}_m g L_2 \tag{3.39}$$

3.2.5.5 Liquid Flow Model at the Low-Point

The liquid mass flow rate at the low-point can also be described by an orifice equation:

$$w_{L,lp} = K_L A_L \sqrt{\rho_L \Delta P_L}, \tag{3.40}$$

in which:

$$\Delta P_L = P_1 + \rho_L g h_1 - P_2 - \overline{\rho}_m g L_2 \tag{3.41}$$

Storkaas and Skogestad [55] proposed a model where the free area for gas flow is calculated precisely using some trigonometric functions. For the sake of simplicity, a quadratic approximation is used in this model.

$$A_G \cong \pi r_1^2 (\frac{h_c - h_1}{h_c})^2, h_1 < h_c \tag{3.42}$$

$$A_L = \pi r_1^2 - A_G \tag{3.43}$$

3.2.5.6 Phase Distribution Model at the Riser Top

In order to calculate the mass flow-rate of the individual phases in the outlet model in equations 3.22 and 3.23, the mixture density at top of riser ρ_t, which is used in the phase distribution at top of the riser, must be known.

Liquid mass fraction at the riser top is:

$$\alpha_{Lm,t} = \frac{\alpha_{L,t}\rho_L}{\alpha_{L,t}\rho_L + (1-\alpha_{L,t})\rho_{G2}} \tag{3.44}$$

Density of two-phase mixture at top of riser:

$$\rho_t = \alpha_{L,t}\rho_L + (1-\alpha_{L,t})\rho_{G2} \tag{3.45}$$

The liquid volume fraction at top of the riser, $\alpha_{L,t}$, can be calculated by the entrainment model proposed by Storkaas [55], but the entrainment equations are complicated and make the model very stiff. Instead of entrainment, a very simple relationship using some physical assumptions is proposed. We use the fact that in a vertical gravity dominant two-phase flow pipe there is approximately a linear relationship between the pressure and the liquid volume fraction. The gradient of pressure along the riser can be supposed to be constant for the desired smooth flow regimes. Because of the assumed linear relationship, the liquid volume fraction also maintains approximately a constant gradient along the riser for the stable flow regimes[32].

$$\frac{\partial \alpha_{L2}}{\partial y} = constant \tag{3.46}$$

This assumption suggests that the liquid volume fraction at middle of the riser is the average of the liquid volume fractions at the two ends of the riser. On the other hand, the liquid volume fraction at middle of the riser is approximately equal to the average liquid volume fraction in the riser given by equation 3.35. Therefore,

$$\overline{\alpha}_{L2} = \frac{\alpha_{L,lp} + \alpha_{L,t}}{2} \tag{3.47}$$

The liquid volume fraction at the bottom of riser, $\alpha_{L,lp}$, is determined by the flow area of the liquid phase at low-point:

$$\alpha_{L,lp} = \frac{A_L}{\pi r_1^2} \tag{3.48}$$

Therefore, liquid volume fraction at the top of the riser, $\alpha_{L,t}$, can be written as:

$$\alpha_{L,t} = 2\overline{\alpha}_{L,2} - \alpha_{L,lp} = \frac{2m_{L2}}{V_2\rho_L} - \frac{A_L}{\pi r_1^2} \tag{3.49}$$

3.2.6 Pipeline and Riser Model

The pipeline and riser models used in this thesis extends from a partial model which defines an interface for components with two multi-ports. The component may transport fluid and may have internal storage for a given fluid medium. They are modeled by Dynamic pipes, which is a base class for a dynamic two-phase pipe model with storage of mass and energy.

In Dymola, these pipes consist of a static pipe segment plus a n-node segment, which represents the dynamics. The models include balance equations for one-dimensional flow, meaning that all flow parameters may be expressed as a function of time and one space coordinate only (usually the measured distance along the path of the flowing fluid), for simplicity. No momentum balance is included, and the partial differential equations are treated with the finite volume method, which is a way of representing and evaluating these equations in the form of algebraic equations [20].

The pipe is split into n-nodes representing the dynamics, equally spread segments along the fluid path (n-nodes = n lumped mass and energy balances across the dynamic pipe). We have used n=10 nodes in our implemented systems. The following parts of this Section will cover the two elements that make the dynamic pipe segment: 1) The static pipe and 2) the node slip.

3.2.6.1 The Dynamics of the Static Pipe

The static part is a model of a straight pipe with constant cross Section and steady-state mass, momentum and energy balances. The fluid properties are taken using the instream operator on port a (inlet of the pipe), independent on the actual flow direction. Flow is assumed turbulent.

Static Pressure Drop

The pressure-drop driving the flow is the total pressure drop (pressure at port a – pressure at port b) minus the static pressure drop:

$$\mathrm{d}p = p_a - p_b - f_{grav} * \rho_{Mstatic} * g * h \tag{3.50}$$

where $\rho_{Mstatic}$ is the density of the fluid held up in the pipe, f_{grav} is a parameter to adjust the static pressure drop (default=1), g is the gravity and h is the height.

The static density is different from the flowing fluid because gas and liquid travels at different velocities, also called slip. The slip factor is defined as the liquid velocity divided by the gas velocity:

$$\alpha_{slip} = \frac{v_l}{v_g} \tag{3.51}$$

To calculate the density of the static fluid, the gas fraction of the static fluid must be calculated based on the slip factor. The mass fraction of gas, based on mass flow rates is:

$$x_G^m = \frac{w_G}{w_G + w_L} = \frac{\rho_G + v_G + A_G}{\rho_G + v_G + A_G + \rho_L + v_L + A_L} \tag{3.52}$$

resulting in:

$$x_G^m = \frac{1}{1 + (\rho_L + v_L + A_L)/(\rho_G + v_G + A_G)} = \frac{1}{1 + (v_L + x_L^a)/((v_G + x_G^a)} \tag{3.53}$$

where w_G,ρ_G,v_G,A_G is the mass flow, density, velocity and area of gas and x_G^a is the the mass fraction of gas at port a. w_L,ρ_L,v_L,A_L x_L^a is the corresponding relations for the liquid phase. This gives the following relationship between mass and area averaged mass fractions:

$$x_G^m = \frac{1}{1 + \alpha_{slip} * (\frac{1-x_G^a}{x_G^a})} \tag{3.54}$$

The relation between area-averaged mass fraction x_G^a ("holdup-fraction") and mass averaged fraction ("flow rate fraction") is given by eq:3.54.

To convert the mass fractions of gas at the flowing conditions and the static conditions, the following relations are derived. For correction, the gas mass fraction becomes:

$$\beta_G = \frac{x_G^m}{x_G^a} = \frac{1 - (1 - \alpha_{slip})x_G^m}{\alpha_{slip}} \tag{3.55}$$

where β_G is the mass fraction of gas with a correction factor due to slip.
And for correction, the liquid mass fraction becomes:

$$\beta_L = \frac{x_L^m}{x_L^a} = \frac{1 - x_G^m}{1 - (\frac{1}{\beta_G})x_G^m} \tag{3.56}$$

where β_L is the corresponding mass fraction of liquid, with a correction factor due to slip.

Fluid Properties

Garcia [20] uniformly describes the relation between mass flow and pressure drop in horizontal two-phase flow with the following formulation:

$$\dot{m}_{flow} = \frac{1}{4} R_e * \pi * D * \mu_L * (\frac{\rho_M}{\rho_L}) \tag{3.57}$$

where R_e is the Reynolds number, D is the pipe diameter. This can be rewritten into:

$$\dot{m}_{flow} = \frac{1}{4} R_e * \pi * D * \mu_M \tag{3.58}$$

where now:

$$\mu_M = \mu_L * (\frac{\rho_M}{\rho_L}) \tag{3.59}$$

where μ_M is the viscosity and ρ_M is the density of the mixture, while ρ_L and μ_L is the density and viscosity of the liquid.

3.2.6.2 The Dynamics of the Node Slip

The nodes are modeled as ideally mixed, simple fluid volumes with the ability to store mass and energy. With slip and slip factor as optional inputs. The nodes contain information about the internal energy and mass of the fluid. It also contains information about mass flow, substance mass flow, enthalpy flow, heat flow and work flow across

the boundaries. The mass flow rate and the substance flow-rate are adjusted to avoid negative fractions inside the volume.

Extended classes of mass fractions and specific enthalpy of the outflowing media, variables for extra mass flow and enthalpy and extra component mass flow can be specified and used.

The outflow enthalpy and outflow mass fractions are set according to equations for slip flow. The mass fractions of the medium flowing out of the node are different from the medium inside the node because the gas and liquid flows are different. The equations are:

$$\beta_G = \frac{1}{X_{nodeG} * (1 - slip) + slip} \tag{3.60}$$

$$\beta_L = \frac{1 - \beta_G * X_{nodeG}}{1 - X_{nodeG}} \tag{3.61}$$

where β_G and β_L are the mass fractions of gads and liquid with a correction factor due to slip. X_{nodeG} is the mass fraction of gas, which equals the mass fraction of gas contained in the node. Slip is a parameter which is the liquid to gas velocity. The outflowing mass fractions are modified to:

$$X_{flowG} = \beta_G * X_{nodeG} \tag{3.62}$$

$$X_{flowL} = \beta_L * X_{nodeL} \tag{3.63}$$

where X_{flowG} and X_{flowL} is the outflowing mass fractions of gas and liquid, while X_{nodeG} and X_{nodeL} is the mass fractions of gas and liquid, contained in the node. The specific enthalpy (internal energy plus the product of its pressure and volume) of the outflowing media is set such that the temperature of the outflowing media equals the media in the node.

3.3 The Implemented Systems

This Section will briefly look at and explain the implemented systems in Dymola.

3.3.1 Riser-Slug System

Based on Jahanshahi's pipeline-riser model[32], we wanted to create a similar case of severe slugging in a pipeline-riser system with the geometry as shown their OLGA test case (Figure 3.4), and then use that model to create terrain-induced well-slugging.

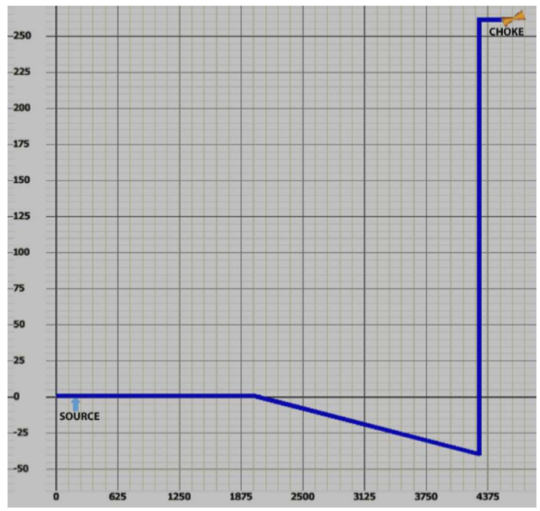

Figure 3.4: Geometry of OLGA pipeline-riser test case [32]

This OLGA test case reference model presented a typical(yet simple) riser slugging problem. As shown in Figure 3.4, the lenght of the pipeline is 4300m. Starting from the inlet, the first 2000m of the pipeline is horizontal and the remaining 2300m inclines downward with a 1° angle. This gives rise to a 40.14m descent and creates a low point at the end of the pipeline. The pipeline diameter is 0.12m. The riser is a vertical 300-m pipe with a diameter of 0.1m. A 100m horizontal Section with the same diameter as that of the riser connects the riser to the outlet choke valve. The feed into the OLGA reference model system is nominally constant at 9 kg/s with $(w_L)_{in}$= 8.64kg/s (oil) and $(w_G)_{in}$=0.36kg/s (gas). The separator pressure (P_s)=50.1bar[32].

In Dymola, we created a similar system, using the riser-slug model from the Subpro library, as shown in Figure 3.5.

The system shown in Figure 3.5 consists of a reservoir model representing the source, a productivity index model to give the correct inflow-performance to the pipeline, a

riser-slug model, a topside choke valve model and a pressure boundary representing a constant separator pressure. There are also multi-phase-metering- and pressure- sensors to measure both flow-rate and pressure both upstream and downstream the riser-slug model.

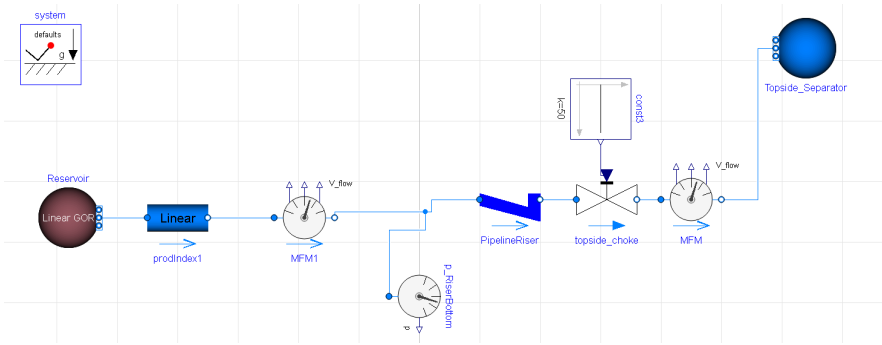

Figure 3.5: Illustration of the riser-slug system in Dymola

The OLGA reference model by Jahanshahi[32] doesn't take into account water production from the reservoir, but the parameters we choose were able to give a steady-state mass flow behaviour as shown in Figure 3.6. He uses a mass gas-oil-ratio (GOR), while Dymola specifies GOR as the standard gas volume to the oil volume(explained in Section 3.2.1). All parameters are shown in table 3.1. The Riser-base pressure is shown in Figure 3.7. As we can see from Figure 3.6, the flow-rate into our pipeline-riser system is a little lower than in the OLGA reference model case [32], but we were able to create riser-slugging at low flow-rates and pressure, using the productivity index model with a 32bar pressure drop(dp_{nom}), to fit the reservoir model with a higher initial pressure.

In table 3.1, the first Section is the reservoir model. The second Section is the productivity index model, third- is the riser-slug model, while the forth and fifth are the choke valve- and topside boundary- models.

The Liquid and gas fractions at the low-point in the pipeline are shown in Figure 3.8. The red values represents the liquid-, and the blue values represents the gas- accumulation in the low-point of the pipeline during a time interval of 50000s (14 hours). Figure 3.8 clearly shows the steps of the severe slugging phenomenon as explained in Section 2.3.1.5.The blue values represent gas fraction and the red values, the corresponding liquid fractions in the low-point of the pipeline. When there is no gas(blue values

Symbol	Description	Values	Units
Pres	initial Reservoir pressure	100	bar
Tres	initial Reservoir temperature	337	K
MM_{gas}	Molecular mass, gas	20E-3	Kg/mol
MM_{oil}	Molecular mass, oil	400E-3	Kg/mol
WC	Water cut	0.4	H2O/liq.(m^3/m^3)
GOR_0	0-Production GOR	100	-
GOR_n	Nominal GOR	100	-
$w_{oil,0}$	0-prod. limit, oil	10	Kg/s
$w_{oil,n}$	Nominal prod., oil	15	Kg/s
dp_{nom}	Nominal pressure drop	32	Bar
w_{nom}	Nominal mass flow-rate	7.5	Kg/s
θ	pipe inclination	1	°C
T_{pipe}	Temperature at pipe inlet	337	K
T_{riser}	Temperature at riser inlet	298.3	K
$slip_{pipe}$	Slip factor pipe	1.1	v_L/v_g
$slip_{riser}$	Slip factor riser	0.5	v_L/v_g
L_{pipe}	Pipe lenght along seabed	4300	m
L_{riser}	Riser lenght	300	m
H_{riser}	Riser height(port b-port a)	300	m
D	Diameter of pipe	0.12	m
K_H	Coeff. liq. level in pipeline	0.7	-
K_L	Coeff. liq. level through lowpoint	9/sqrt(5e5*900)	-
K_G	Coeff. gas flow through lowpoint	K_L	-
C_v	choke-valve flow coeff.	200	USG/min
P_{sep}	Pressure boundary topside	50.1	bar
T_{sep}	Temperature boundary topside	285	K

Table 3.1: Parameters of the Riser-slug system in Dymola

are 0), the low-point is full of liquid(the red values equal 1). Then gas starts to build-up pressure, while the liquid values are decreasing. At some point, when the pressure is high enough, the gas pushes the liquid out of the riser (red values are at their bottom values). Then the cycle repeats.

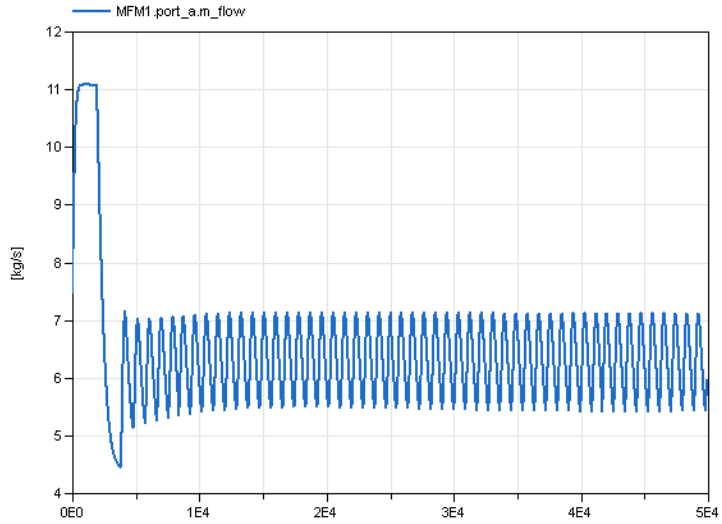

Figure 3.6: Mass flow-rate into the pipeline in the riser-slug model in Dymola

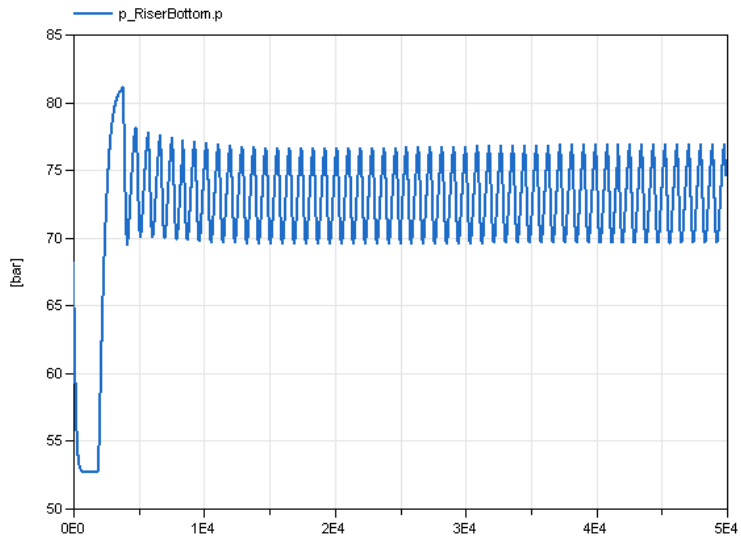

Figure 3.7: Riser Bottom Pressure in the riser-slug model in Dymola

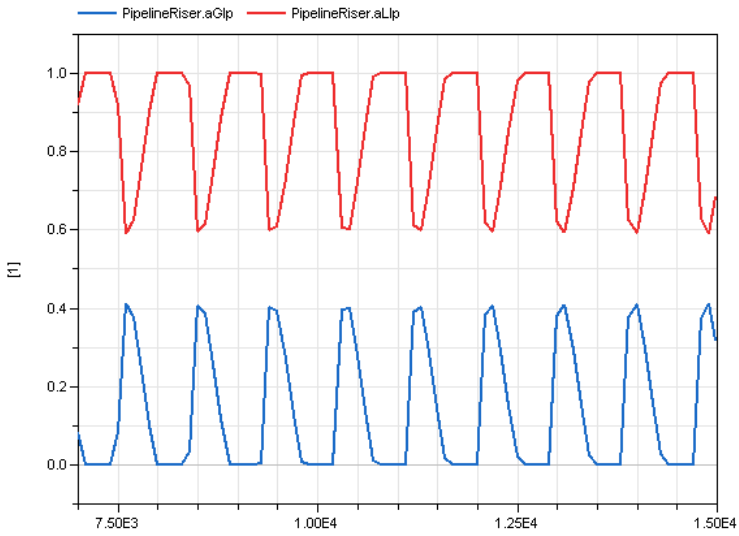

Figure 3.8: Gas and Liquid area fractions in the Low-point of the pipeline

3.3.2 Well-Slug Systems

The area fraction of gas and liquid in the low-point indicates terrain induced riser-slugging(explained in Section 2.3), and shown in Figure 3.8. This causes pressure fluctuations(Figure 3.7) and mass flow fluctuations (Figure 3.6). Using the same setup, we identified the factors in the model that created the slugging behaviour, and changed the geometry into three different well-systems as shown in Figure 3.9.

The obvious condition that changes when converting the riser-slug model into a well-slug model is the higher average pressure down-hole, as well as higher flow-rates of the different phases. Also, when considering that a well is closer to the reservoir, the capacity of the tubing at the bottom hole is generally smaller than the capacity of the pipeline. Therefore, severe slugging at the bottom of the well-bore is less likely to occur[40]. Terrain-induced slugging in the low-point of the well-bore has been concluded to be a rare phenomenon. The casing-heading mechanism (Section 2.3.1.3) and the density-wave instability (Section 2.3.1.4) is more likely to occur, but it has also been proven numerically that severe slugging may happen in the bottom of a well-bore in a horizontal well with extended reach geometry[40].

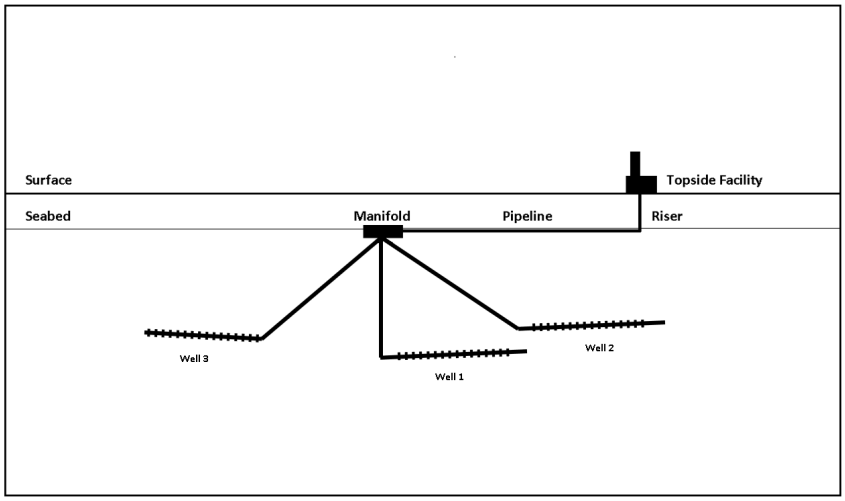

Figure 3.9: Simple illustration of the three different wells together in an integrated system

By using the working riser-slug model in Figure 3.5, we moved that model downhole. By adding a pipeline model, a riser model and another choke valve model, we obtained more complex system dynamics, that describe an offshore production system. To compensate for the initial pressure increase and geometry changes, the conditions that needed to be manipulated were:

- Inflow-conditions through the productivity index model
- Slip-factor in the pipeline/riser Section of the well-slug model
- Water-cut in the reservoir model
- GOR in the reservoir model

The resulting three wells are all deviations from the pipeline-riser model[32]. All reservoirs are modelled as near-wellbore reservoirs as shown in Figure 3.9. The first well (Well 1) is the closest in terms of geometry, but the vertical Section is made significantly higher. The second well (Well 2) is the one that deviates the most from the pipeline-riser geometry, looking more like the extended-reach well in [40]. The third well (Well 3) has a geometry, which does not deviate as much from the pipeline-riser model[32] as the

well-2 system. All wells are shown in Figure 3.9 and will be explained in more detail in the following Sections.

The well- and reservoir conditions are made different for each well, but every well is considered to have a significant amount of gas through a high Gas-Oil-Ratio (GOR). The medium: **ThreePhaseStatoil** contains oil, gas and water, explained in Section 3.2.2, implemented in all systems.

Every well is connected to the same type of pipeline-riser system, as well as the same type of topside choke-valve and a pressure boundary. These components yield the same properties, diameter and geometries for all systems, because the three well-systems are later connected in an integrated 3-well system, explained in Section 3.3.3.

The pipeline for all systems is horizontally laid on the seafloor, 3000m long with a diameter of 0.28m. The height difference between the outlet (port b) and the inlet (port a) is -100m, yielding a slightly defined low-point at the end of the pipeline. The riser is a 300m long, vertical pipe with a diameter of 0.28m, and the topside pressure boundary is set at a constant of 30 bar (separator pressure). The parameters and values for the pipeline model, riser model, choke valve models and the topside boundary model, which is the same for all systems, is given in table 3.2.

Symbol	Description	Values	Units
L_{pipe}	Lenght of the pipeline	3000	m
D_{pipe}	Diameter of the pipeline	0.28	m
ϵ_{pipe}	roughness of the pipeline	2.5e-5	m
$slip_{pipe}$	Slip factor pipeline	1.4	v_L/v_g
H_{pipe}	Pipeline height(port b-port a)	-100	m
$T_{a,start,pipe}$	Initial Temperature at pipe inlet(port a)	337	K
$T_{b,start,pipe}$	Initial Temperature at pipe outlet(port b)	300	K
$P_{a,start,pipe}$	Initial Pressure at pipe inlet(port a)	60	bar
$P_{b,start,pipe}$	Initial Pressure at pipe outlet(port b)	40	bar
L_{riser}	Length of the riser	300	m
D_{riser}	Diameter of the riser	0.28	m
ϵ_{riser}	roughness of the riser	2.5e-5	m
$slip_{riser}$	Slip factor riser	0.7	v_L/v_g
H_{riser}	Riser height(port b-port a)	300	m
$T_{a,start,riser}$	Initial Temperature at riser inlet(port a)	300	K
$T_{b,start,riser}$	Initial Temperature at riser outlet(port b)	285	K
$P_{a,start,riser}$	Initial Pressure at riser inlet(port a)	40	bar
$P_{b,start,riser}$	Initial Pressure at riser outlet(port b)	30	bar
C_{v1}	Prod.choke valve flow coeff.	200	USG/min
C_{v2}	Topside choke valve flow coeff.	200	USG/min
P_{sep}	Pressure boundary topside	30	bar
T_{sep}	Temperature boundary topside	285	K

Table 3.2: Parameters of the pipeline and riser model, choke valve models and the topside boundary model of the separated well 1,2,3 systems and the integrated 3-well system, implemented in Dymola

3.3.2.1 Well 1

This well is the deepest of the three wells, drilled 2600m vertically, then horizontal with a 1 degree inclination for 3000m as illustrated in Figure 3.9. The well geometry is shown in Figure 3.10. Figure 3.11 shows the system implemented in Dymola. In the creation process of this well, the goal was to match the inflow conditions in Jahanshahi's pipeline-riser model[32] as good as possible. We've focused on the mass fraction of the

different phases, the total mass flow, Bottom-Hole Pressures and area-fractions of gas and liquid in the low-point of the well to present key aspects to optimal production and the slugging behavior.

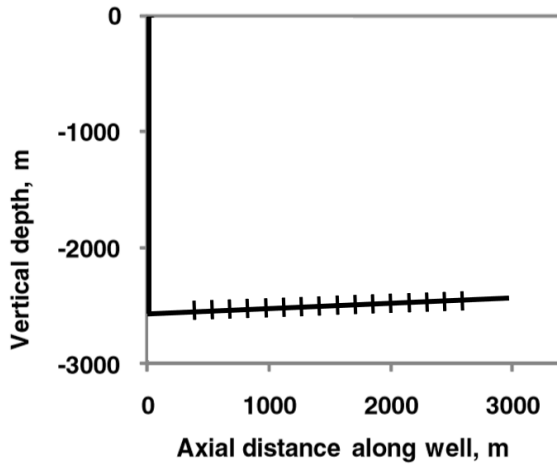

Figure 3.10: Geometry of the well-1 system

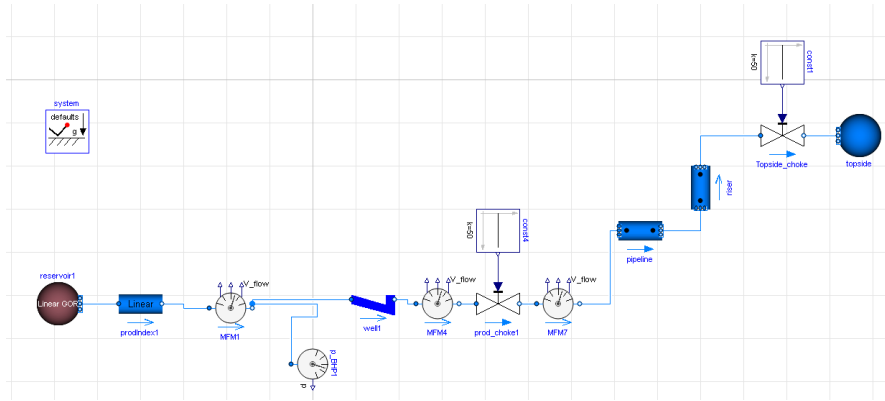

Figure 3.11: Well 1 system, implemented in Dymola

The reservoir model in this system has an initial reservoir pressure at 350bar, which, because of the depth, is the highest of the three well-systems. The boundary Water cut in the reservoir is 0.4, defined as the volume of H2O divided by the volume of liquid

(m^3/m^3). The gas-oil-ratio (GOR) (explained in Section 3.2.1) is 100, indicating that it's a gas well, which is the case for all the wells. The well-slug model has a diameter of 0.12m in both the horizontal and vertical Section. Initially, as shown in Figure 3.11, the valve openings of both the production choke(Z_1) and the topside choke(Z_2) are set to a constant opening of 50%, yielding slugging behaviour. The bifurcation diagram of well 1 is shown in Figure 3.12.

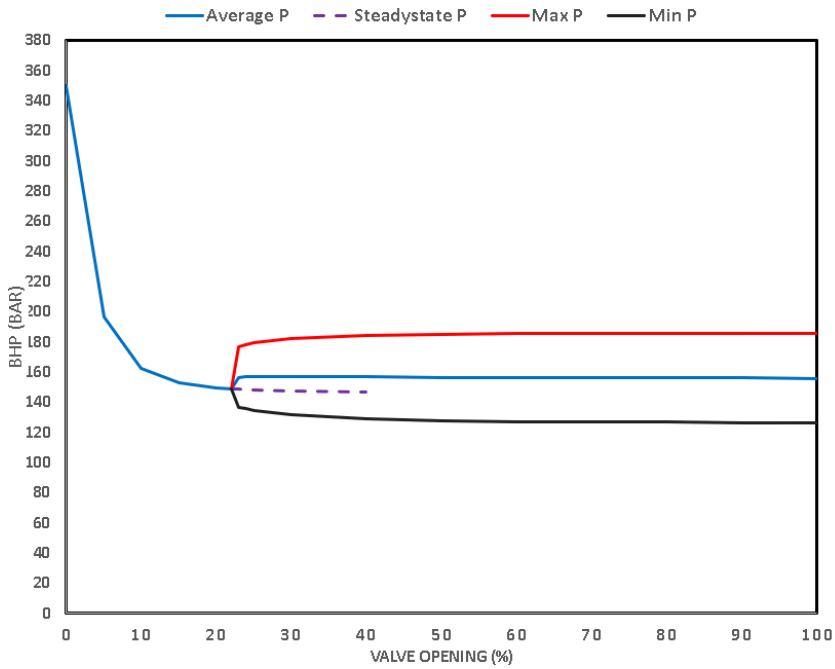

Figure 3.12: Bifurcation diagram of Well 1

This diagram shows the behaviour of the Bottom-Hole Pressure (BHP), over the whole working range of the production choke valve[56]. The critical value of the relative valve opening of the production choke valve for the transition between a stable non-oscillatory flow regime and riser-slugging in the well is Z_1=23%. In Figure 3.12, the red line represents the max value of the pressure oscillations and the black line is the corresponding min value, for valve openings larger than 23%. The blue line is the average pressure and the purple line is the steady-state pressure.

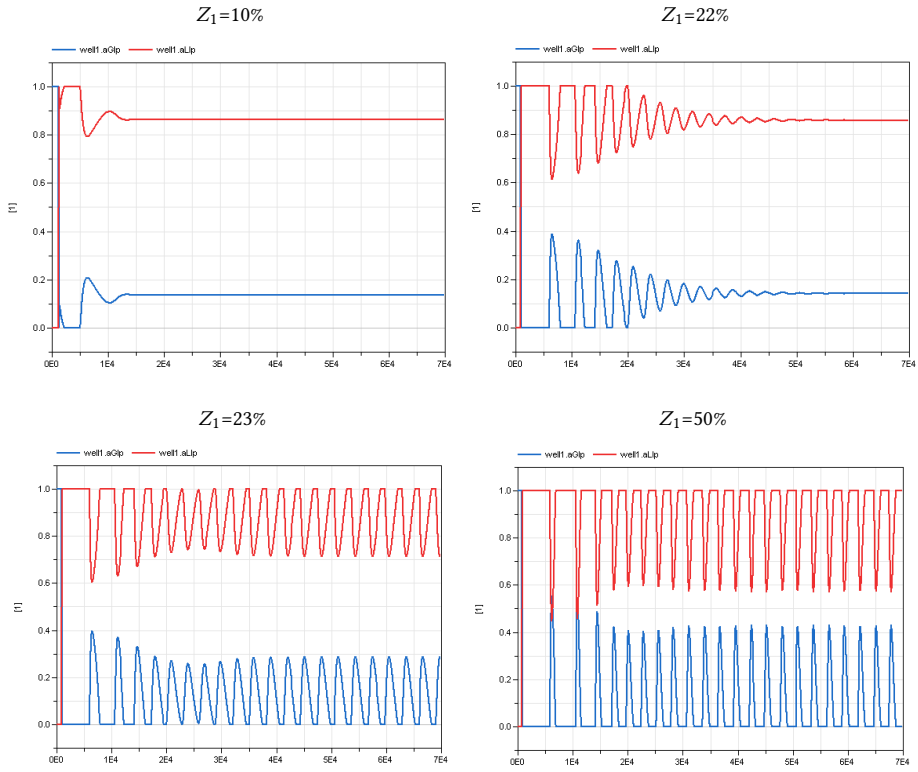

Figure 3.13: Gas and Liquid area fractions in the Low-point of well 1 for different valve openings

The multi-phase metering sensor (MFM1) bottom-hole in Figure 3.11 gives us all the necessary information about the inflow performance to the well, like total mass flow, pressure, volume flow, densities and mass fractions. At valve opening Z_1=22%, the system is in a no-slug regime, without any steady-state gas and liquid accumulation in the low-point of the well, as shown in Figure 3.13. At Z_1=23%, the liquid starts to accumulate, and at Z_1=50%, the liquid slugs are longer and more severe.

Figure 3.14 shows the system response between a no-slug regime(Z_1=22%) and the critical valve opening (Z_1=23%) down-hole. As we can see, the productivity index model regulates the inflow-performance of the well, generating a constant mass flow of oil, gas and water w_{in}=8.03kg/s in a no-slug scenario (Z_1=22%).

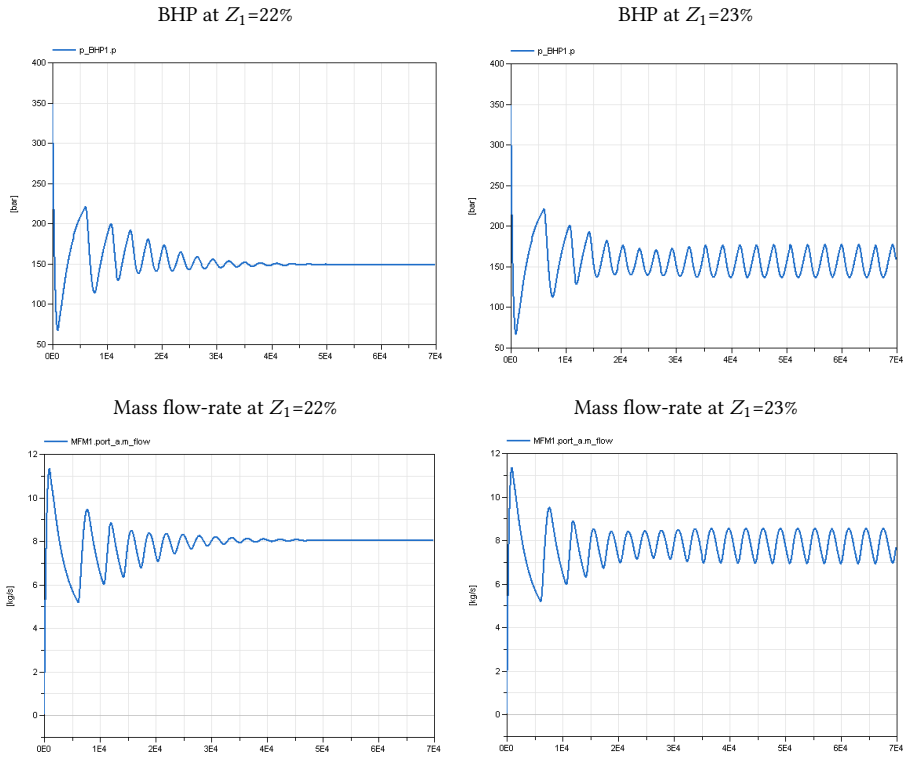

Figure 3.14: Simulations of Well 1, showing BHP(bar) and mass flow-rate(kg/s) for different valve-openings

The periodic time of the oscillations (from top to top) provides information about the frequency of the system response, which is the same for each valve opening. By looking at Figure 3.15, taking a steady-state time interval with a valve opening Z_1=50%, we get a periodic time of the oscillations, T=2800s. Since the frequency is the inverse of the periodic time, this becomes f=1/2800=3.571428e-4 Hz (1/s).

The mass fractions measured on the multi-phase-metering sensor (MFM1) are shown in Figure 3.16. The mass fraction of oil is 0.545, water is 0.404 and gas is 0.051.

Figure 3.17 shows the mass flow-rate measurements down-hole vs topside for two different valve openings in the slug-regime, where the red line is the bottom-hole measurement and the blue line represents the topside measurement. The responses of

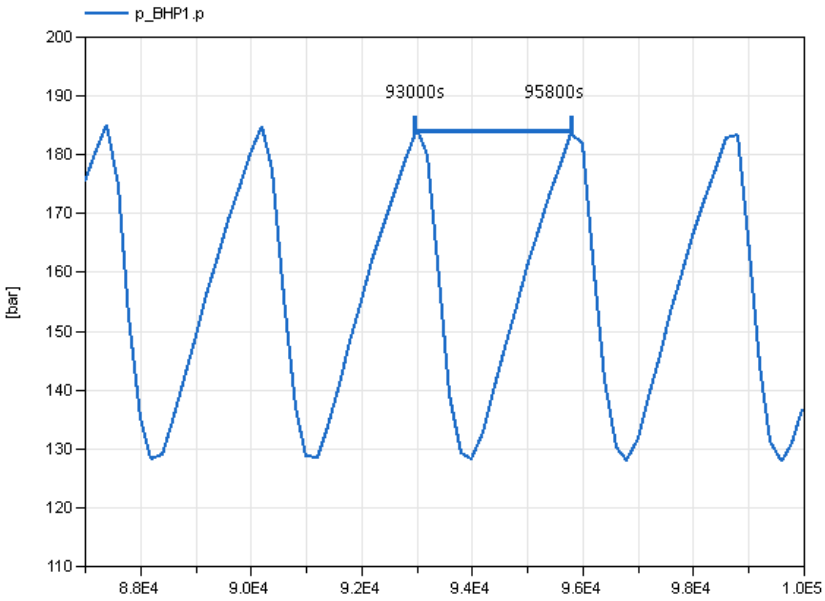

Figure 3.15: Period time of the pressure oscillations bottom-hole of well 1

both valve openings indicate that riser-slugging bottom-hole has a significantly bad influence on the topside mass flow-rate, which is undesirable.

The numerical values for all parameters of the Reservoir model, productivity index model and the well-slug model are given in table 3.3.

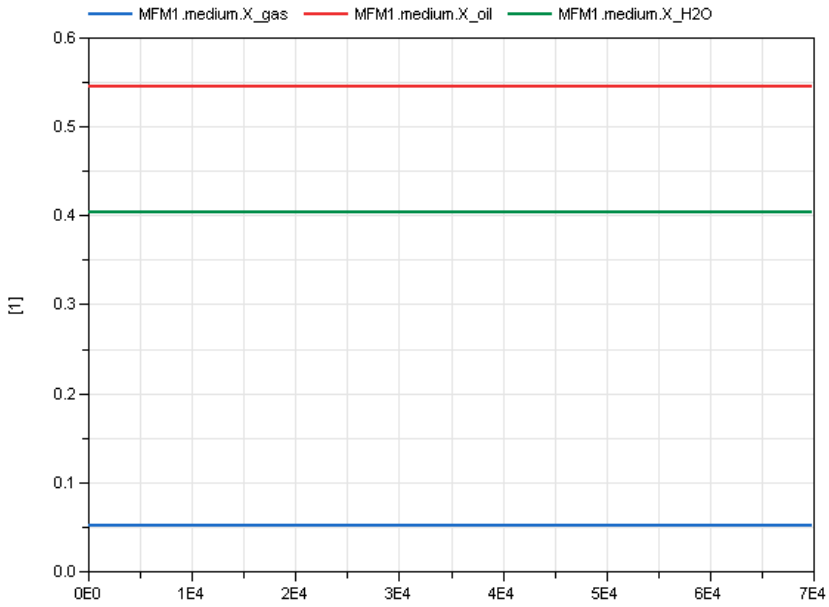

Figure 3.16: Mass fractions bottom-hole for Well 1

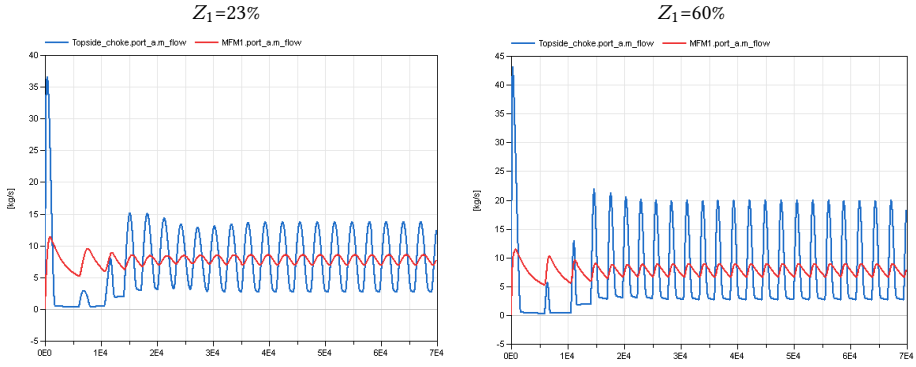

Figure 3.17: Bottom-hole measurements vs topside measurements of massflow-rate at different valve openings in the Well 1 system.

Symbol	Description	Values	Units
Pres	Reservoir pressure	350	bar
Tres	Reservoir temperature	378	K
MM_{gas}	Molecular mass, gas	20e-3	Kg/mol
MM_{oil}	Molecular mass, oil	400e-3	Kg/mol
WC	Water cut	0.4	H2O/liq.(m^3/m^3)
GOR_0	0-Production GOR	100	-
GOR_n	Nominal GOR	100	-
$w_{oil,0}$	0-prod. limit, oil	10	Kg/s
$w_{oil,n}$	Nominal prod., oil	15	Kg/s
dp_{nom}	Nominal pressure drop	1	Bar
w_{nom}	Nominal mass flow-rate	0.04	Kg/s
θ	pipe inclination	1	°C
T_{pipe}	Temperature at pipe inlet	378	K
T_{riser}	Temperature at riser inlet	350	K
$P_{start,pipe}$	Initial Pressure at pipe inlet	349	bar
$P_{start,riser}$	Initial Pressure at riser inlet	280	bar
$slip_{pipe}$	Slip factor pipe	2.7	v_L/v_g
$slip_{riser}$	Slip factor riser	0.9	v_L/v_g
L_{pipe}	Pipe lenght along seabed	3000	m
L_{riser}	Riser lenght	2600	m
H_{riser}	Riser height(port b-port a)	2600	m
D	Diameter of pipe	0.12	m
K_H	Coeff. liq. level in pipeline	0.7	-
K_L	Coeff. liq. flow through lowpoint	4.24e-4	-
K_G	Coeff. gas flow through lowpoint	K_L	-

Table 3.3: Parameters of the Reservoir model, productivity index model and well-slug model of Well 1 implemented in Dymola

3.3.2.2 Well 2

As mentioned in Section 3.3.2, the well-2 system is the one with the geometry closest to the one tested numerically in [40]. The geometry of this well is shown in Figure 3.18. It was made for the purpose of being close to a realistic extended-reach-horizontal well. The geometry of this well is a 3000m horizontal section and a 3000m vertical Section. The horizontal section has got a 1 degree inclination angle along the seabed. The height difference between the output and input of the vertical Section is 2000m, yielding a significant deviation from the vertical. The implementation in Dymola can be seen in Figure 3.19.

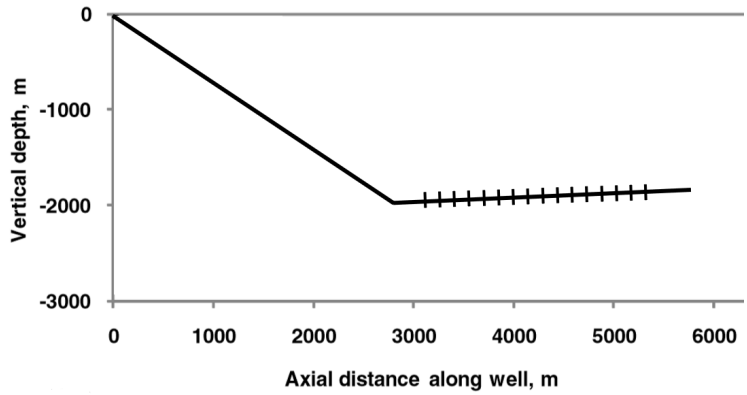

Figure 3.18: Geometry of the well-2 system

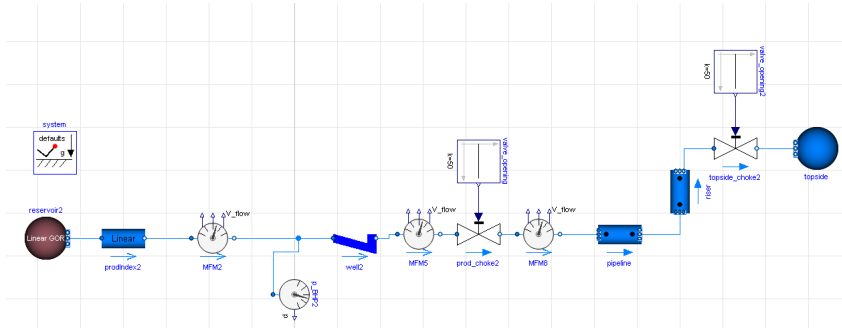

Figure 3.19: Well 2 system, implemented in Dymola

The reservoir model in this system has an initial reservoir pressure at 280 bar, which is lower than Well 1, because of the depth. The boundary water-cut is 0.55 and the gas-oil-ratio (GOR) is 90. The well-slug model has a diameter of 0.089m in both the horizontal and vertical section. The bifurcation diagram of well 2 is shown in Figure 3.20

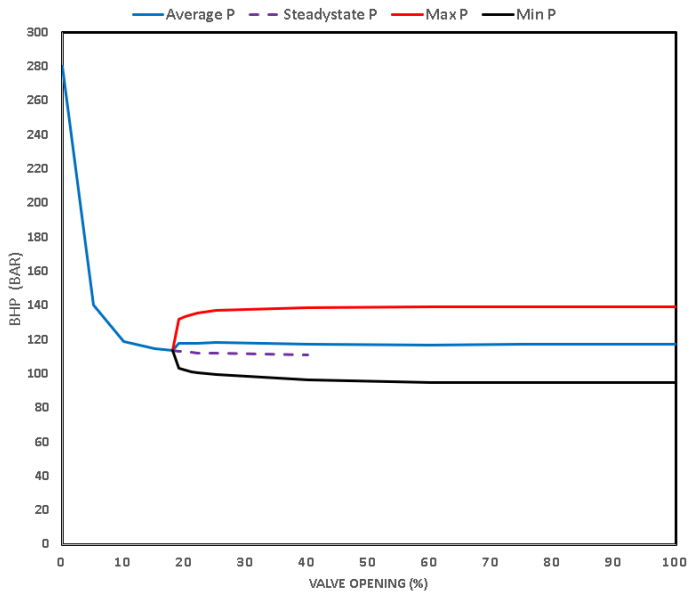

Figure 3.20: Bifurcation diagram of Well 2

The critical value of the relative valve opening of the production choke valve for the transition between a stable non-oscillatory flow regime and riser-slugging is Z_1=19% for this well. In Figure 3.20, we can see that pressure oscillations in the BHP goes from 95 bar, all the way up to 140 bar. At valve opening Z_1=18%, the system is in a no-slug regime, without any steady-state gas and liquid accumulation in the low-point of the well, as shown in Figure 3.21. At Z_1=19%, the liquid starts to accumulate and at Z_1=50%, the liquid slugs are longer and more severe.

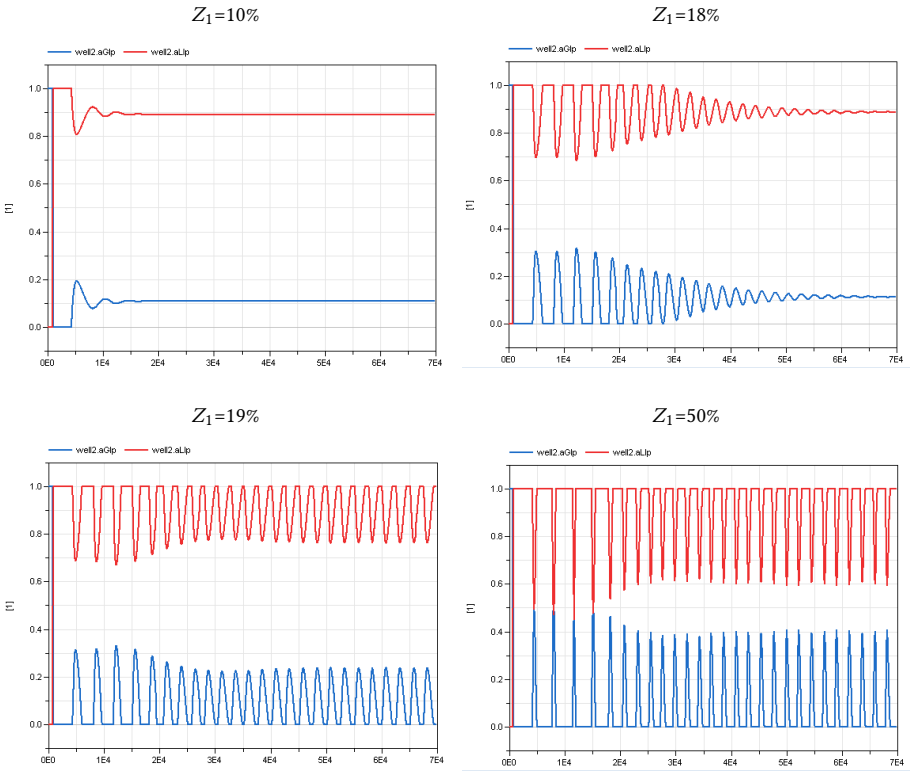

Figure 3.21: Gas and Liquid area fractions in the Low-point of Well 2 for different valve openings

Figure 3.22 shows the system response between a no-slug regime(Z_1=18%) and the critical valve opening (Z_1=19%) down-hole. The productivity index model regulates the inflow-performance of the well, generating a constant mass flow of oil, gas and water w_{in}=6.65kg/s in a no-slug scenario (Z_1=18%).

The periodic time of the oscillations (from top to top) is shown in Figure 3.23. By looking at a steady-state time interval with a valve opening Z_1=50%, we get a periodic time of the oscillations, T=2200s. The frequency becomes f=1/2200=4.5454e-4 Hz (1/s).

The mass fractions measured on the Bottom-hole sensor(MFM2) are shown in Figure 3.24. The mass fraction of oil is 0.41, water is 0.55 and gas is 0.034.

Figure 3.25 shows the mass flow-rate measurements down-hole vs topside for two

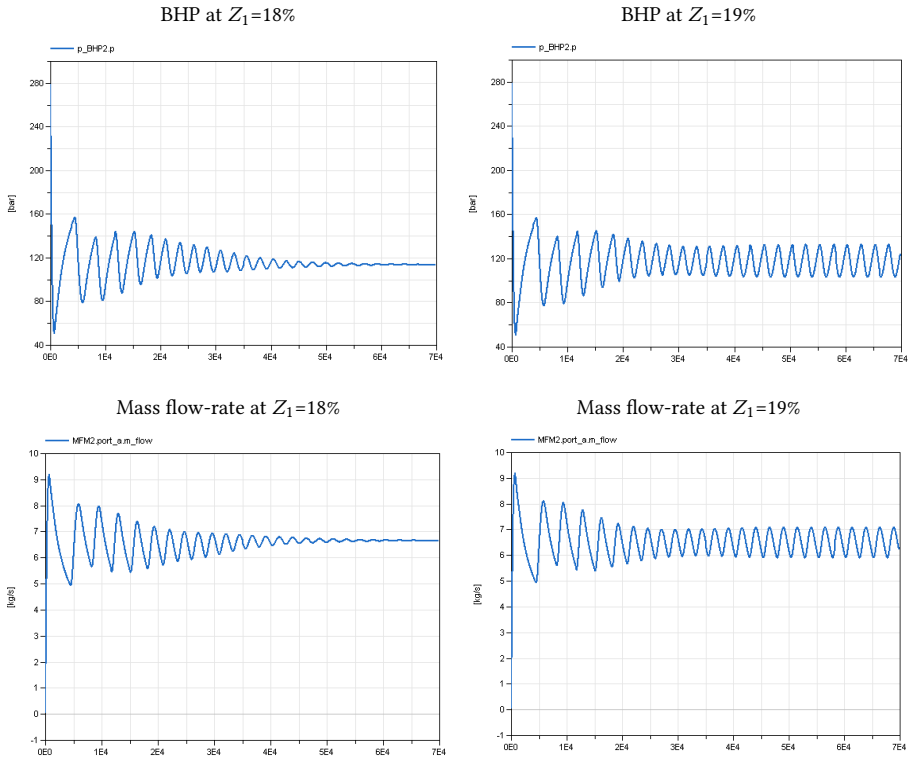

Figure 3.22: Simulations of Well 2, showing BHP(bar) and mass flow-rate(kg/s) for different valve-openings

different valve openings in the slug-regime, where the red line is the bottom-hole measurement and the blue line represents the topside measurement. Te responses of both valve openings indicate that riser-slugging bottom-hole has a significantly bad influence on the topside mass flow-rate, which is undesirable. The numerical values for all parameters of the Reservoir model, productivity index model and the well-slug model are given in table 3.4.

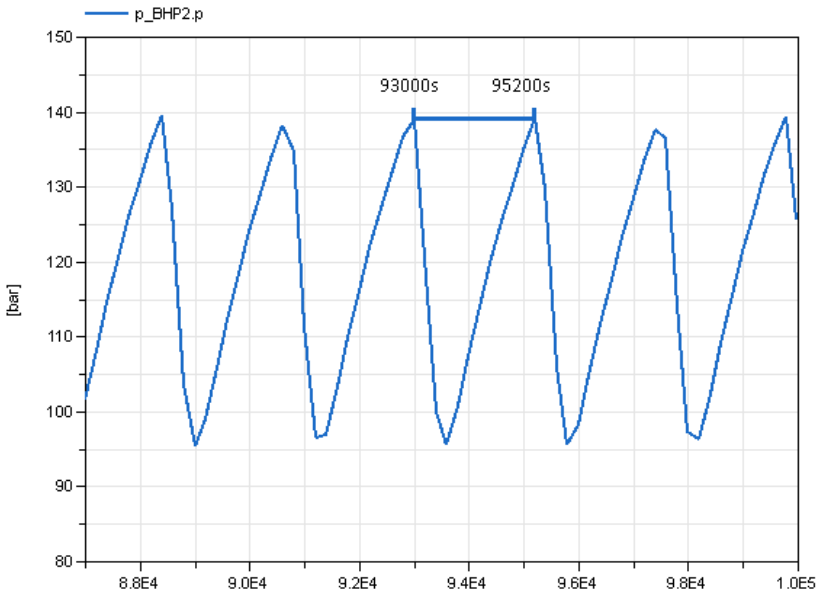

Figure 3.23: Period time of the pressure oscillations bottom-hole of well 2

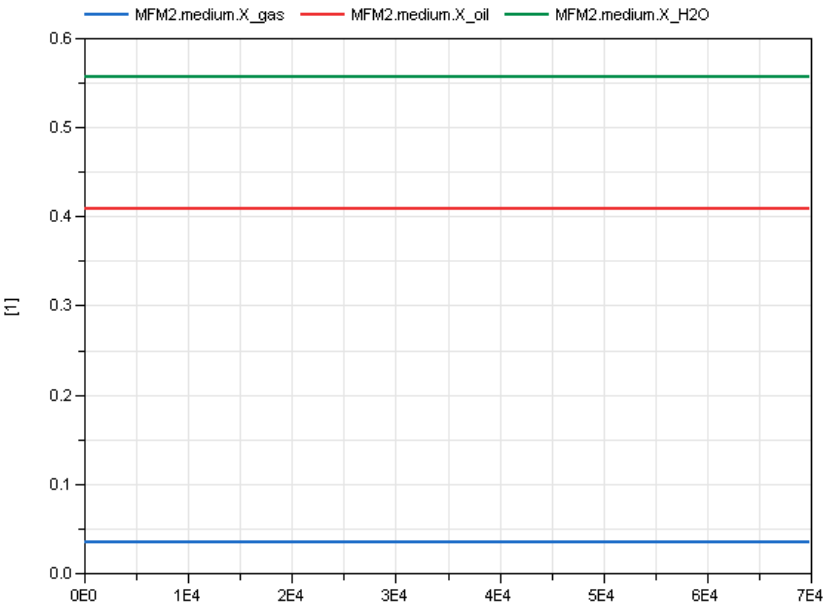

Figure 3.24: Mass fractions bottom-hole for Well 2

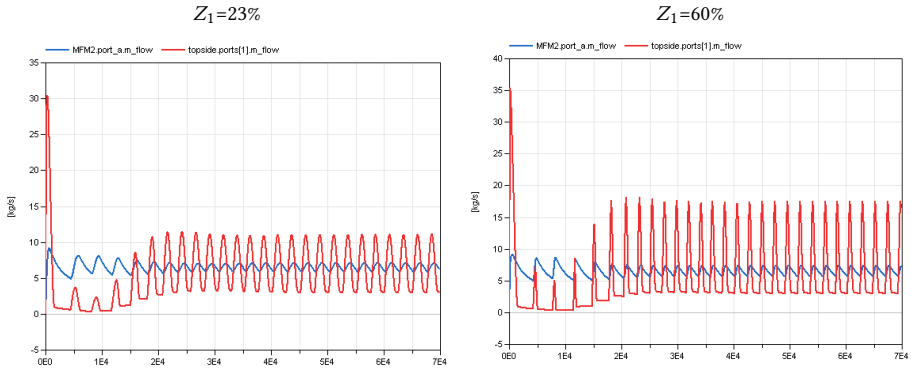

Figure 3.25: Bottom-hole measurements vs topside measurements of massflow-rate at different valve openings in the Well 2 system.

Symbol	Description	Values	Units
Pres	Reservoir pressure	280	bar
Tres	Reservoir temperature	378	K
MM_{gas}	Molecular mass, gas	20e-3	Kg/mol
MM_{oil}	Molecular mass, oil	400e-3	Kg/mol
WC	Water cut	0.55	H2O/liq.(m^3/m^3)
GOR_0	0-Production GOR	90	-
GOR_n	Nominal GOR	90	-
$w_{oil,0}$	0-prod. limit, oil	10	Kg/s
$w_{oil,n}$	Nominal prod., oil	15	Kg/s
dp_{nom}	Nominal pressure drop	1	Bar
w_{nom}	Nominal mass flow-rate	0.04	Kg/s
θ	pipe inclination	1	°C
T_{pipe}	Temperature at pipe inlet	378	K
T_{riser}	Temperature at riser inlet	350	K
$P_{start,pipe}$	Initial Pressure at pipe inlet	279	bar
$P_{start,riser}$	Initial Pressure at riser inlet	210	bar
$slip_{pipe}$	Slip factor pipe	4	v_L/v_g
$slip_{riser}$	Slip factor riser	1.9	v_L/v_g
L_{pipe}	Pipe lenght along seabed	3000	m
L_{riser}	Riser lenght	3000	m
H_{riser}	Riser height(port b-port a)	2000	m
D	Diameter of pipe	0.089	m
K_H	Coeff. liq. level in pipeline	0.7	-
K_L	Coeff. liq. flow through lowpoint	4.24e-4	-
K_G	Coeff. gas flow through lowpoint	K_L	-

Table 3.4: Parameters of the Reservoir model, productivity index model and well-slug model of Well 2 implemented in Dymola

3.3.2.3 Well 3

The geometry of this well is a 2400m long horizontal section and a 2600m vertical Section as shown in Figure 3.26. The horizontal section got a 1 degree inclination angle along the seabed. The height difference between the output and input of the vertical section is 2200m, yielding some deviation from the vertical. The implementation in Dymola can be seen in Figure 3.27

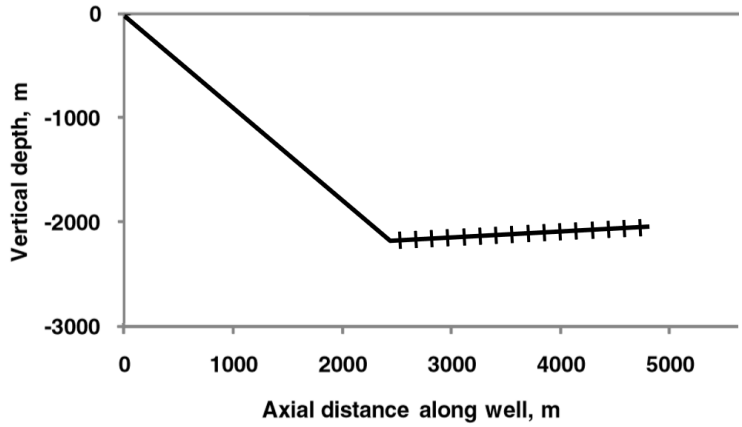

Figure 3.26: Geometry of the well-3 system

The reservoir model in this system has an initial reservoir pressure at 340 bar. The boundary water-cut is 0.65 and the gas-oil-ratio (GOR) is 180. The well-slug model has a diameter of 0.1m in both the horizontal and vertical section. The bifurcation diagram

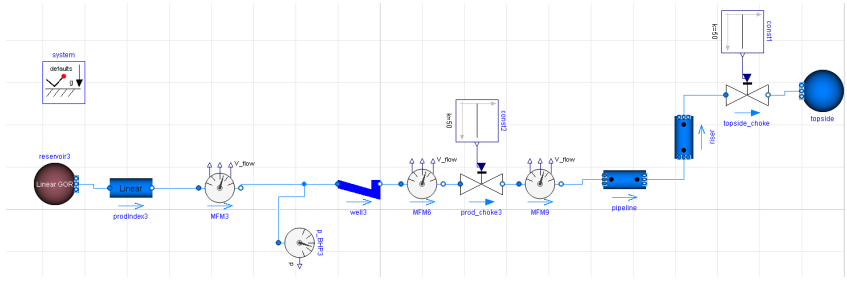

Figure 3.27: Well 3 system, implemented in Dymola

of well 3 is shown in Figure 3.28

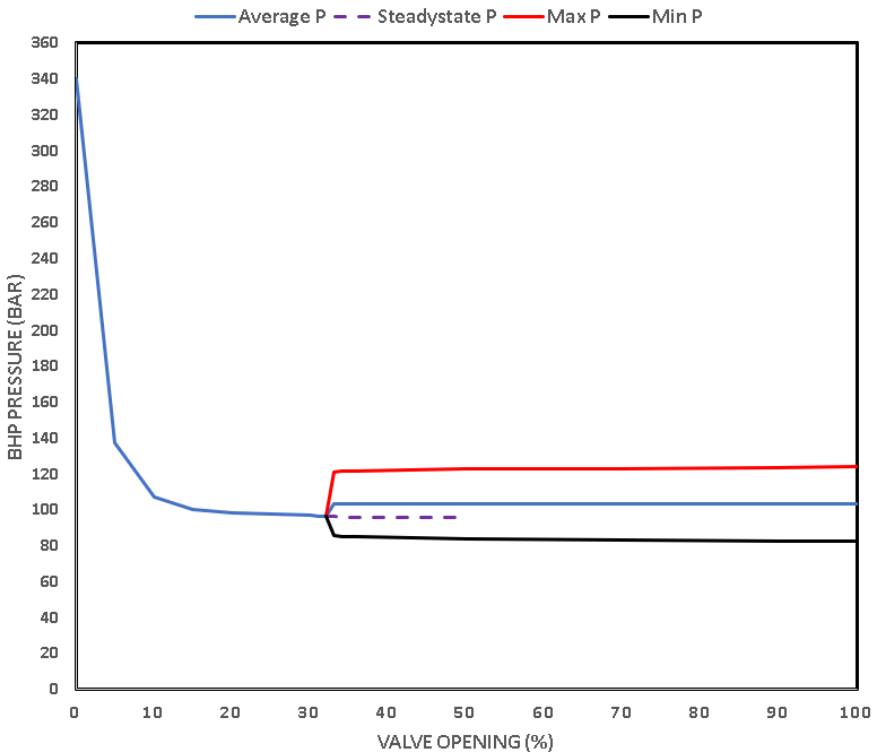

Figure 3.28: Bifurcation diagram of Well 3

The critical value of the relative valve opening of the production choke valve for the transition between a stable non-oscillatory flow regime and riser-slugging is Z_1=33% for this well. In Figure 3.28 we can see that pressure oscillations in the BHP goes from 82 bar all the way up to 124 bar. At valve opening Z_1=32% the system is in a no-slug regime, without any steady-state gas and liquid accumulation in the low-point of the well, as shown in Figure 3.29. At Z_1=33%, the liquid starts to accumulate and at Z_1=60%, the liquid slugs are longer and more severe.

Figure 3.30 shows the system response between a no-slug regime(Z_1=32%) and the critical valve opening (Z_1=33%) down-hole. The productivity index model regulates the inflow-performance of the well, generating a constant mass flow of oil, gas and

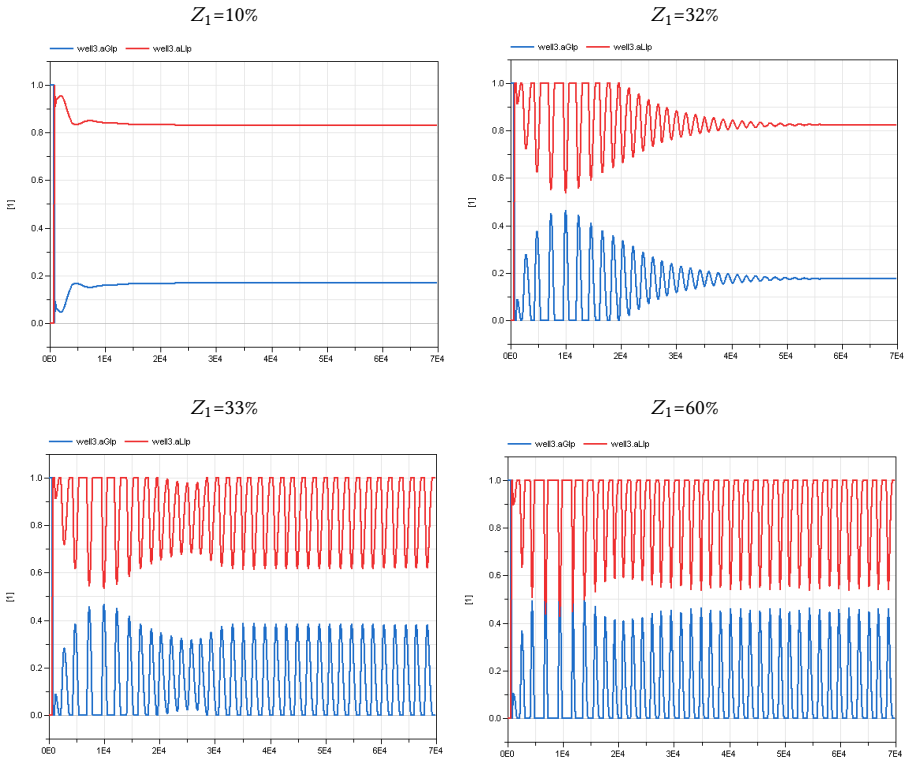

Figure 3.29: Gas and Liquid area fractions in the Low-point of Well 3 for different valve openings

water w_{in}=7.3kg/s in a no-slug scenario (Z_1=32%). The mass fractions measured on the Bottom-hole sensor(MFM3) is shown in Figure 3.31. The mass fraction of oil is 0.31, water is 0.64 and gas is 0.052.

The periodic time of the oscillations (from top to top) is shown in Figure 3.32. By taking a steady-state time interval with a valve opening Z_1=50%, we get a periodic time of the oscillations, T=1800s. The frequency becomes f=1/1800=5.5556e-4 Hz (1/s).

Figure 3.33 shows the mass flow-rate measurements down-hole vs topside for two different valve openings in the slug-regime, where the red line is the bottom-hole measurement and the blue line represents the topside measurement. Te responses of both valve openings indicates that riser-slugging bottom-hole has a significantly bad

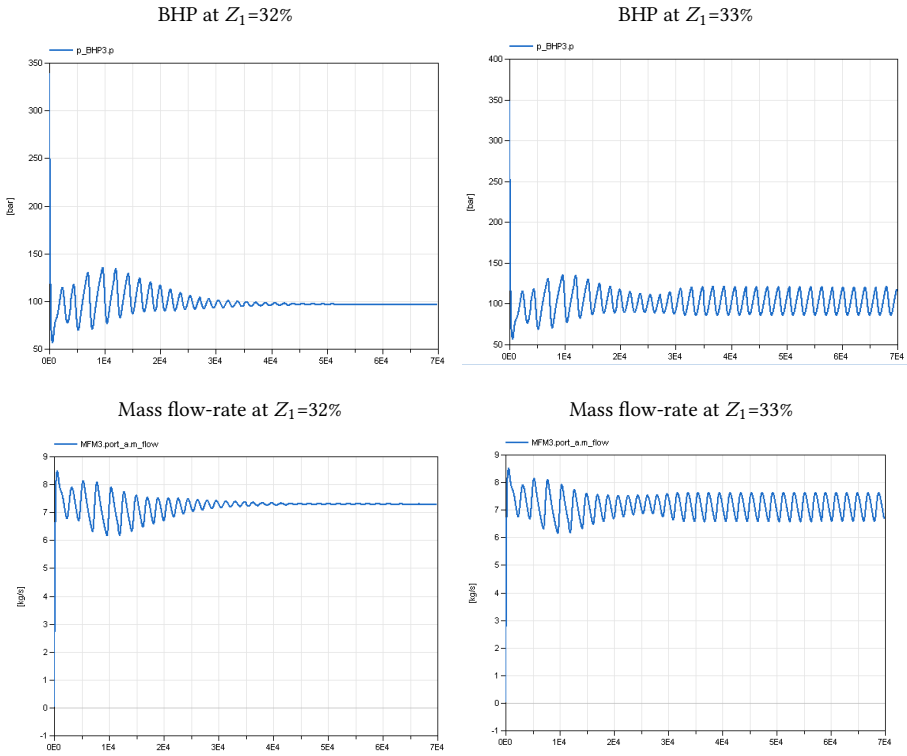

Figure 3.30: Simulations of Well 3, showing BHP(bar) and mass flow-rate(kg/s) for different valve-openings

influence on the topside mass flow-rate, which is undesirable. The numerical values for all parameters of the Reservoir model, productivity index model and the well-slug model is given in table 3.5.

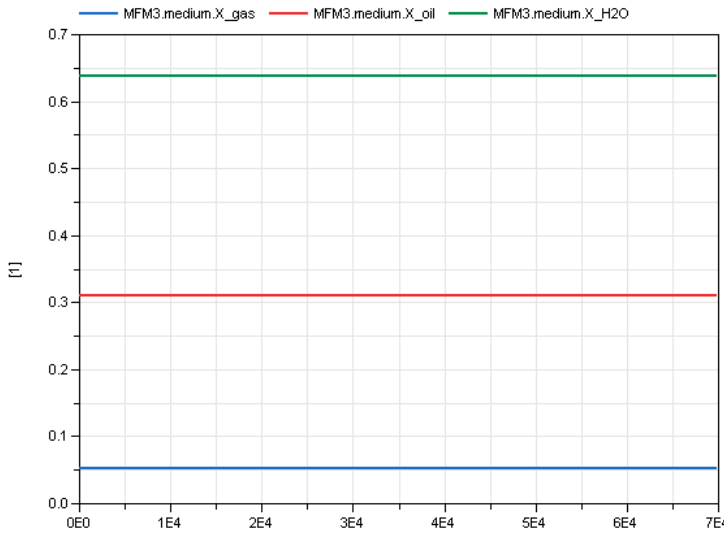

Figure 3.31: Mass fractions bottom-hole for Well 3

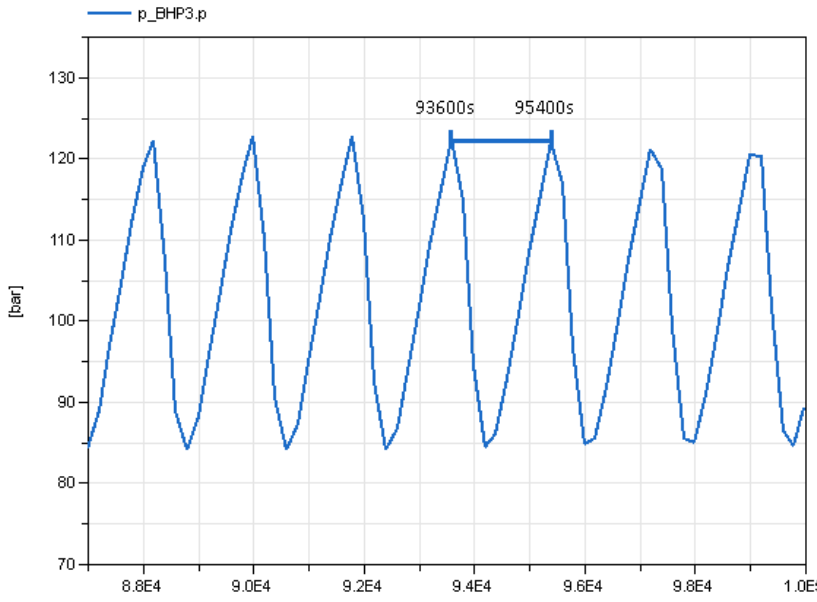

Figure 3.32: Period time of the pressure oscillations bottom-hole of well 3

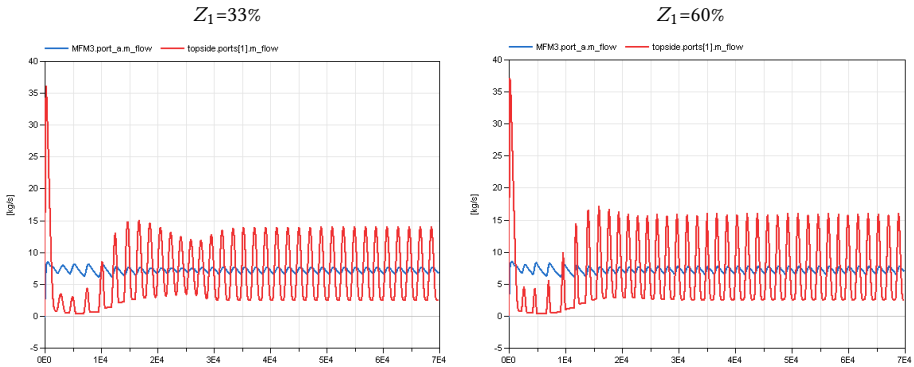

Figure 3.33: Bottom-hole measurements vs topside measurements of massflow-rate at different valve openings in the Well 3 system.

Symbol	Description	Values	Units
Pres	Reservoir pressure	340	bar
Tres	Reservoir temperature	378	K
MM_{gas}	Molecular mass, gas	20e-3	Kg/mol
MM_{oil}	Molecular mass, oil	400e-3	Kg/mol
WC	Water cut	0.65	H2O/liq.(m^3/m^3)
GOR_0	0-Production GOR	180	-
GOR_n	Nominal GOR	180	-
$w_{oil,0}$	0-prod. limit, oil	10	Kg/s
$w_{oil,n}$	Nominal prod., oil	15	Kg/s
dp_{nom}	Nominal pressure drop	1	Bar
w_{nom}	Nominal mass flow-rate	0.03	Kg/s
θ	pipe inclination	1	°C
T_{pipe}	Temperature at pipe inlet	378	K
T_{riser}	Temperature at riser inlet	350	K
$P_{start,pipe}$	Initial Pressure at pipe inlet	349	bar
$P_{start,riser}$	Initial Pressure at riser inlet	240	bar
$slip_{pipe}$	Slip factor pipe	4.5	v_L/v_g
$slip_{riser}$	Slip factor riser	2	v_L/v_g
L_{pipe}	Pipe lenght along seabed	2400	m
L_{riser}	Riser lenght	2600	m
H_{riser}	Riser height(port b-port a)	2200	m
D	Diameter of pipe	0.1	m
K_H	Coeff. liq. level in pipeline	0.7	-
K_L	Coeff. liq. flow through lowpoint	4.24e-4	-
K_G	Coeff. gas flow through lowpoint	K_L	-

Table 3.5: Parameters of the Reservoir model, productivity index model and well-slug model of Well 3 implemented in Dymola

3.3.3 Integrated 3-Well System

The three seperate wells are connected together to the pipeline, where the input (port a) is representing the manifold as shown in Figure 3.34. The geometry of this integrated 3-well system is shown in Figure 3.9

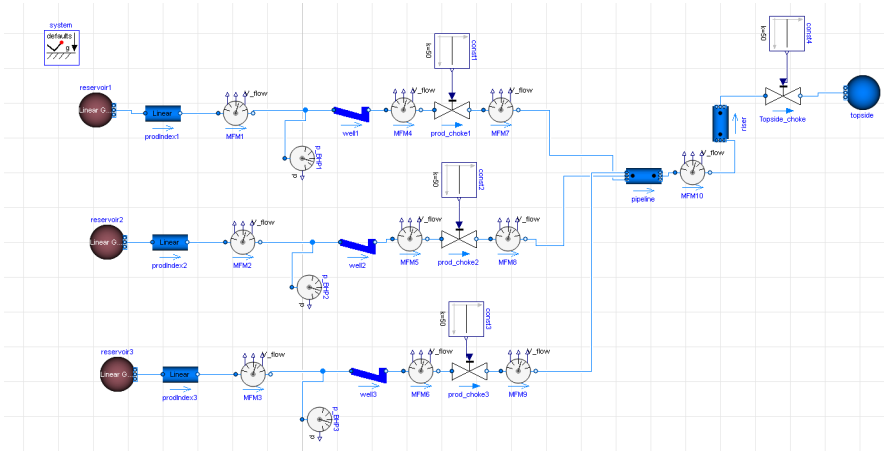

Figure 3.34: Integrated 3-well system, implemented in Dymola

Together, the three wells result in a more complex system dynamics. At production choke openings (Z_1,Z_2 and Z_3 = 50%) representing the production choke openings of well 1,2 and 3 respectively, the pressure measured bottom-hole for each well is shown in Figure 3.35. The blue values represent the BHP of well 1, and red and green values represent the corresponding pressures of well 2 and well 3.

The steady-state BHP of all three wells is shown in Figure 3.36. From the analysis of every well in the previous Sections, it was concluded that the three wells had different frequencies. As we can see from the pressure responses in Figure 3.36, the three wells now got the same frequency f=1/2200s = 4.4545 Hz (1/s). This seems a bit odd at first sight, but there's actually an explanation to this behavior.

To understand how connected systems work in this modeling environment, we can use an electrical circuit analogy. Pressure is like voltage and mass flow is like the current flowing through the system. The main difference between an electrical circuit and fluid circuit lie in the fact that Ohms law (U=R*I) is a linear equation (doubling the voltage, doubles the current), while the fluid equations are generally nonlinear (doubling the

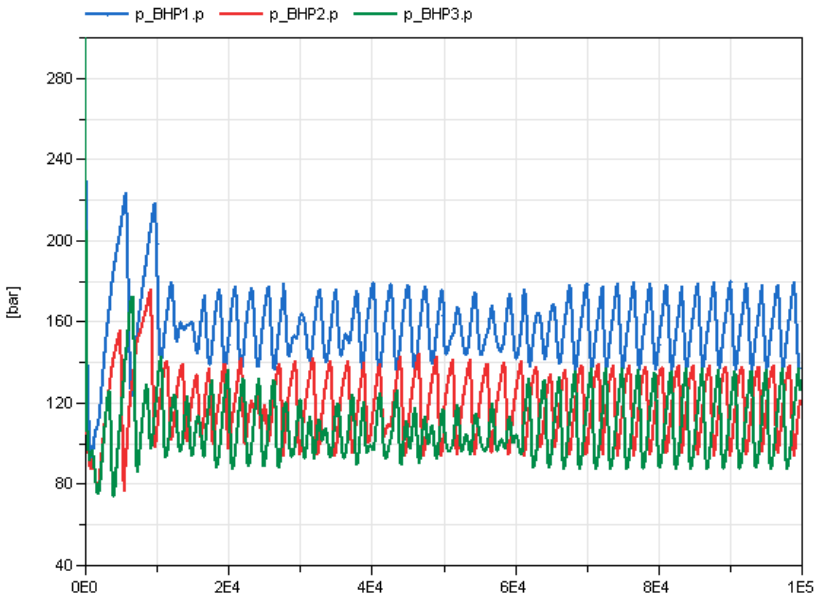

Figure 3.35: Bottom-Hole Pressures of well 1,2 and 3 in the Integrated 3-well system

pressure drop does not double the flow-rate unless the flow is laminar)[39]. If three systems are connected together in parallel, like the one in Figure 3.34, the pressure loss is the same in all pipes[39]:

$$\mathrm{d}p = \mathrm{d}p_1 = \mathrm{d}p_2 = \mathrm{d}p_3 = \mathrm{d}p_n \tag{3.64}$$

And the mass flow (kg/s) becomes the sum of the flow in each pipe can be written:

$$m = m_1 + m_2 + m_3 + m_n \tag{3.65}$$

The reason why the three wells got the same frequencies is because of the framework conditions at the input and output of the system. For each of the three well-systems, the reservoir conditions are different, but the pipeline-riser conditions are the same for each well. Because the pipeline-riser conditions are the same, when connected, the framework conditions where the three wells meet, now become a hub with mutual influence to all the wells. Due to these conditions, the dynamics change, and the pressures get the same

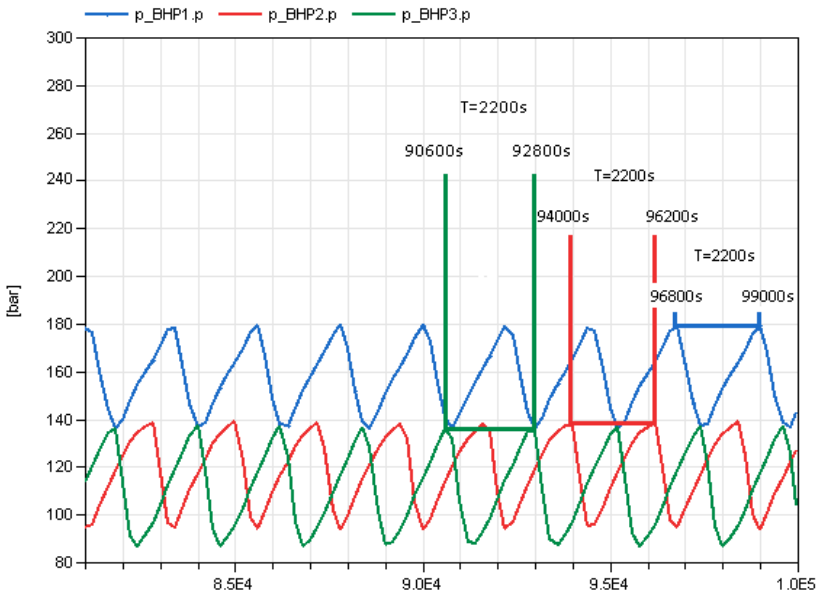

Figure 3.36: Steady-state BHP of well 1,2 and 3 in the Integrated 3-well system

frequencies.

The mass fractions into each well are given in table 3.6, and the mass fractions of each phase entering the riser in Figure 3.34 are given in Figure 3.37

	X_{oil}	X_{water}	X_{gas}
Well 1	0.545	0.404	0.051
Well 2	0.41	0.55	0.034
Well 3	0.31	0.64	0.052

Table 3.6: Mass fractions of well 1,2 and 3, measured bottom-hole

By looking at table 3.6 and Figure 3.37, we can see that the mass fractions of the oil, water and gas phases change when entering the riser, compared to the bottom-hole conditions. In table 3.6, we read that Well 1 got the most mass of oil, while well 3 got the least amount of oil. Well 3 got most mass of water and well 1 got the least amount of water. Both of them got approx the same mass amount of gas. The values of the water-

and oil- mass fractions of well 2 are approximately the average of the other two wells, and the gas mass fraction is significantly lower.

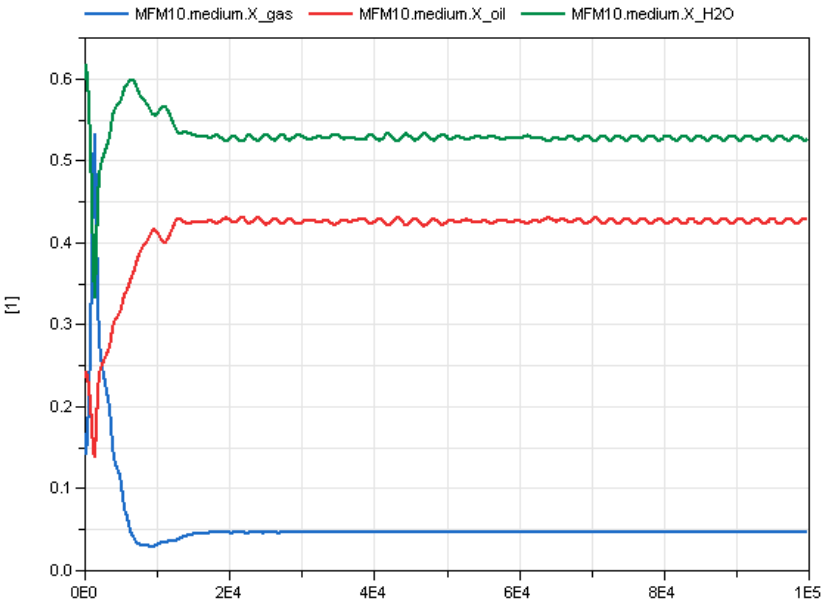

Figure 3.37: Mass fractions entering the riser of the 3-well system

Figure 3.37 shows that mass fraction of oil entering the riser is approximately $X_{oil,riser}$ = 0.4291. The mass fraction of water $X_{water,riser}$ = 0.529 and the mass fraction of gas is $X_{gas,riser}$ = 0.046.

Those values are the approximate averages of well 1,2 and 3 of each phase. This means that the mass fractions of the total mass received at the topside facility are roughly 43% oil, 53% water and 4.6% gas. Figure 3.38 shows the mass flow-rates of the different wells in the 3-well system.

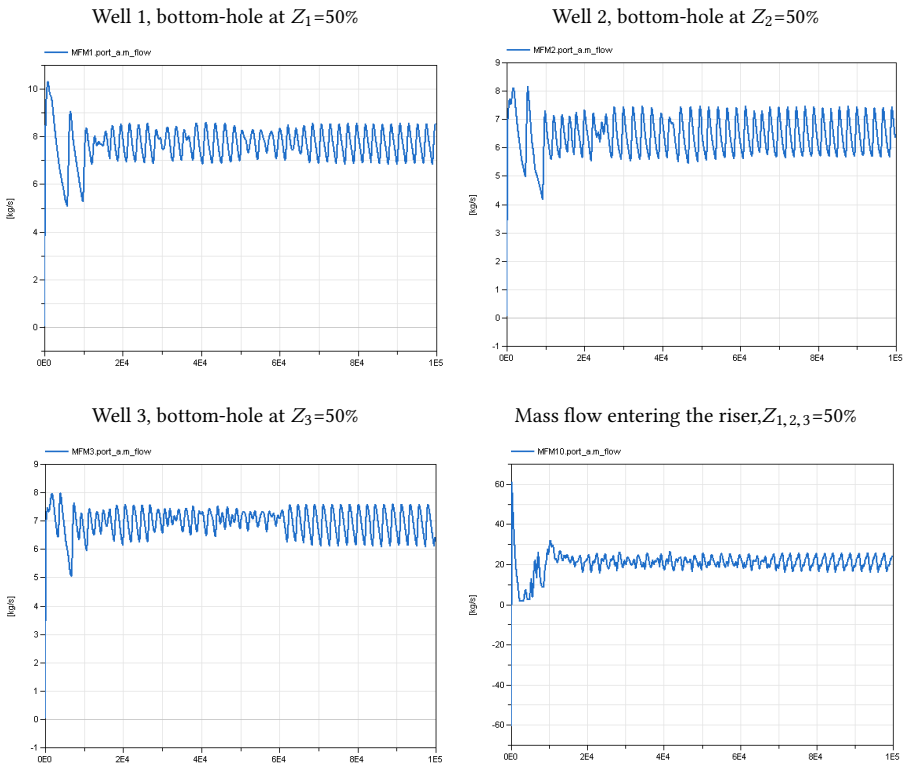

Figure 3.38: Different mass flow-rate measurements in the 3-well system (kg/s)

We clearly see that the three separate wells influence each other by looking that disturbances in the flow-rate measurements. The total flow into the riser is also the sum of the three wells, entering the pipeline in Figure 3.34.

The area Fraction of the gas and liquid phases in the low-point of each well in the 3-well system compared to the three individual wells for Production choke-valve openings at 50%, is shown in Figure 3.39.

By looking at the comparison between the separate systems and the 3-well system, we can see that the low-point area fractions of gas and liquid change when we connect the three wells together. The wells influence each-other and cause disturbances in the system dynamics as shown in Figure 3.39. This leads to disturbances in both the pressures (Figure 3.35) and mass flow-rates(Figure 3.38).

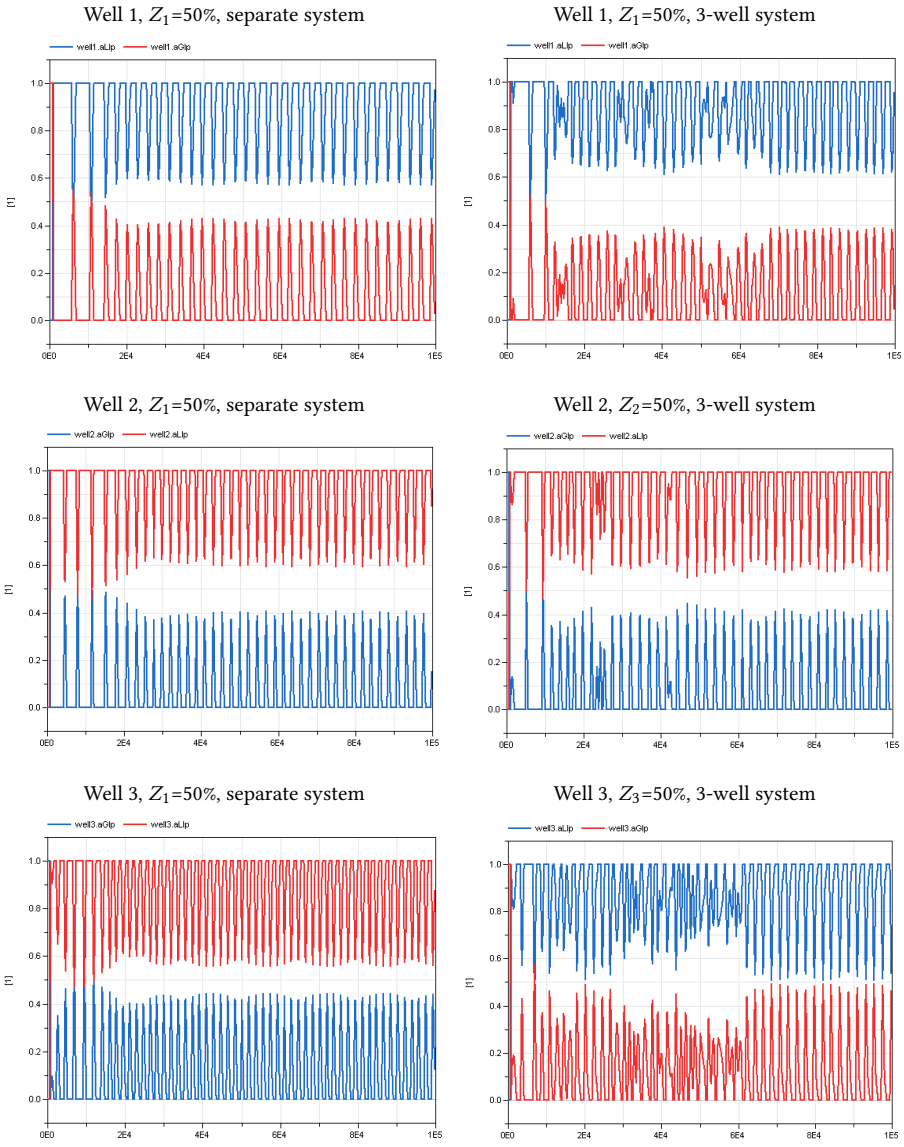

Figure 3.39: Gas and Liquid area fractions in the Low-point of well 1,2 and 3 for both the seperate systems and the integrated 3-well system

As explained in Section 3.3.2.1, the separate well 1 system had a critical valve opening in the transition between a no-slug regime and slugging of Z_1=23%. If we reduce the valve opening to 22%, it would indicate a steady state no-slug regime for this system. By letting Z_1=22% and further down to 10% opening in the 3-well system, comparing to the separate well 1 system, we get the area gas and liquid fractions in the low-point as shown in Figure 3.40.

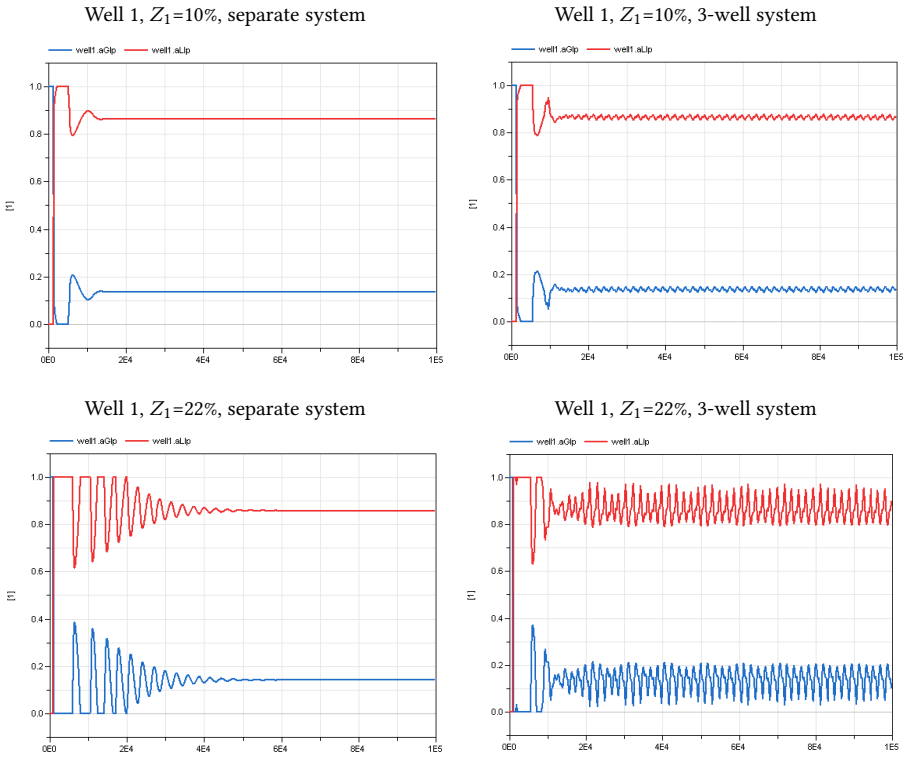

Figure 3.40: Gas and Liquid area fractions in the Low-point of well 1 for both the separate systems and the integrated 3-well system

The responses in Figure 3.40 further prove the fact that the dynamics of well 2 and 3 affect the dynamics of well 1, when connected together. This provides disturbance to the system, resulting in more complex system dynamics. Figure 3.41 shows the low-point relations of well 2 and 3. As explained in Section 3.3.2.2, the critical opening of the

production choke valve Z_1 in the separate well 1 system was 19%. The critical opening of the choke in the well 3 system was 33%, as explained in Section 3.3.2.3. Figure 3.41 shows the area fractions in the low-point of well 2 and 3, for openings lower than the critical valve opening for both systems, which indicated a no-slug regime in the separate systems.

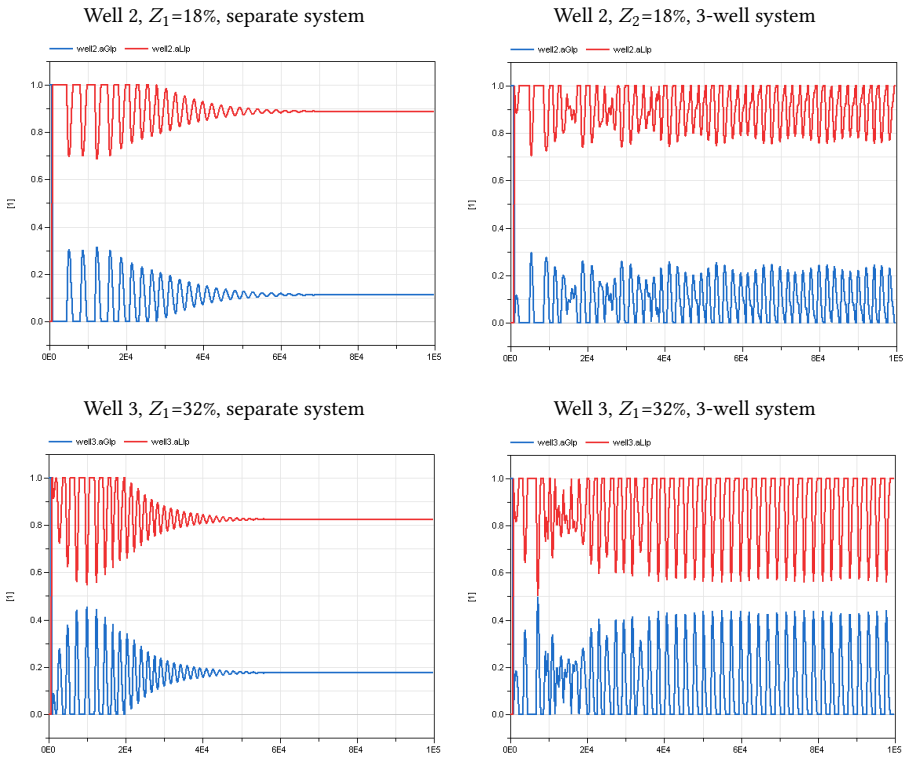

Figure 3.41: Gas and Liquid area fractions in the Low-point of well 2 and 3 for both the separate systems and the integrated 3-well system

By looking at the low-point relations of gas and liquid in Figure 3.40 and Figure 3.41, we can conclude that without any anti-slug control, these three well-systems connected together will stabilize at much lower valve openings than for the separate well-systems, due to influence the three wells have on each-other.

Chapter 4

Anti Slug Control Solutions

This Chapter will cover the Anti-slug control solutions applied to the different systems implemented in Dymola as described in Section 3.3.

As mentioned in Section 2.5.4, feedback control strategies are common solutions for dealing with unstable flow in an offshore production system. Figure 4.1 shows a block diagram of a usual feedback control loop, where u is the manipulated input (controller output), d the disturbance, y the controlled output, and y_s the setpoint(reference) for the controlled output. $g(s) = \frac{\Delta y}{\Delta u}$ denotes the process transfer function and $c(s)$ is the feedback part of the controller [51].

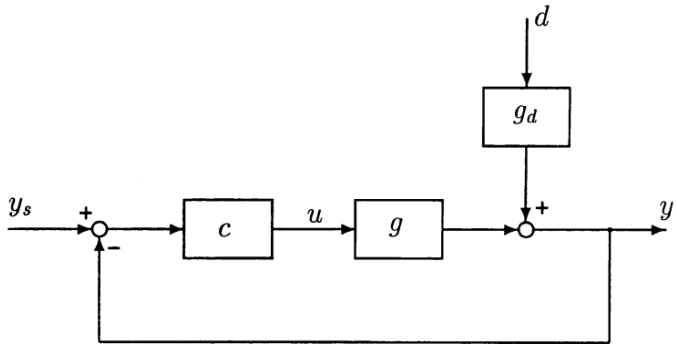

Figure 4.1: Block diagram of feedback control system [51]

The bifurcation diagrams of the separated Well-systems, like the one for Well-3 in

Figure 3.28, tells us something about the control-possibilities of these systems. The unstable steady-state (purple) value in Figure 3.28 is like the equilibrium of an inverted pendulum, and can be stabilized by dynamic feedback control. Because the steady-state value is lower than the average Pressure (blue value), anti-slug control can stabilize the system at lower Pressure set-points. This will result in an increased production rate and economical benefits [43].

The severe slugging in the wells of all the implemented systems in Dymola, is mitigated with PI controllers. All the separated well-systems are considered Single-Input-Single-Output (SISO) systems, which means that the controller got one single input and output in the control-structure. Jahanshahi[30] proved that the Bottom-Hole Pressure (BHP) and the Riser-Base Pressure were the best controller variables (CVs) for these kind of systems. Suggestions that the origin of severe slugging instability is located at the bottom-hole of the well [50] also concluded that the Pressure at this position is the best Controlled Variable (CV). Therefore, the focus of the slug control in this thesis has been to use the Bottom-Hole Pressure(BHP) as the main Control Variable (CV) and the production choke valve opening as the main Manipulated Variable (MV). In case the BHP is unavailable, which often might be the case, we have also tested other possible CVs like the Riser Top pressure together with the topside choke valve opening as an alternative MV. Because this is an experimental modeling environment, we also tried using the mass flow-rate down-hole as our second MV for the cascade gain-scheduling implementation in Section 4.2.4.3. However, using these measurements in a real scenario might be impossible due to lack of sensor-data[11].

The well-2 system, which has got the geometry closest to the extended reach horizontal well[40](explained in Section 3.3.2.2), has received the most attention during the anti-slug control part of this work.

When we implement PI-controllers in each well in the integrated 3-well system, we get multiple control inputs- and outputs-. Because all the wells in this system (as explained in Section 3.3.3) influence each-other, this system behaves like a Multiple-Input-Multiple-Output (MIMO) system. Therefore, it is more complicated to tune it, as mentioned in Section 4.2.2.4.

To handle plant-changes we implemented a Gain-Scheduling PI strategy to the well-2 system, managing to adapt to a certain range of reservoir-based changes in Pressure, GOR and Water-Cut.

Table 4.1 shows all the controllers implemented in the different systems in Dymola, denoted by X. In general, the top row is written: $Type_{CV,MV}$. GS stands for Gain-Scheduling, $P1$ and $P2$ is the BHP and Riser Top Pressure(RTP) respectively. Z_1 is the production choke valve opening and Z_2 is the topside choke valve opening. The $\star$ denotes if the system has got tuned parameters. If not, the tuning is done by trial and error. The **X** denoting bottom-hole PI-control of the 3-well system means that there are 3 PI-controllers, one for each well, resulting in a total of 9 different PI-control structures in the implemented systems.

	PI_{P1,Z_1}	PI_{P2,Z_2}	PI, GS_{P1,Z_1}
Well-1 system	$X^\star$		
Well-2 system	$X^\star$	$X^\star$	X
Well-3 system	$X^\star$		
3-Well system	**X**	$X^\star$	

Table 4.1: All the different controllers, implemented in Dymola

4.1 Steady-State Gain

By looking at the separate well 1,2 and 3 systems, explained in Section 3.3, we can obtain the system responses. For the well 1 system, if we apply a step in the production choke valve opening in a no-slug regime from Z_1=15% to Z_1=19%, as shown in Figure 4.2, we get a response in the BHP as shown in Figure 4.3. The step is applied after t=50000s.

From Figure 4.3, We get a underdamped second-order system response without time-delay in the following form [9]:

$$\frac{Y(s)}{U(s)} = \frac{K}{T^2 s^2 + 2T\zeta s + 1} \tag{4.1}$$

where K is the steady-state gain, T is the period time and ζ is the damping coefficient. The steady state gain K, can be found by taking the steady state output difference divided by the input(step) change [51]:

$$K = \frac{\Delta y(\infty)}{\Delta u} = \frac{y_2 - y_1}{u_2 - u_1} = \frac{150.27 - 153.221}{19 - 15} = -0.73775 \tag{4.2}$$

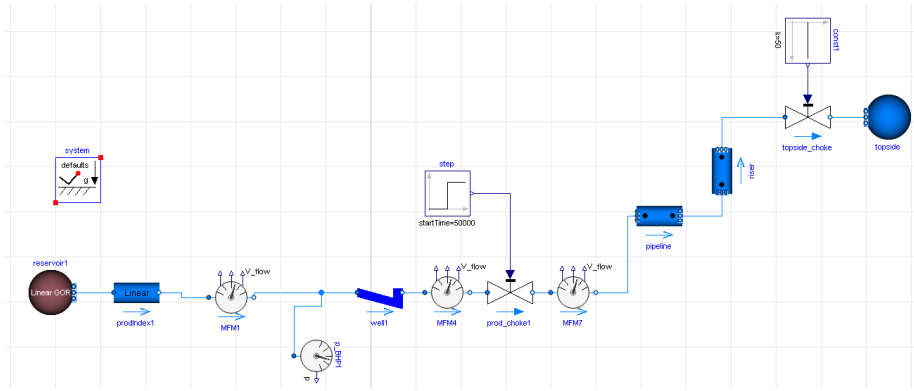

Figure 4.2: Implementing a step in the well 1 system

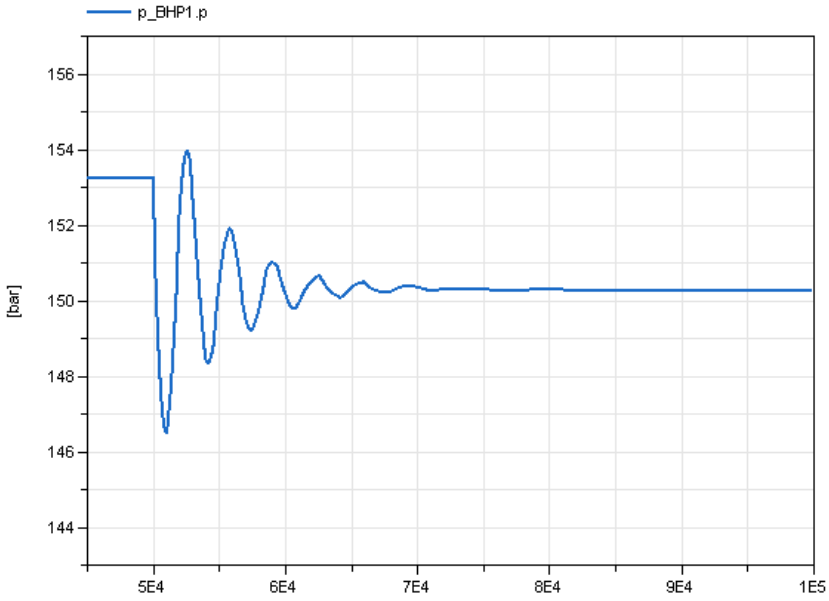

Figure 4.3: BHP response to the step change in the well 1 system

As shown in eq: 4.2 The steady-state gain K is negative. This is the case for all the implemented systems, and will affect the implementation of the controllers in the following Sections.

4.2 PI-Control

As mentioned in Section 2.5.4.1, active feedback control of the production choke using a Proportional Integral-controller or PI-controller has been a favored solution in the industry for anti-slug control due to it's efficiency, simplicity and low cost. It can be used to stabilize or reduce well instabilities. The integral part enables the controller to eliminate offsets. The PI-controller can be used on systems with large disturbances, but may fail when the control input is highly nonlinear[46].

A PI- controller has the form:

$$u(s) = K_c e(s) + \frac{K_i e(s)}{s} \tag{4.3}$$

Which can be rewritten as:

$$u(s) = K_c e(s)(1 + \frac{1}{T_i s}) \tag{4.4}$$

Where T_i, the integral time is the ratio between the proportional gain K_c and the integral gain K_i:

$$T_i = \frac{K_c}{Ki} \tag{4.5}$$

and the error signal $e(s)$ is the difference between the desired output signal, i.e the reference(set-point) signal $y_d(s)$ and the output signal$y(s)$:

$$e(s) = y_d(s) - y(s) \tag{4.6}$$

Using eq: 4.6 in eq: 4.3, we get:

$$u(s) = (y_d(s) - y(s))(K_c + \frac{K_i}{s}) \tag{4.7}$$

Because we got a negative stead-state gain in Section 4.1, eq: 4.7 can be rewritten into:

$$u(s) = -(y_d(s) - y(s))(K_c + \frac{K_i}{s}) = -e(s)(K_c + \frac{K_i}{s}) \tag{4.8}$$

This form of the PI-controller, shown in eq: 4.8, is the one implemented in Dymola,

and it shows that, because the error signal $e(s)$ is negative, the K_c and K_i parameters has to be negative in order for the feedback control system to work.

The PI controller implemented in Dymola(Figure 4.4), has the following form in the time domain:

$$u(t) = -K_c e(t) - K_i \int_0^t e(\tau) d\tau \tag{4.9}$$

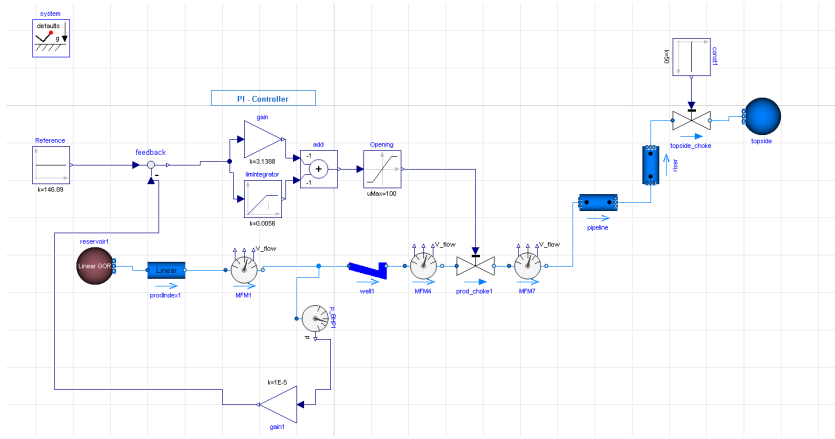

Figure 4.4: PI control of the Well 1 system

In Figure 4.4, the error, $e(t)$ which is the feedback term, has two inputs: the reference signal (y_d) and the measurement from the BHP (y). A gain block connected to the BHP sensor is used to match the reference signal, converting from Pascal (Pa) to bar. The integral block has an integrated limiter, keeping the integral gain within bounds (an upper and lower limit). The sum block after the proportional- and integral- gain block, is negative, because of the negative steady-state gain (Section 4.1). The negative sum block shown in Figure 4.4, means that we can implement positive K_c and K_i values for the system to be on the form of eq: 4.9. If the sum block is positive, which is the case in the predesigned PI-controller block in the Subpro library in Dymola, used in Section 4.2.4.3, then the K_c values has to be negative. The T_i stays positive at all times because of eq: 4.5. There is also a limiter on the output signal from the controller, keeping the values within the range of the choke valve opening (0-100%).

4.2.1 PI Tuning Strategy

We decided to use the set-point overshoot method[48] for PI-tuning on all the separated well systems as well as the topside control of the 3-well system. This method is based on Skogestad's SIMC method[53] and requires one closed-loop step set-point response experiment using a P-controller.

First, we need to use a P-controller with gain K_{c0}, and apply a set-point change of amplitude Δy_S. K_{c0} should be selected so that we get a proper overshoot in the set-point response (in the process output). An example of a setpoint response can be shown in Figure 4.5.

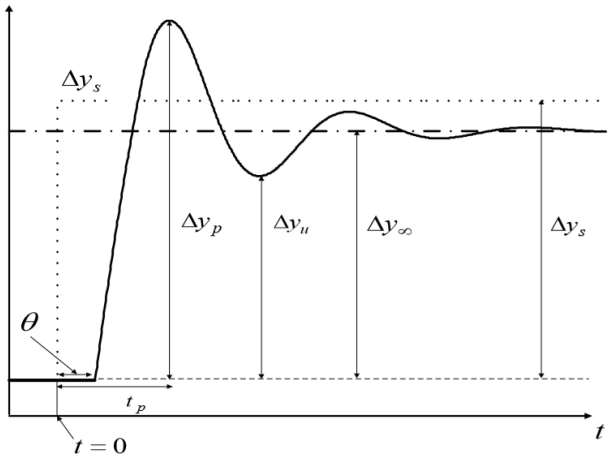

Figure 4.5: Closed-loop step set-point response with P-only control[48]

From the set-point response, we read off the maximum response, y_{max}, and the steady-state response, $y(\infty)$, and the time to reach the peak, t_p. We assume that the process output has value y_0 before the set-point change. From the above quantities, the actual overshoot is calculated:

$$S = \frac{\Delta y_p - \Delta y_\infty}{\Delta y_\infty} = \frac{y_{max} - y(\infty)}{y(\infty) - y_0} \tag{4.10}$$

The relative steady-state change of the process output is calculated by the following equation:

$$b = \frac{\Delta y_\infty}{\Delta y_S} = \frac{y(\infty) - y_0}{\Delta y_S} \tag{4.11}$$

To avoid waiting for the response to settle at a steady-state value, Shamsuzzoha[48] suggests that the estimate $y(\infty) = 0.45(y_{max} + y_{min})$ where y_{min} is the value of an assumed undershoot in the response.

Define the following parameters:

$$F = 1 \tag{4.12}$$

The factor F is a tuning parameter and $F = 1$ gives the "fast and robust" SIMC settings corresponding to τ_c=θ[53]. To detune the response and get more robustness, select $F > 1$ to speed up the closed-loop response.

$$A = 1.152 * S^2 - 1.607 * S + 1.0 \tag{4.13}$$

The PI parameter settings are:

$$K_c = K_{c0} * \frac{A}{F} \tag{4.14}$$

$$T_i = \min\left(0.86At_p \frac{b}{1-b},\ 2.44t_pF\right) \tag{4.15}$$

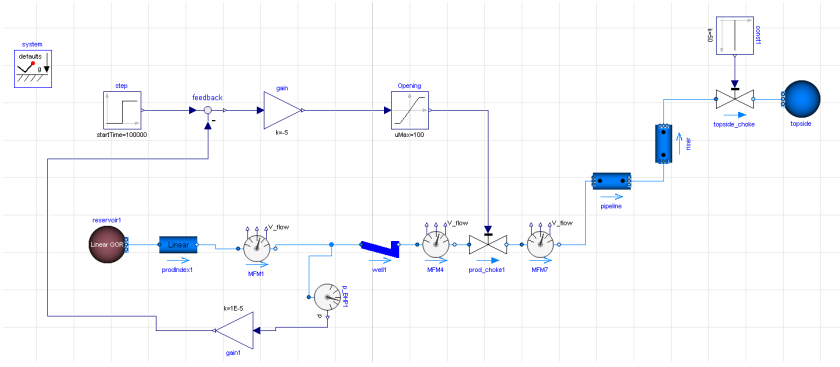

Figure 4.6: Step implemented to a P-controller in the Well 1 system

The controller gain K_{c0} was chosen to to get a proper overshoot in the BHP response after the step-change. The set-point-change Δy_{SP} was chosen (> 1 with the intention of applying PI-parameters covering an extended range of set-point pressures) within the range of the BHP oscillations at the critical valve opening of each well.

For the well-1 system, we applied K_{c0} =-5 and Δy_S=3, starting at y_{SP}=145 bar, with the step happening after the BHP had reached steady-state(t=100000s). We got the BHP response as shown in Figure 4.7. The simulation time was set to t=200000s

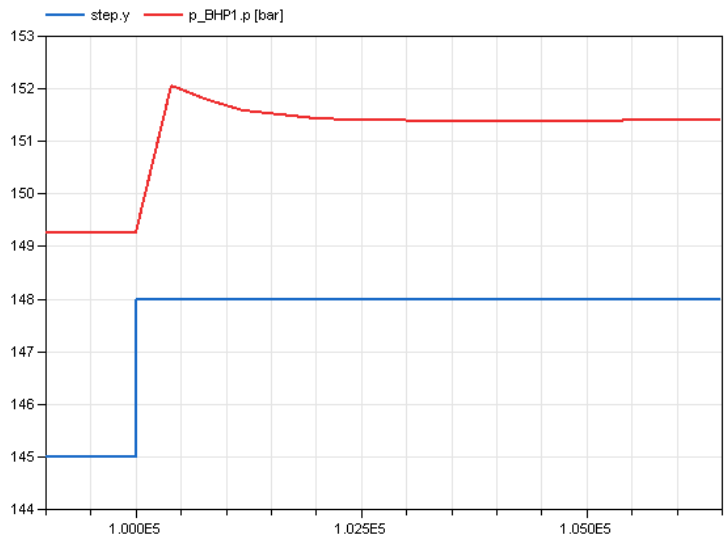

Figure 4.7: BHP response after the step-change in the well 1 system

From this response, we get the actual overshoot:

$$S = \frac{y_{max} - y(\infty)}{y(\infty) - y_0} = \frac{152.056 - 151.421}{151.421 - 149.256} = 0.2933025 \tag{4.16}$$

The relative steady-state change of the process output becomes:

$$b = \frac{y(\infty) - y_0}{\Delta y_S} = \frac{151.421 - 149.256}{3} = 0.7217 \tag{4.17}$$

The tuning parameter was chosen F=1, and

$$A = 1.152 * 0.2933^2 - 1.607 * 0.2933 + 1.0 = 0.6278 \tag{4.18}$$

This lead to the PI parameter settings:

$$K_c = K_{c0} * \frac{A}{F} = 5 * \frac{0.6278}{1} = 3.139 \tag{4.19}$$

The time to reach the first peak, t_p can be read from the BHP step response to be 400s, and the integral time becomes:

$$T_i = \min\left(0.86At_p\frac{b}{1-b},\ 2.44t_pF\right) = \min(560, 976) = 560s \tag{4.20}$$

Similar closed loop step-response tests, as the one shown in Figure 4.6, were conducted with the BHP($P1$) as our CV and the production choke valve opening(Z_1) as our MV on the separated well-2 and well-3 systems. The tuning parameter was $F = 1$ and the set-point change was Δy_S=3 for all systems. The proportional gains K_c are implemented as positive values for all systems implemented because of the negative sum block, as the one shown in Figure 4.4, except for the system implemented in Section 4.2.4.3, where the K_c values are negative because of the positive sum inside the premade PI-controller block. For implementation in our systems, K_i can be calculated using eq: 4.5. The tuned PI-parameters and measured values as shown in table 4.2

PI_{P1,Z_1}	K_{c0}	t_p	K_c	T_i
Well-1 system	5	400s	3.139	560s
Well-2 system	10	800s	7.9631	1248s
Well-3 system	5	800s	4.1166	1400s

Table 4.2: Tuned PI-parameters using BHP as CV and production choke valve opening as MV

By using the same tuning strategy, using the RTP($P2$) as our CV and the topside choke valve opening(Z_2) as our MV on the Separate well-2 system and the integrated 3-well system, we got the tuned PI-parameters for these systems. Two things worth mentioning are that we expanded the step-change (Δy_S) from 3bar to 5bar on the 3-well system and changed the tuning parameter F from 1 to 6, in order to handle the complex dynamics of this system and get a good response. The tuned PI-parameters

and measured values from the closed-loop tests are shown in table 4.3

PI_{P2,Z_2}	F	Δy_S	K_{c0}	t_p	K_c	T_i
Well-2 system	1	3	4	1600s	3.3207	3365s
3-Well system	6	5	7	800s	0.9038	4854s

Table 4.3: Tuned PI-parameters using RTP as CV and Topside choke valve opening as MV

4.2.2 PI-control Using Bottom-Hole CV and MV

4.2.2.1 Well - 1 system

By using the tuned PI-parameters found in Section 4.2.1, table 4.2, we implemented a PI-controller as shown in Figure 4.8. The best setpoint (P_{ref}), was found by trial and error, using the lowest possible set-point for the highest possible mass flow-rate, which is desirable.

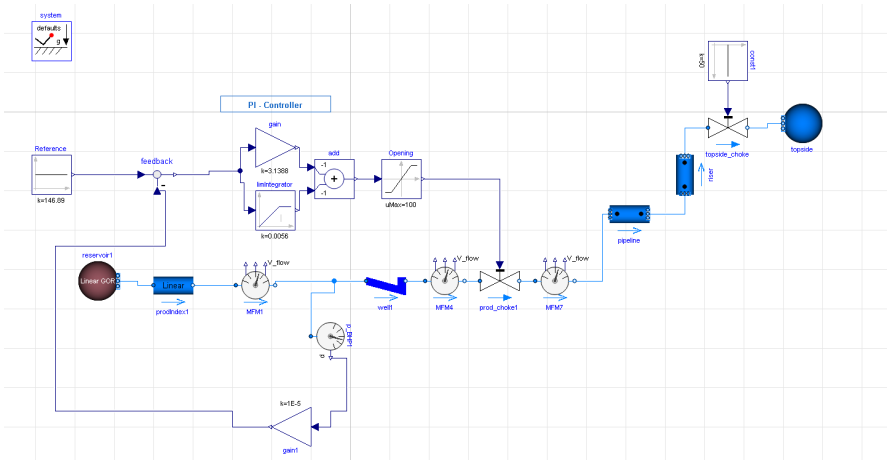

Figure 4.8: PI control of the well-1 system

The simulation results for the PI-control structure in the Well-1 system is shown in Figure 4.9. When the simulation starts, the production choke valve opening is set to Z_1=23%, which is within the slug-regime of this system. At t=200000s, the controller

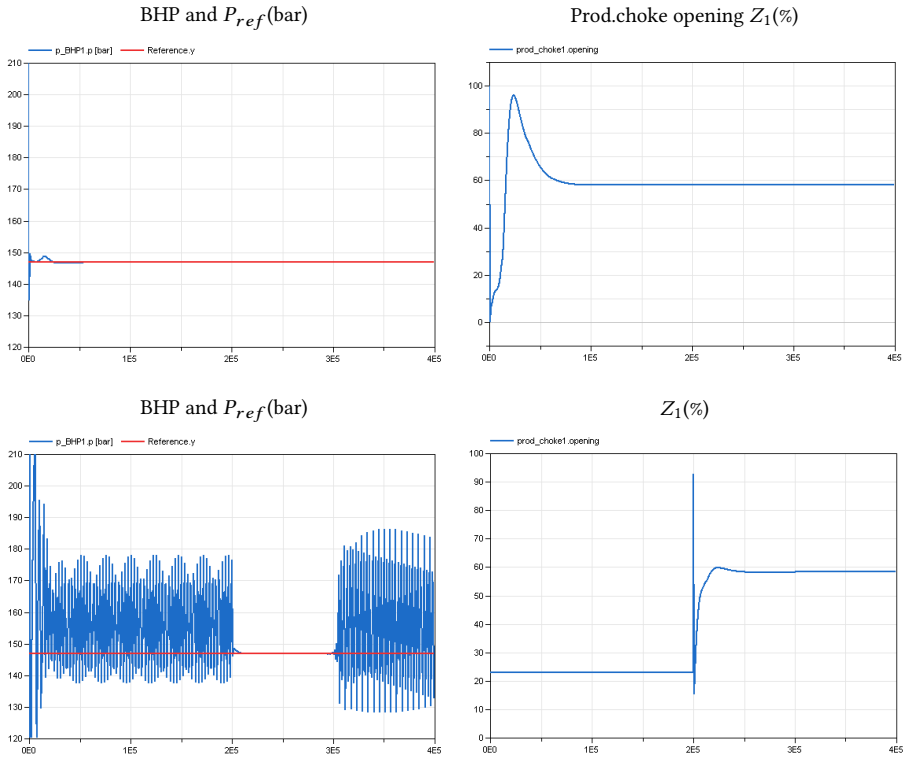

Figure 4.9: PI-control of the well-1 system

turns on, and at t=300000s, the controller turns off and slugging continues at the steady-state valve opening of the production choke valve. We can see that using a PI-controller with the tuned parameters, the system stabilizes at Z_1=58.36%, both when the controller is on at all times and when we turn it on and off.

Figure 4.9 proves that the PI-controller is able to track the reference pressure P_{ref} and that it's crucial to have it on at all times. Figure 4.9 shows that the oscillations in the BHP are magnified at a larger valve opening (when the controller turns off). The resulting mass flow-rate from the PI-control, measured on the multi-phase metering sensor(MFM1) bottom-hole, is shown in Figure 4.10, and we can see that the mass flow-rate stabilizes at around 8.12kg/s.

We introduced plant-changes to the reservoir to test the robustness of the PI-

controller, as shown in Figure 4.8. We applied a ramp, starting at t=50000s, increasing it from 0.4 to 0.6. The ramp uses 70000s to reach the new value, and we get the response as shown in Figure 4.11

From Figure 4.11, we see that the PI-controller is unable to track the set-point when we apply a plant-change in water-cut increase to this system. If we increase the set-point P_{ref}=180 bar, we get the response shown in Figure 4.12

From Figure 4.12, we can see that by increasing the set-point to the controller, we manage to stabilize the BHP when we introduce increased Water-cut as a plant-change to the system. This results in a lower flow-rate, which is undesirable.

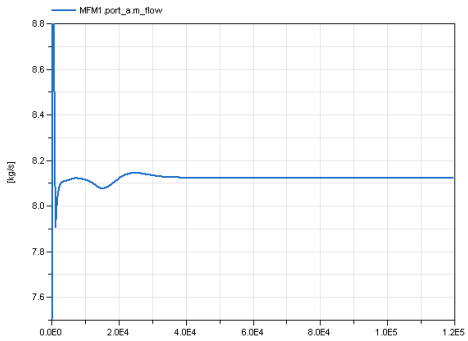

Figure 4.10: Mass flow-rate (kg/s)

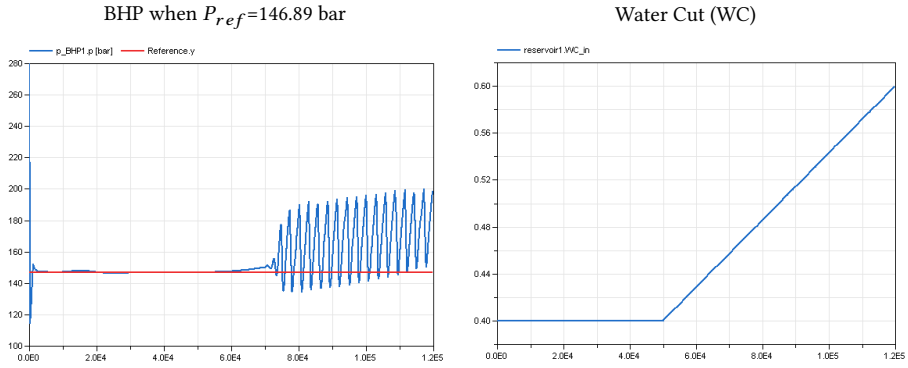

Figure 4.11: Applying plant-changes (WC) to the well-1 system

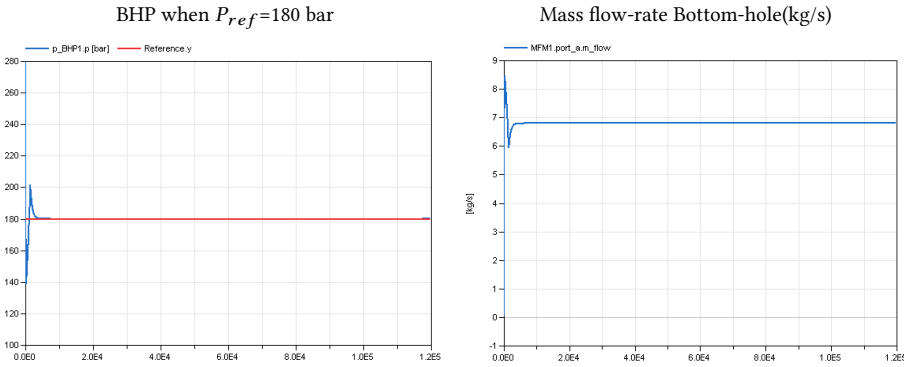

Figure 4.12: BHP response when increasing the set-point P_{ref}

4.2.2.2 Well - 2 System

This system is implemented the same way in Dymola as the well-1 system, explained in Section 4.2.2.1. By trial and error, the optimal set-point was found to be P_{ref}=111.2 bar. The simulation results for the PI-control structure in the Well-2 system are shown in Figure 4.13.

From Figure 4.13, we can see that the well-2-system stabilizes at a higher valve opening Z_1 than the well-1-system, shown in Figure 4.9. The PI-controller in the well-2 system stabilizes at Z_1=69%. Because this system stabilizes at a higher valve opening, we had to increase the simulation time from 400000s to 500000s. The controller turns

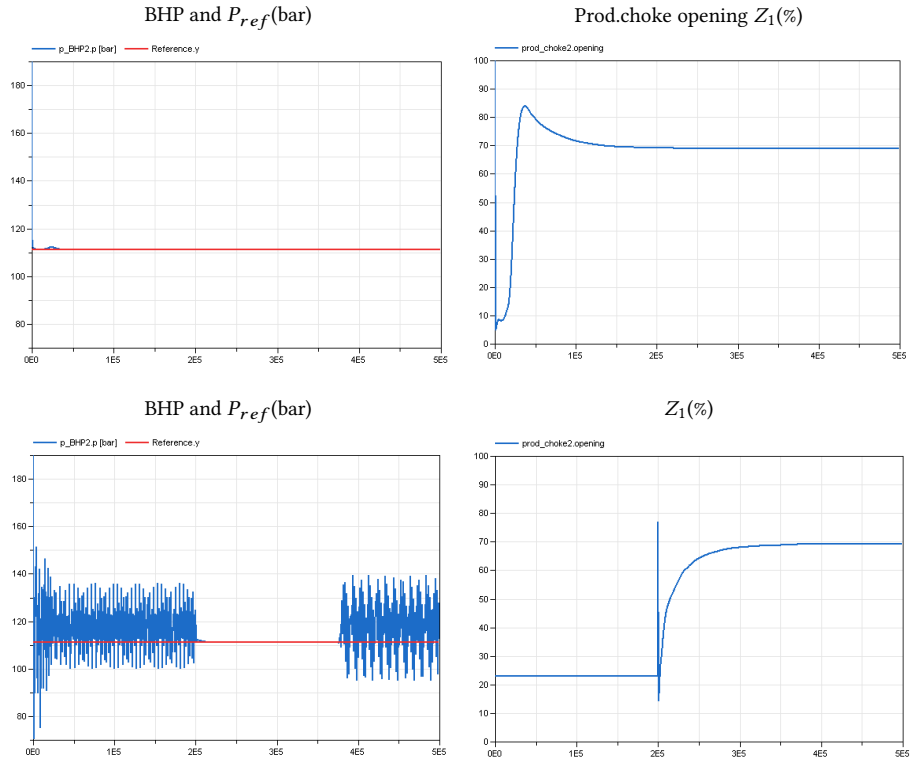

Figure 4.13: PI-control of the well-2 system

on at t=200000s and turns off at t=380000s as illustrated in Figure 4.13.

The resulting mass flow-rate from the PI-control, measured on the multi-phase metering sensor bottom-hole, is shown in Figure 4.14, and we can see that the mass flow-rate stabilizes at around 6.75kg/s.

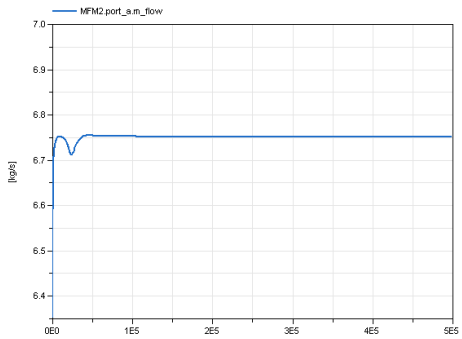

Figure 4.14: Mass flow-rate (kg/s)

4.2.2.3 Well - 3 System

The step-change of the closed loop step response with a P-controller for this system was between 95 and 98 bar, with Δy_S=3, and the BHP response resulted in the PI-parameters shown in table 4.2. The optimal set-point was found to be P_{ref}=95.9 bar. The simulation results for the PI-control in the Well-3 system are shown in Figure 4.15.

Figure 4.15 shows that the PI-control in the well-2 system stabilizes Z_1 at 63.86% opening. The PI-controller turns on at t=200000s and turns off at t=500000s. As illustrated in Figure 4.15, the controller manages to track the set-point and stabilize the BHP both when on all the time and when turned on during a slug regime. It proves for all systems that the controller must be turned on at all times, because at higher valve openings, the pressure oscillations increases, and become more severe. This is undesirable as it may result in an unstable production and wear-and tear on equipment.

The resulting mass flow-rate from the PI-control, measured on the multi-phase metering sensor bottom-hole, is shown in Figure 4.16. We can see that the mass flow-rate stabilizes at around 7.32 kg/s at the given set-point P_{ref}=95.9 bar.

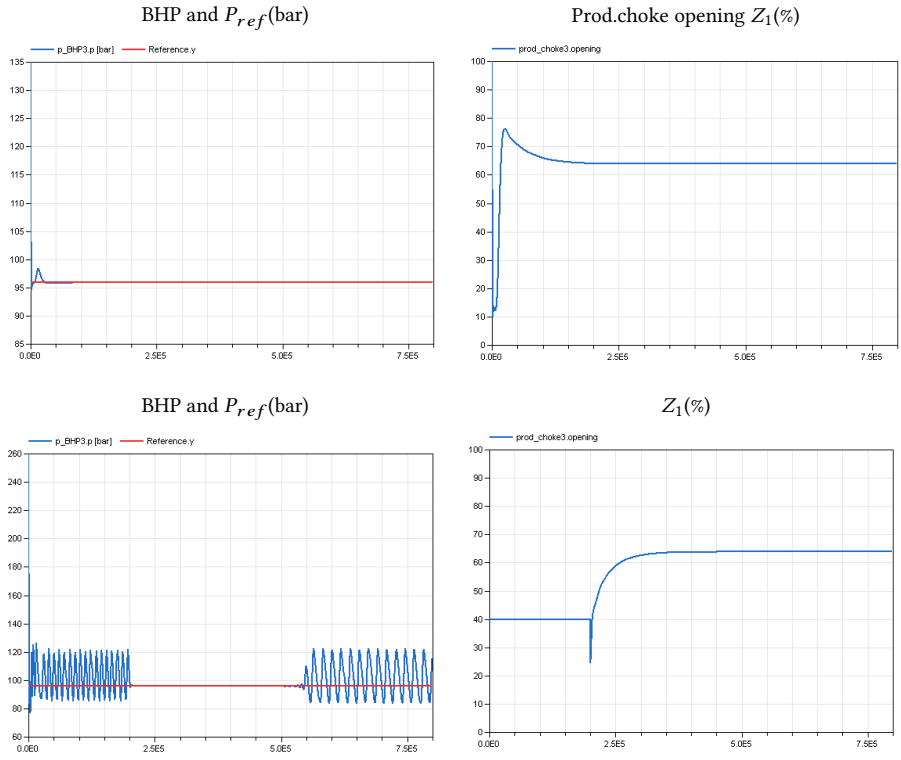

Figure 4.15: PI-control of the well-3 system

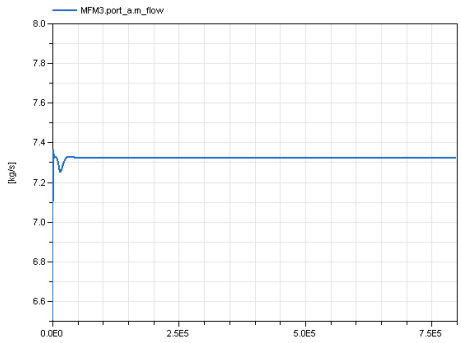

Figure 4.16: Mass flow-rate (kg/s)

4.2.2.4 3 - Well System

PI-control was implemented in the 3-well system as shown in Figure 4.17.

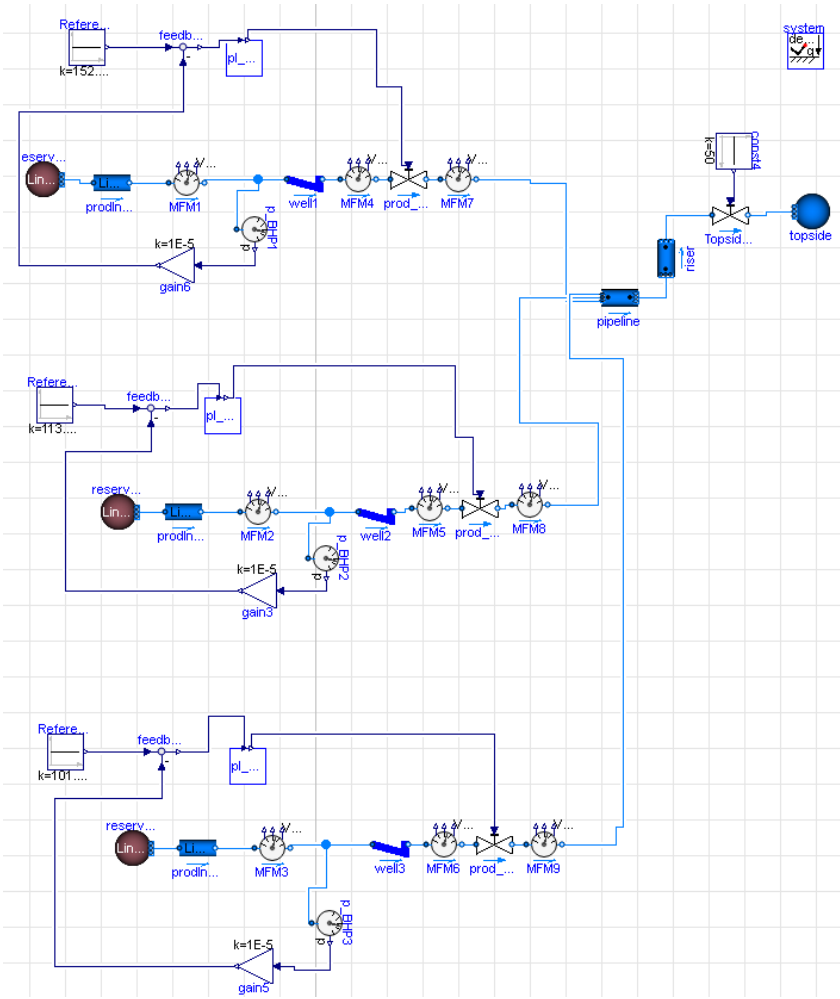

Figure 4.17: PI-control of the 3-well system using Bottom-hole CV and MV

The PI-control block in Figure 4.17 contains an on/off switch, as illustrated in Figure 4.18

The PI-controller of well 1,2 and 3 in the 3-well system is modelled in the way

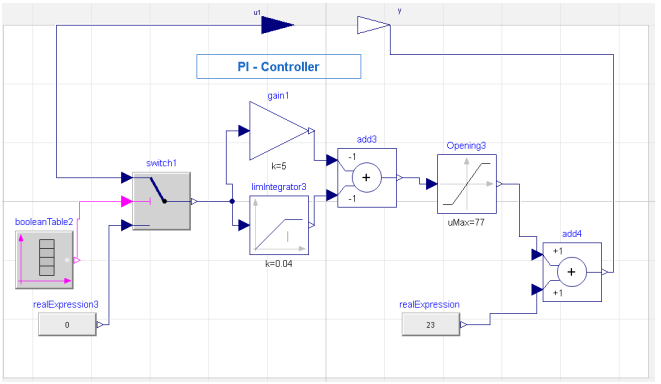

Figure 4.18: PI-control subblock in Dymola - 3-well system

that it does not start to process the feedback signal until it's turned on. The switch in Figure 4.18 triggers when the simulation time reaches the table value, turning on the controller. The "0" value input ensures that the controller input is zero as long as it is turned off. The sum block after the limiter ensures that the valve opening (%) starts on a preset value within the slug-regime of each well. The controller then turns on, at a specific time.

Because of the dynamics of the system in Figure 4.17, it's very hard to tune each well separately. Every well in this "parallel" connected MIMO system influences each-other, so the tuning on one well will affect the others and vice versa. Because of this, the PI-parameters for well 1,2 and 3 in this system, as well as the optimal set-points, were found by trial and error, ensuring as high valve openings as possible.

The PI parameters for each well is shown in table 4.4, and simulation results of each PI-controller is shown in Figure 4.19

PI_{P1,Z_1}	P_{ref}(bar)	K_c	T_i
Well-1	152.838	1.9	1900s
Well-2	113.65	3	3000s
Well-3	101.88	2	2000s

Table 4.4: Tuned PI-parameters using BHP as CV and production choke valve opening as MV

As shown in Figure 4.19, the blue values are the BHP of well 1 and the red and green values are the corresponding pressures of well-2 and 3 respectively. The reference pressures P_{ref} are also plotted for all the wells. We can see that the PI controllers with the parameters as shown in table 4.4 are able to track the set-points P_{ref} when the controllers are turned on after t=200000s. The production choke valve openings Z_1 can also be seen for all the wells. The blue values represent Z_1 for well 1, and the red and green are the corresponding valve openings of well-2 and 3 respectively.

Table 4.5 shows the difference between the valve openings Z_1 for the separate well 1,2 and 3 systems compared to the 3-well system using PI control with bottom-hole CV and MV. The $\star$ notation indicates that the systems are tuned using the Set-point overshoot method[48].

PI_{P1,Z_1}	Separate well systems* (%)	3-well system (%)
Well-1	58.36	68.526
Well-2	69	55.46
Well-3	63.86	65

Table 4.5: Prod. choke valve openings Z_1 of the Separate well 1,2,3 systems compared to the 3-well system using PI control with bottom-hole CV and MV

Table 4.6 shows the mass flow-rate comparisons between the separate well 1,2 and 3

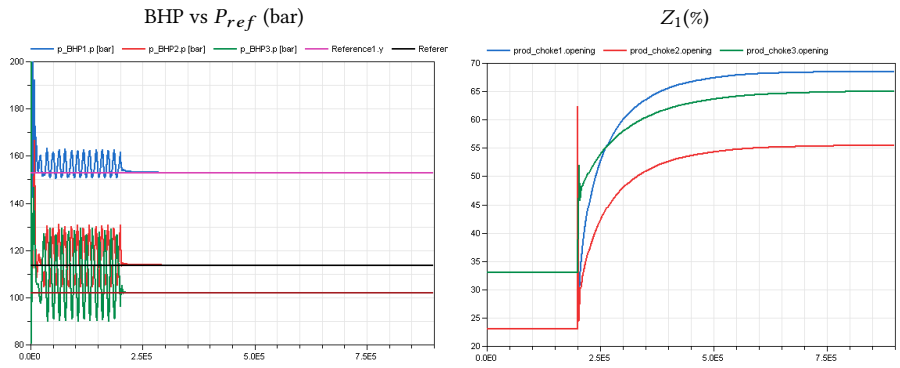

Figure 4.19: PI-control of well 1,2 and 3 in the 3-well system using Bottom-hole CV and MV

systems and the 3-well system using PI control with bottom-hole CV and MV. Here, $\diamond$ indicates that the total mass flow-rate is entering the riser of the 3-well system(Figure 4.17) and is not a fictional summation of the separate wells.

PI_{P1,Z_1}	Separate well systems* (kg/s)	3-well system (kg/s)
Well-1	8.12	7.886
Well-2	6.75	6.6537
Well-3	7.32	7.143
Total	22.19	21.683$^\diamond$

Table 4.6: mass flow-rate- comparisons between the separate well 1,2 and 3 systems and the 3-well system using PI control with bottom-hole CV and MV

4.2.3 PI-Control using Topside CV and MV

4.2.3.1 Well-2 system

In case the BHP-measurements were unavailable, this system was also tested with a PI-controller implemented topside, using the Riser-Top Pressure as our CV and the topside choke valve as our MV. This implementation is shown in Figure 4.20

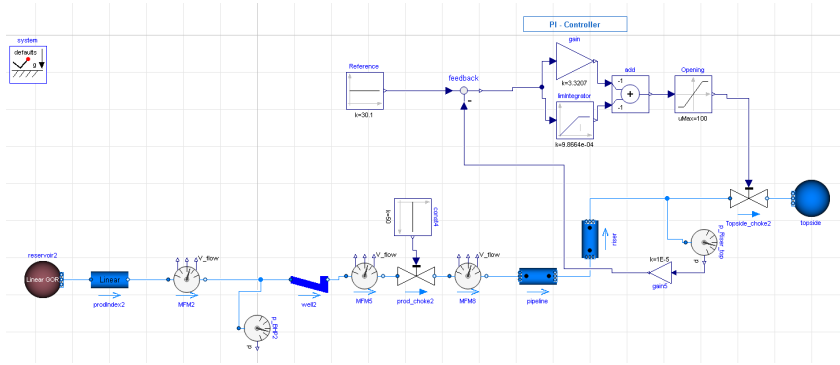

Figure 4.20: PI control topside in well-2 system

The optimal set-point for this system was found to be P_{ref}=30.2 bar, and the simulation results of the PI-control structure implemented topside in the Well-2 system are

shown in Figure 4.21.

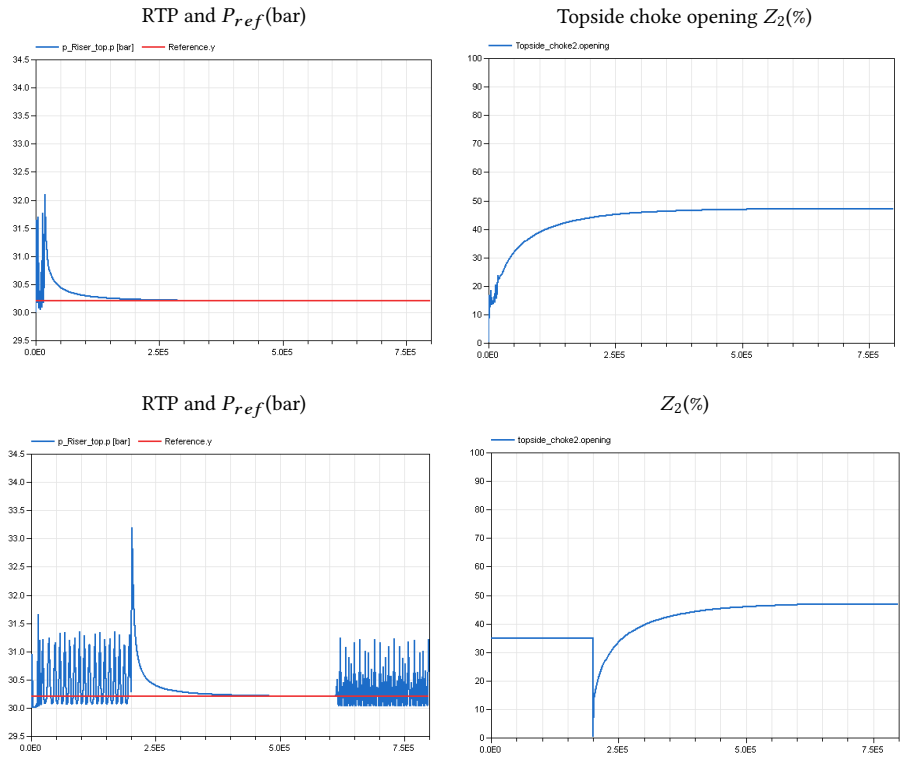

Figure 4.21: PI-control topside of the well-2 system

As shown in Figure 4.21, we can stabilize the well instabilities by using a PI-controller with topside pressure measurements RTP, actuating the topside choke valve opening Z_2. On this control system, we used the same tuning procedure as for the PI-controller, measuring the BHP, actuating the production choke valve Z_1 in Section 4.2.2.2.

As shown in Figure 4.21, the PI-controller stabilizes the system at Z_2=46.8% valve opening. The controller is turned on at t=200000s and turned off when the choke opening has reached steady-state, at t=600000s. By implementing a PI-control strategy with the RTP as our CV and the topside choke valve (Z_2) as our MV to mitigate well-slugging, it clearly shows that even at lower steady-state valve openings, the system takes long time to stabilize. By looking at the Topside choke opening (Z_2) when the controller is

turned on and off, in Figure 4.21, we can see that after the controller is turned on at t=200000s, Z_2 struggles and dips to zero opening before stabilizing, which is undesirable, and may cause wear-and tear on the choke valve.

The BHP and the mass flow-rate as a result of the topside PI-control, is shown in Figure 4.22

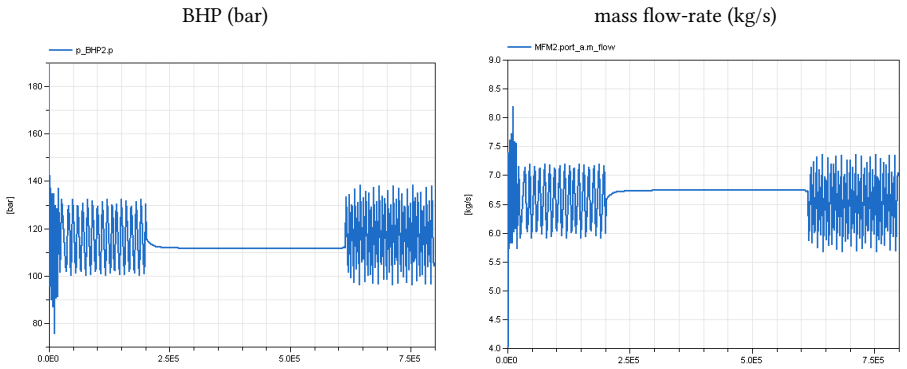

Figure 4.22: Down-hole conditions as a result of the topside PI-control on the well-2 system

As shown in Figure 4.22,when turned on, the PI-controller using topside measurements and actuators, is able to stabilize the BHP at a steady-state mass flow-rate = 6.74kg/s, which is approximately the same as using the BHP as CV and Z_1 as MV. We conclude that well-instabilities of this system can be stabilized by using both bottom-hole- and topside- Pressure measurements and actuators.

4.2.3.2 3-Well System

We implemented a PI-controller topside of the 3-well system as illustrated in Figure 4.23. By using the same PI-tuning strategy as explained in Section 4.2.1, we came up with the PI-parameters in table 4.3. By choosing the optimal P_{ref}=31.85 bar, by trial and error, simulating over a significant time period t=600000s, we got the simulation results, as shown in Figure 4.24.

As shown in Figure 4.24, the PI controller manages to track the reference P_{ref} and stabilize both the RTP and BHP of all wells. The Topside choke valve opening stabilizes

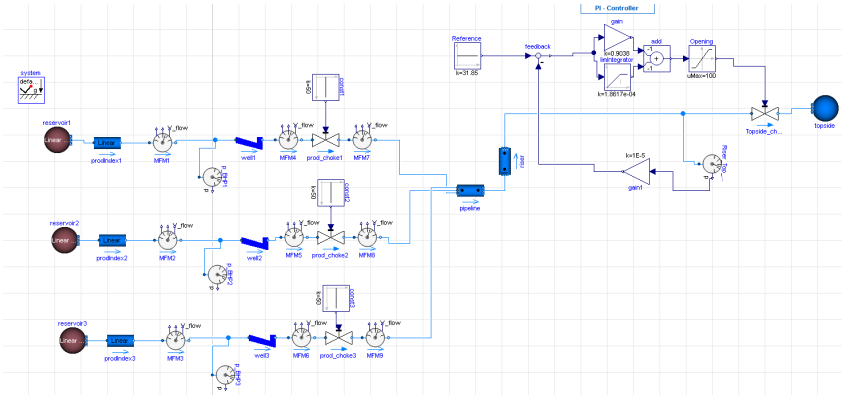

Figure 4.23: PI-control of the 3-well system using Topside CV and MV

at Z_2=55.38%, and the total mass flow-rate at steady-state, entering the riser as a result of this control is 21.77kg/s. This is approximately the same total flow as the result of the PI-control implemented in all the wells in the 3-well system in Section 4.2.2.4. An interesting observation from Figure 4.24 is that we were able to stabilize the BHP in all the wells by manipulating the topside choke valve and stabilizing the RTP.

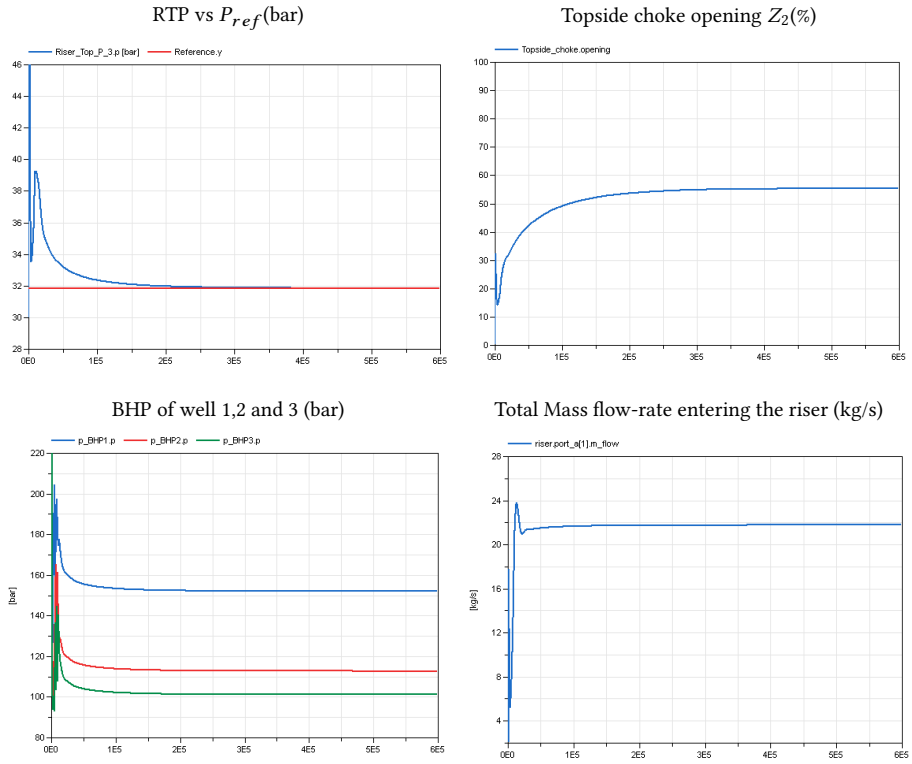

Figure 4.24: Topside PI-control of the 3-well system

4.2.4 Nonlinear Control Solution

Existing anti-slug control systems may become unstable after some time, because of inflow disturbances or plant-changes[30], also proved in Figure 4.11. Plant changes may come as a result of a reduction in the reservoir Pressure, an increase in Water-Cut or or increased Gas-Oil-Ratio (GOR). The nonlinearity at different operating conditions is one source of plant changes. In addition, the time delay is another problematic factor for stabilization[33]. The nonlinearity of the system is one problem for a linear controller, because of the gain of the system changes drastically at different operating conditions. This nonlinearity can be counteracted by model-based nonlinear controllers, or by gain scheduling of multiple linear controllers. Model-based control strategies and nonlinear

control strategies are mentioned in Section 2.5.4.2.

4.2.4.1 Gain-Scheduling Control

The basic limitation of a linear controller, is the that the controller is guaranteed to work only in some neighborhood of a single operating(equilibrium) point. It might be possible to model the system in such way that the operating points are parameterized by one or more variables, called scheduling variables. In such situations, we may linearize the system at several equilibrium points, design a linear feedback controller at each point, and implement the resulting family of linear controllers as a single controller whose parameters are changed by monitoring the scheduling variables. A such controller is called a gain-scheduling controller [38].

A gain-scheduling of linear controllers has been proven to be well-suited for anti-slug control when a subsea Pressure measurement is available. Compared to the nonlinear model-based controllers, the gain-scheduling controller is more robust and requires less modeling effort[54].

4.2.4.2 Cascade Control System

Cascade control strategies, using several controllers in series, have been proven to work well, suppressing both riser slugging, high frequent hydrodynamic slugging and terrain slugging[25]. A control system of this nature was implemented, offshore at Gullfaks C for the tie-in of the Tordis subsea field in 2003. The proposed control system that was installed, consisted of a slug suppression system (Cascade control) and a slug handling by advanced level control of the inlet separator using a Model Predictive Control (MPC) to handle nonlinear behaviour and manipulate the level set-points[25]. The control structure implementation is shown in Figure 4.25.

In Figure 4.25, a Pressure controller in outer loop provided the set point to a slave flow controller. This flow controller used the topside choke to get a desired volumetric flow through the choke. The volumetric flow was not measured directly, but computed from a simplified valve equation and measurements of density and choke Pressure loss. Standard PID controllers were programmed in the topside process control system [25]. The same control structure was also implemented at the Heidrun field in 2001, using PI-controllers [24].

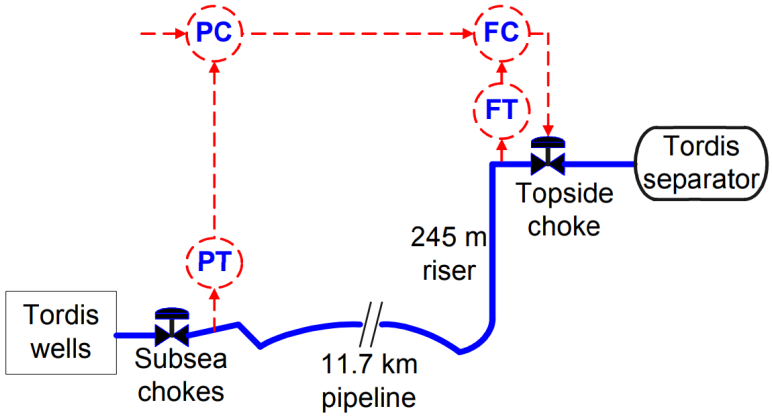

Figure 4.25: Cascade control of inlet Pressure and choke volumetric flow at Tordis [25]

Godhavn also proposed a new cascade control solution using the top Pressure (upstream the control choke) in a slow outer loop and the flow through the choke in an inner loop, using PI and PID controllers [23]. This control system is shown in Figure Figure 4.26.

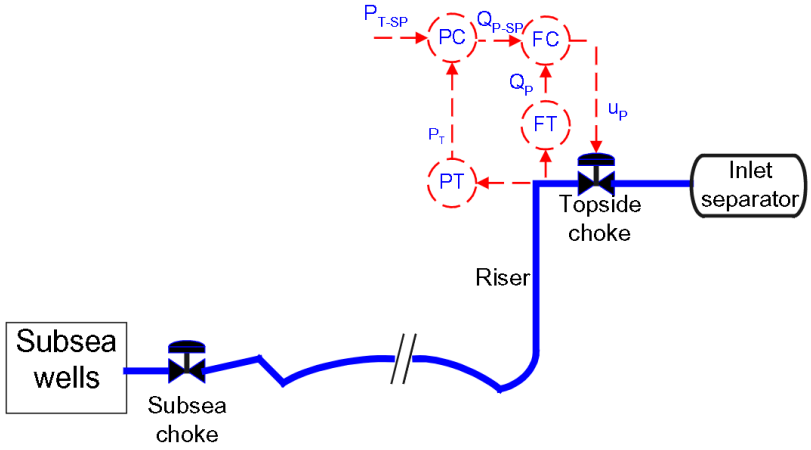

Figure 4.26: Top Pressure and volumetric flow cascade control [23]

Subsea pressure measurements are expensive to install and maintain and sometimes less available and less reliable than topside measurements. Topside measurements are

usually updated more often and they are in many cases more accurate than subsea measurements [23].

The next Section will cover the Gain-Scheduling PI-control system, implemented in the separate well-2 system, to handle plant-changes. As an experimental setup in Dymola, both the Bottom-hole Pressure (BHP) and the mass flow-rate down-hole is measureable and used in our control system.

4.2.4.3 Implementation in Dymola

To handle nonlinearity, i.e plant-changes, we implemented a cascade feedback control-system with one PI-controller in the outer loop, and a PI-gain scheduling controller in the inner loop as shown in Figure 4.27.

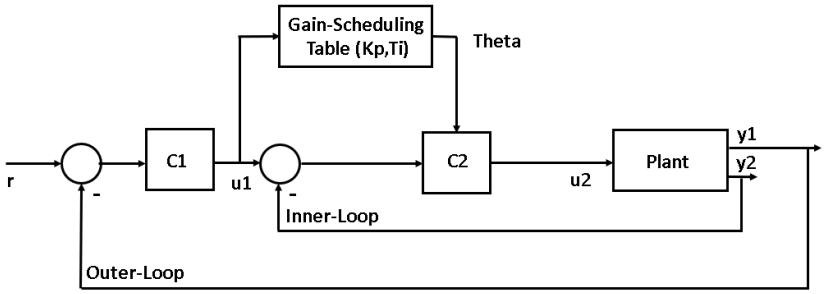

Figure 4.27: Cascade Gain-Scheduling PI-control-Structure of the Well-2 system

In Figure 4.27, the outer-loop ensures that the system tracks the reference **r**, which in our case is a desired mass flow-rate. Using bottom-hole measurements of the mass flow-rate **y1**, the outer-loop controller **C1** provides the controller output **u1**(Pressure), which is the set-point for the inner loop. The inner loop controller **C2** stabilizes the BHP (**y2**) by manipulating the Production choke valve opening **u2**. The Scheduling-variable for this system is **u1**, which is the controller output of **C1** and the set-point (Pressure) for the inner loop. The gain-scheduling table linearly interpolates between 7 different PI controllers for different operating conditions(set-points(**u1**)), choosing the optimal controller to track the reference **r**. The **Plant** represents the Well-2 system-dynamics and the implementation in Dymola is shown in Figure 4.28.

As mentioned (shown in Figure 4.27), the set-point P_{ref} equals the controller output

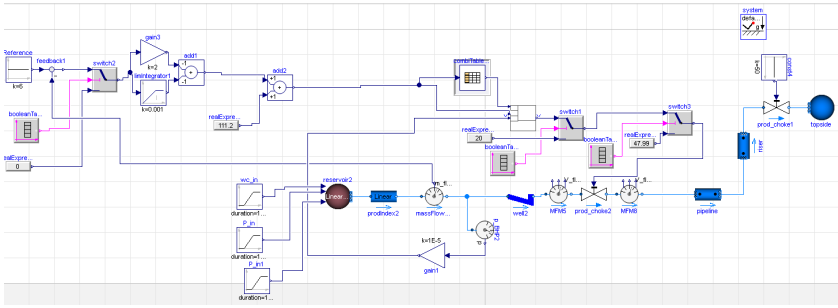

Figure 4.28: Cascade Gain-Scheduling PI-control-Structure of the Well-2 system in Dymola

u1. The operating range of this system is limited by the different controllers in the Gain-scheduling table, which are linearized around 7 different operating conditions (different set-points). The gain-scheduling table uses set-points P_{ref} from 111.2, up to 130 bar, covering the operating range of this system. P_{ref}=111 bar was the lowest possible set-point Pressure to stabilize this system at the highest possible valve opening, resulting in the highest mass flow-rate(Section 4.2.2.2). P_{ref}=130 bar is the set-point needed to maintain a mass flow-rate of w_{ref}=6kg/s without plant-changes, which in our system, is the reference **r** in Figure 4.27.

As shown in Figure 4.27, the inner loop contains the Gain-shceduling PI-controller **C2** . The PI-paramters for P_{ref} = 111.2 bar was found using the Overshoot method in Section 4.2.1, and the proposed parameters for the well-2 system at this set-point are shown in table 4.2. The PI-parameters for the flow-controller **C1** (outer loop in Figure 4.27) was found by trial and error. The PI-parameters for the other 6 controllers in the Gain-scheduling table were also found by trial and error.

The different PI-controllers in the gain-scheduling table are shown in table 4.7. The switching between the controllers is done by linear interpolation in one dimension of the Gain-scheduling table. The interpolation is efficient, because a search for a new interpolation starts at the interval used in the last call. If the input (set-point) is outside of the defined interval (111.2-130 bar), the corresponding values (K_c and T_i), are also determined by linear interpolation through the last or first two points of the table.

The plant changes introduced to the system are shown in table 4.8, and the simulation time is set to t=600000s. The reference of the outer loop is w_{ref}=6kg/s, and both

	P_{ref} = **u1**	K_c	T_i
$C2_1$	111.2 bar	-7.9631	1248s
$C2_2$	112 bar	-7.5	1000s
$C2_3$	113 bar	-7	800s
$C2_4$	120 bar	-7	800s
$C2_5$	121 bar	-6	600s
$C2_6$	122 bar	-4	450s
$C2_7$	130 bar	-4	450s

Table 4.7: The different controllers used in the Gain-scheduling PI-controller **C2**

controllers are turned off at initialization. The initial set-point Pressure P_{ref} = **u1** for the inner loop is set to 111.2 bar.

Plant Changes	Before	After	Change (%)
Water Cut (WC)	0.55	0.6589	+19.8
Gas Oil Ratio(GOR)	90	120	+33
Reservoir Pressure	280 bar	261 bar	-6.78

Table 4.8: Plant changes introduced to the Well-2 system over a period of 100000s = 28 hours

The simulation results are shown in Figure 4.29. As shown in Figure 4.29, at t= 100000s, both controllers are turned on and the outer loop tries to stabilize the system, to track the desired mass flow-rate of w_{ref}=6kg/s. The gain-scheduling PI-controller starts to work and switches between different controllers to match the desired mass flow-rate at P_{ref} = **u1**=130 bar. At t=200000s , we introduce plant changes to the system, shown in table 4.8. At t=500000s, the controllers turn off again and the system enters the unstable flow-regime again. The PI-parameters from the gain-scheduling table are shown in Figure 4.30.

As shown in Figure 4.30, the upper plot is the K_c values, and the lower plot is the corresponding T_i values. At t=100000s when the controllers turn on, the Gain-scheduling PI-controller interpolates between 3 different controllers to reach the desired set-point of w_{ref}=6kg/s. Between t=200000s and t=300000s, we introduce plant-changes, and

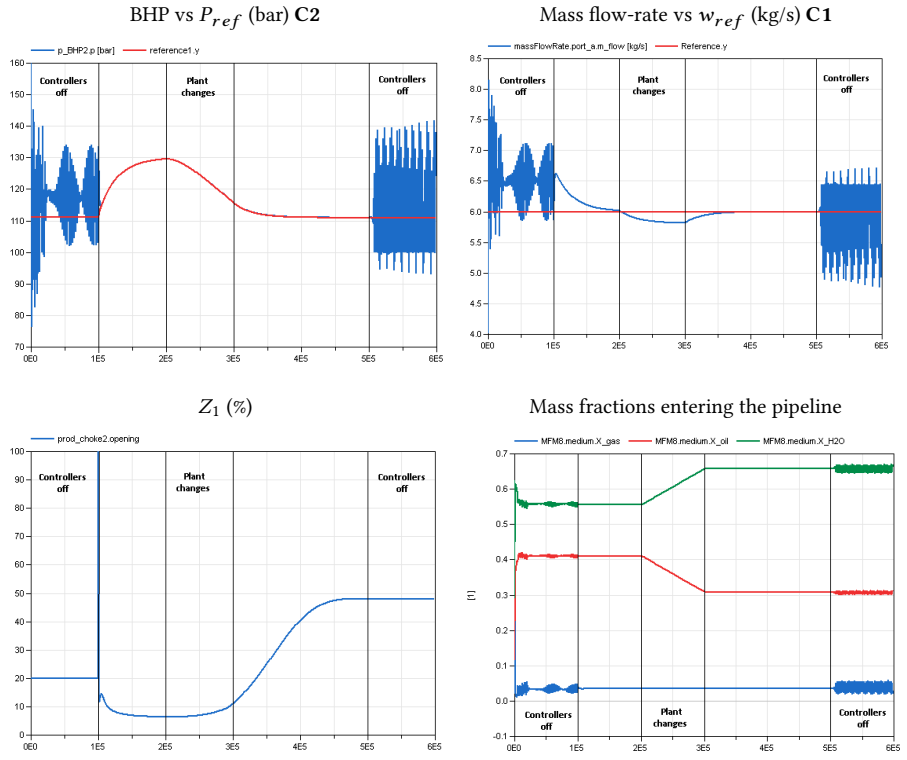

Figure 4.29: Cascade Gain-Scheduling PI-control the Well-2 system

the gain-scheduling controller has to compensate in order to stabilize the system at w_{ref}=6kg/s.

Figure 4.29 shows that both the flow-controller **C1** (outer loop) and the gain-scheduling Pressure controller **C2**(inner-loop) are able to stabilize the system with plant-changes shown in table 4.8. An interesting observation is that the choke opening is Z_1=7% without plant-changes and changes to Z_1=48% to compensate for the plant-changes, achieving the same mass flow-rate w_{ref}=6kg/s.

The mass fractions of the different phases entering the pipeline are also shown in Figure 4.29. The green values is the mass fraction of water, and the red and blue are the corresponding mass fractions of oil and gas for this system.

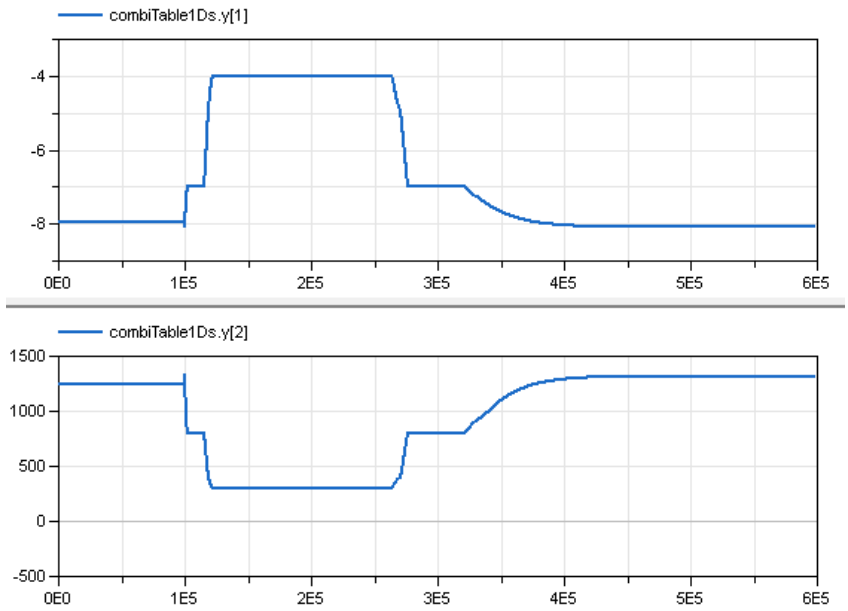

Figure 4.30: K_c and T_i values from the Gain-scheduling table, given to the inner-loop controller **C2**

Chapter 5

Conclusions and Future Work

Well slugging is, in many researchers' eyes, a phenomenon we cannot explain for certain because of the lack of information provided. Severe slugging in horizontal wells, like we have described in this thesis, is a very rare phenomenon, and the casing-heading- and density-wave- instability has been shown to more frequent in the research of unstable wells (covered in Section 2.3). It has, though, been proven numerically using OLGA that, with a specific geometry, severe slugging may occur in the low-point of an extended reach horizontal well[40]. For this work, this type of slugging was then remodelled in Dymola and we provided several different well-slug systems. The focus on the implementation of these systems has been to create extreme conditions bottom-hole to simulate severe slugging.

This chapter will cover all the results of this work and also give recommendations for further studies.

5.1 Research

The research has not shown any previous works that describe this kind of well instability, implemented in Dymola. OLGA or other multi-phase flow simulators have been proven to give accurate simulations of slugging in pipeline-riser systems[30], but may be difficult to use when describing well-instability [37]. Because of the lack of previous works regarding modeling of severe slugging in wells, we may consider questioning the

reliability of the simulation results in Dymola.

5.2 Modeling and Implementation

We tried to replicate Jahanshahi's riser-slug model[32]and the extended reach well-slug model[40] as accurately as possible to create the same type of behaviour provided in these papers. It might not be possible to describe well-slugging with a riser-slug model in a real environment, but the research has not shown any available well-slug models, representing the severe slugging phenomenon in wells. We ended up using most components from the Subpro library in Dymola, including a riser-slug model [32], with the possibilities of changing the geometry, properties and inflow-conditions to try to describe a slugging well. Because we didn't have any working slug-model from simulation (i.e OLGA), we had to identify the different parameters by a systematic trial and error approach in Dymola that would create a working slug-model. The parameters that would create this behaviour down-hole were: the inflow-conditions through the productivity-index model, the slip-factor in the horizontal and vertical section of the well as well as the pressure, water-cut and the Gas-oil-ratio(GOR) in the reservoir. When the riser-slug model in Dymola achieved the desired behaviour (similar to the Jahanshahi model[32]), it was easier to turn riser-slug model into well-slug models, by changing the parameters identified in the implementation of the riser-slug model.

We then connected 3 well-slug models with different inflow-conditions, geometry and reservoir conditions into a integrated 3-well system. When separated, the 3 wells had different frequencies, but when connected, they shared the same frequency. This is because of the framework conditions at the input and output of the system. The input framework conditions of each well are different and the output framework conditions are the same for all systems. When connected, the output framework conditions now become a hub with mutual influence to all the wells. This might also be numerical solver issue and we cannot confirm that this is how an integrated large, multi-well system behaves in a real scenario, but it is an interesting observation.

5.3 Anti-Slug Control

The main focus of the anti-slug control implementation was to use PI (Proportional - Integral) controllers due to their simplicity and because they are widely used in the industry(as explained in Section2.5.4.1). 9 controllers were implemented in 4 different systems to mitigate severe terrain induced riser-slugging in wells. PI-controllers using bottom-hole measurements and actuators were applied to all the different systems. PI-controllers using topside measurements and actuators were applied to the separated well-2 system and the integrated 3-well system. A cascade gain-scheduling PI control structure was implemented to the separated well-2 system using bottom-hole measurements and actuators. The main controlled variable (CV) used was the bottom-hole pressure (BHP) and the main manipulated variable (MV) was the production-choke valve opening, but we also tested using the riser-top pressure as our CV and the topside choke valve opening as our MV.

The main tuning procedure for the PI-parameters was the setpoint overshoot Method[48], used on 5 of the 9 implemented controllers. The challenge was to identify, design and implement a control structure to handle nonlinearity, i.e plant changes. We ended up using a cascade gain-scheduling PI-control structure with the intention of working in a wide range of operating conditions.

When the 3 well-slug models were connected, they influenced each-other, resulting in a more complex anti-slug control implementation than for the separated well-slug systems. Because of this, we ended up using the trial and error method for PI-parameter tuning of this system.

5.4 Simulations and Results

To be consistent, we chose a numerical solver that could fit the stiffness of the systems in all our simulations. This could possibly be an error source in this work and could affect the simulation results to be different compared to a real scenario.

All the PI-controllers implemented with bottom-hole measurements and actuators managed to stabilize the bottom-hole pressure (BHP) at a relatively high openings. When introducing a plant-change (increase in reservoir water-cut), the PI controller implemented bottom-hole in the separate well-2 system did not manage to stabilize the

BHP at a low pressure set-point. When increasing the set-point pressure, the controller managed to stabilize the BHP, yielding a lower flow-rate. This is undesirable and proves the need for a nonlinear control strategy to handle plant-changes. The PI-controllers implemented bottom-hole in each well of the integrated 3-well system managed to stabilize the BHP at approximately the same valve openings as the results provided in the separate well-systems.

By using topside measurements and actuators compared to a bottom-hole implementation in the separate well-2 system, the simulations showed that steady-state mass flow-rate as a result of the PI-control was approximately the same.

PI-control using topside measurements and actuators were also applied to the integrated 3-well system and the simulations showed that this kind of implementation achieved approximately the same mass flow-rate entering the riser as the PI-controller implemented down-hole in the same system.

By implementing a cascade gain-scheduling PI-control structure in the separate well-2 system, we managed to stabilize the system at a desired mass flow-rate when plant-changes were introduced. The outer loop of the cascade control system stabilized the flow-rate and providing a set-point (pressure) to the inner loop. The inner loop stabilized the BHP, manipulating the production choke valve opening. The plant changes were applied in the reservoir and, over time, it resulted in a 19.8% increase in the water-cut, a 33% increase in Gas-oil-ratio (GOR) and 6.78% decrease in the reservoir pressure. An interesting observation was that the valve opening without plant-changes stabilized the system at a 7% valve opening to track the desired set-point (mass flow-rate). The plant-changes pushed the valve opening all the way up to 48%, to achieve stabilization at the same desired mass flow-rate.

Because the results are numerical solutions from the specific modeling environment provided by Dymola, we do not know if our work will be appliable for future works regarding anti-slug control in wells. Though, we have proved that in this modeling environment we can mitigate slugging down-hole using PI-controllers.

5.5 Recommendations for Future Works

5.5.1 Modeling and Implementation

Because the focus of this work was to implement well-slug models representing severe riser-induced slugging, one recommendation for further works could be to expand the research-area by looking at other types of slugging, occurring in wells like the density-wave- or the casing-heading- instability(as explained in Section2.3), and implement them in Dymola.

5.5.2 Anti-Slug Control

We ended up using only Dymola for anti-slug control implementation. However, Matlab and Simulink have been shown to be more effective when designing and implementing more advanced anti-slug control strategies. A Functional-Mock-up-Interface or FMU, enables the possibility to connect different modeling platforms(Dymola and simulink), and we may be able to design more complex control strategies than the ones used in this thesis.

Because of the influence the wells had on each other in the integrated 3-well system, we found the PI-parameters as well as the optimal set-points through trial and error. As a recommendation for future works on anti-slug control implementation of this type of MIMO system in Dymola, a Model Predictive Control (MPC) design could be implemented as a solution [61]. This controller is widely used in the industry. It is able to effectively incorporate process constraints directly and control MIMO processes which have strong interaction in an effective way.

References

[1] T Ahmed. *Reservoir Engineering Handbook, Third Edition.* El-sevier, Oxford, UK, 2006.

[2] Q. Bai, Y.and Bai. *Subsea Pipelines and Riser.* Elsevier Science Ltd, Oxford, 2005.

[3] Q. Bai, Y.and Bai. *Subsea Engineering Handbook.* Gulf Professional Publishing, 2012.

[4] N. Barrett and D. King. Bp exploration operating company, oil/water slugging of horizontal wells – symptom, cause and design. *SPE Annual Technical Conference and Exhibition, New Orleans, Louisiana*, 1998.

[5] K. Bendiksen, D. Maines, R. Moe, and S. Nuland. The dynamic two-fluid model olga: Theory and application. *SPE production engineering*, 1991.

[6] J. P. Brill and H. D. Beggs. *Two-Phase Flow In Pipes.* Tulsa, Oklahoma, University of Tulsa, 1991.

[7] T. Burgess. Horizontal drilling comes of age. *Oil Field Review*, 2(3):22–25, 1991.

[8] A. M. Cheng. Inflow performance relationships for solution-gas-drive slanted/horizontal wells. *SPE 20720*, 1990.

[9] C. J. Chou and C. T. Huang. Estimation of the underdamped second-order parameters from the system transient. *Industrial Engineering Chemistry Research*, 33:174–176, 1994.

[10] R Cossê. *Handbook of Marine Craft Hydrodynamics and Motion Control*, chapter Basics Of Reservoir Engineering. Institut français du pétrole (IFP), Pa, 1993.

[11] M. Dalsmo, E. Halvorsen, and O. Slupphaug. Active feedback control of unstable wells at the brage field. *SPE Annual Technical Conference and Exhibition, San Antonio, Texas*, 2002.

[12] F. Di-Meglio. *Dynamics and control of slugging in oil production*. PhD thesis, Centre Automatique et Systemes, Unit ‘ e Math ematiques et Systemes, MINES Paris- ‘ Tech, 60 bd St Michel 75272 Paris Cedex 06, France, 2011.

[13] F. Di-Meglio, G.O. Kaasa, and N. Petit. A first principle model for multi-phase slugging flow in vertical risers. *Joint 48th IEEE Conference on Decision and Control and 28th Chinese Control Conference*, 2009.

[14] F. Di-Meglio, G.O. Kaasa, N. Petit, and V. Alstad. Reproducing slugging oscillations of a real oil well. *In: 49th IEEE Conference on Decision and Control. Atlanta, Georgia, USA*, pages 4473–4479, 2010.

[15] F. Di-Meglio, G.O. Kaasa, N. Petit, and V. Alstad. Model-based control of slugging: Advances and challenges. *IFAC Workshop on Automatic Control in Offshore Oil and Gas Production*, pages 109–115, 2012.

[16] Dymola. *Dassault Systêmes*. [Online]. Available from: `https://www.3ds.com/products-services/catia/products/dymola/`. 2019.

[17] G. O. Eikrem. *Stabilization of Gas-Lift Wells by Feedback Control*. PhD thesis, Department of Engineering Cybernetics, Norwegian University of Science and Technology, Trondheim, Norway, 2006.

[18] G. O. Eikrem and O. M. Aamo. Anti-slug control of gas-lift wells-experimentalresults. *IFAC Nonlinear Control Systems, Stuttgart, Germany*, 2004.

[19] M. G. L. Evers and V. L. van Beusekom. Appearance and mitigation of density waves in continuously gas-lifted oil wells. *14th International Conference on Multiphase Production Technology, 17-19 June, Cannes, France*, 2009.

[20] F. Garcia, J. Garcia, R. Garcia, and D. Joseph. Friction factor improved correlations for laminar and turbulent gas-liquid flow in horizontal pipelines. *International Journal of Multiphase Flow*, (33):1320–1336, 2007.

[21] H. Genceli, K. A. Kuenhold, O. Shoham, and J. P. Brill. Simulation of slug catcher behavior. *Annual Technical Conference and Exhibition of Society of Petroleum Engineers, Houston*, 1988.

[22] C. A. Glandt. Reservoir management employing smart wells: A review. *SPE Drilling and completion*, 2005.

[23] J-M. Godhavn, M. P. Fard, and P. H. Fuchs. New slug control strategies, tuning rules and experimental results. *Journal of Process Control*, 15:547–557, 2005.

[24] J. M. Godhavn and G. Skofteland. Suppression of slugs in multiphase flow lines by active use of topside choke - field experience and experimental results. *11th BHR Group Multiphase Production International Conference, San Remo, Italy*, pages 527–542, 2003.

[25] J. M. Godhavn, S. Strand, and G. Skofteland. Increased oil production by advanced control of receiving facilities. *16th Triennial World Congress, Prague, Czech Republic*, 2005.

[26] J. P. Hartnett and T. F. Irvine Jr. Two-phase slug flow. In *Advances in Heat Transfer*, page 83. Academic Press inc, San Diego, 1990.

[27] B. Hu. *Characterizing gas-lift instablilities.* PhD thesis, Department of Petroleum Engineering and Applied Geophysics, NTNU, 2004.

[28] L. S. Imsland. *Output Feedback and Stabilization and Control of Positive Systems.* PhD thesis, Department of Engineering Cybernetics, Norwegian University of Science and Technology, Trondheim, Norway, 2002.

[29] ISA75.01, Control Valve Sizing Equations. . [Online]. Available from: `https://www.isa.org/isa75-01/`. 2007.

[30] E. Jahanshahi. *Control Solutions of Multiphase flow, Linear and Nonlinear approaches to Anti-slug Control.* PhD thesis, Norwegian University of Science and Technology, Trondheim, Norway, 2013.

[31] E. Jahanshahi, S. Skogestad, , and A.H. Helgesen. Controllability analysis of severe slugging in well-pipeline-riser systems. *IFAC Workshop on Automatic Control in Offshore Oil and Gas Production, NTNU, Trondheim, Norway*, pages 101–108, 2012.

[32] E. Jahanshahi and S. Skogestad. Simplified dynamical models for control of severe slugging in multiphase risers. *18th IFAC World Congress, Milano, Italy*, 2011.

[33] E. Jahanshahi and S. Skogestad. Comparison between nonlinear model-based controllers and gain-scheduling internal model control based on identified model. *52nd IEEE Conference on Decision and Control December 10-13, 2013. Florence, Italy*, 2013.

[34] O. F. Jahnsen and M. Storvik. Subsea processing and boosting in a global perspective. *10th Offshore Mediterranean Conference and Exhibition in Ravenns, Italy March 23 – 25*, 2011.

[35] B. Jansen, M. Dalsmo, L. Nøkleberg, K. Havre, V. Kristiansen, and P. Lemetayer. Automatic control of unstable gas lifted wells. *SPE Annual Technical Conference and Exhibition, Houston, Texas*, 1999.

[36] F. Jansen, O. Shoham, and Y. Taitel. The elimination of severe slugging - experiments and modeling. *International Journal of Multiphase Flow*, 22(6):1055–1072, 2005.

[37] G. O. Kaasa, V. Alstad, J. Zhou, and M. Aamo, O. Nonlinear model-based control of unstable wells. *Modeling, Identification and control*, 28(3), 2007.

[38] H. K Khalil. *Nonlinear Systems*, chapter Gain-Scheduling. Prentice Hall, Inc., 2002.

[39] Kudela, H. *Pipeline Systems*. PDF [Online]. Available from: `http://www.itcmp.pwr.wroc.pl/~znmp/dydaktyka/fundam_FM/Lecture_no7_Pipeline_Systems.pdf`.

[40] R. Malekzadeh and R. F. Mudde. A modeling study of severe slugging in wellbore. *NOrth Africa Technical Conference and Exhibition , Cairo, Egypt, 20-22 Februrary*, 2012.

[41] W. Meng and J. J. Zhang. Modeling and mitigation of severe riser slugging: A case study. *SPE Annual Technical Conference and Exhibition, New Orleans, Louisiana*, 2001.

[42] D. Naizhong, G. Zhimin, W. Helin, W. Zengshun, L. Lixin, H. Qingquan, and X. Zhihui. Application of multi-branch horizontal well technology in cbm drilling. *IADC/SPE Asia Pacific Drilling Technology Conference and Exhibition*, (4), 2012.

[43] A. Ogazi, Y. Cao, H. Yeung, and L. Lao. Slug control with large valve openings to maximize oil production. *SPE Journal*, 15(3):812–821, 2010.

[44] S. Pedersen, P. Durdevic, and Y. Zhenyu. Review of slug detection, modeling and control techniques for offshore oil and gas production processes. *2nd IFAC Workshop on Automatic Control in Offshore Oil and Gas Production*, 48(6):89–96, 2015.

[45] P. F. Pickering, G. F. Hewitt, and C. P. Watson, M. J.and Hale. The prediction of flows in production risers, truth and myth? *IIR Conference. Aberdeen*, pages pp 1–16, June 2001.

[46] K. S Rao and R. Mishra. Comparative study of p, pi and pid controller for speed control of vsi-fed induction motor. *SSTC, Bhilai, Chhattisgarh, India*, 2(2), 2014.

[47] A. Sayda and J. Taylor. Modeling and control of three-phase gravity separators in oil production facilities. *American Control Conference*, 2007.

[48] M. Shamsuzzoha, S. Skogestad, and I. J. Halvorsen. On-line pi controller tuning using closed-loop setpoint response. *9th International Symposium on Dynamics and Control of Process Systems (DYCOPS 2010, Leuven, Belgium)*, 2010.

[49] L. Sinêgre, N. Petit, and P. Menegatti. Predicting instabilities in gas-lifted wells simulation. *American Control Conference, Minnesota, USA*, page 5530–5537, 2006.

[50] J. M. Skofteland, G.and Godhavn and T. Kulset. Implementation of a slug control system for subsea wells in an integrated operation environment. *in: 13th International Conference on Multiphase Production Technology. Edinburgh, UK*, pages pp. 225–236, 2007.

[51] S. Skogestad. Simple analytic rules for model reduction and pid controller tuning. *Journal of Process Control*, 13:291–309, 2003.

[52] S. Skogestad. Chemical and energy process engineering. *Boca Raton, FL, CRC Press, Taylor and Francis Group*, 2009.

[53] S. Skogestad and C. Grimholt. The simc method for smooth pid controller tuning. *Chapter for PID book (planned: Springer, 2011, Editor: R. Vilanova) This version: September 7, 2011*, 2011.

[54] S. Skogestad and E. Jahanshahi. Nonlinear control solutions to prevent slugging flow in offshore oil production. *Journal of Process Control*, 54:138–151, 2017.

[55] E. Storkaas and S. Skogestad. A low-dimensional dynamic model of severe slugging for control design and analysis. *11th International Conference on Multiphase flow, San Remo, Italy, BHR Group*, 2003.

[56] E. Storkaas and S. Skogestad. Controllability analysis of two-phase pipeline-riser systems at riser slugging conditions. *Control Engineering Practice*, 15(5):567–581, 2007.

[57] Y. Taitel. Stability of severe slugging. *International Journal of Multiphase Flow*, 12:203–217, 1986.

[58] Y. Taitel, D. Barnea, and A. E. Dukler. Modeling flow pattern transitions for steady upward gas liquid flow in vertical tubes. *AIChE Journal*, pages 345–354, 1980.

[59] The schlumberger oilfield glossary. . [Online]. Available from: `https://www.glossary.oilfield.slb.com`. 2007.

[60] T. Tollin. Unstable multi-phase flow in well-pipeline- riser systems. Specialization Project, 2018.

[61] X. Wang and M. Chen. Cluster-level feedback power control for performance optimization. *2008 IEEE 14th International Symposium on High Performance Computer Architecture*, 2008.

[62] R. J. Wilkens. Flow assurance. In J. Saleh, editor, *Fluid Flow Handbook*, chapter 29. McGraw-Hill, 2002.

[63] L. Xing, H. Yeung, J. Shen, , and Y. Cao. Experimental study on severe slugging mitigation by applying wavy pipes. *Chemical Engineering Research and Design*, 91:18–28, 2013.

[64] B. Yocum. Offshore riser slug flow avoidance: Mathematical models for design and optimization. *SPE European Meeting. Society of Petroleum Engineers, London. United Kingdom*, (4312), 1973.

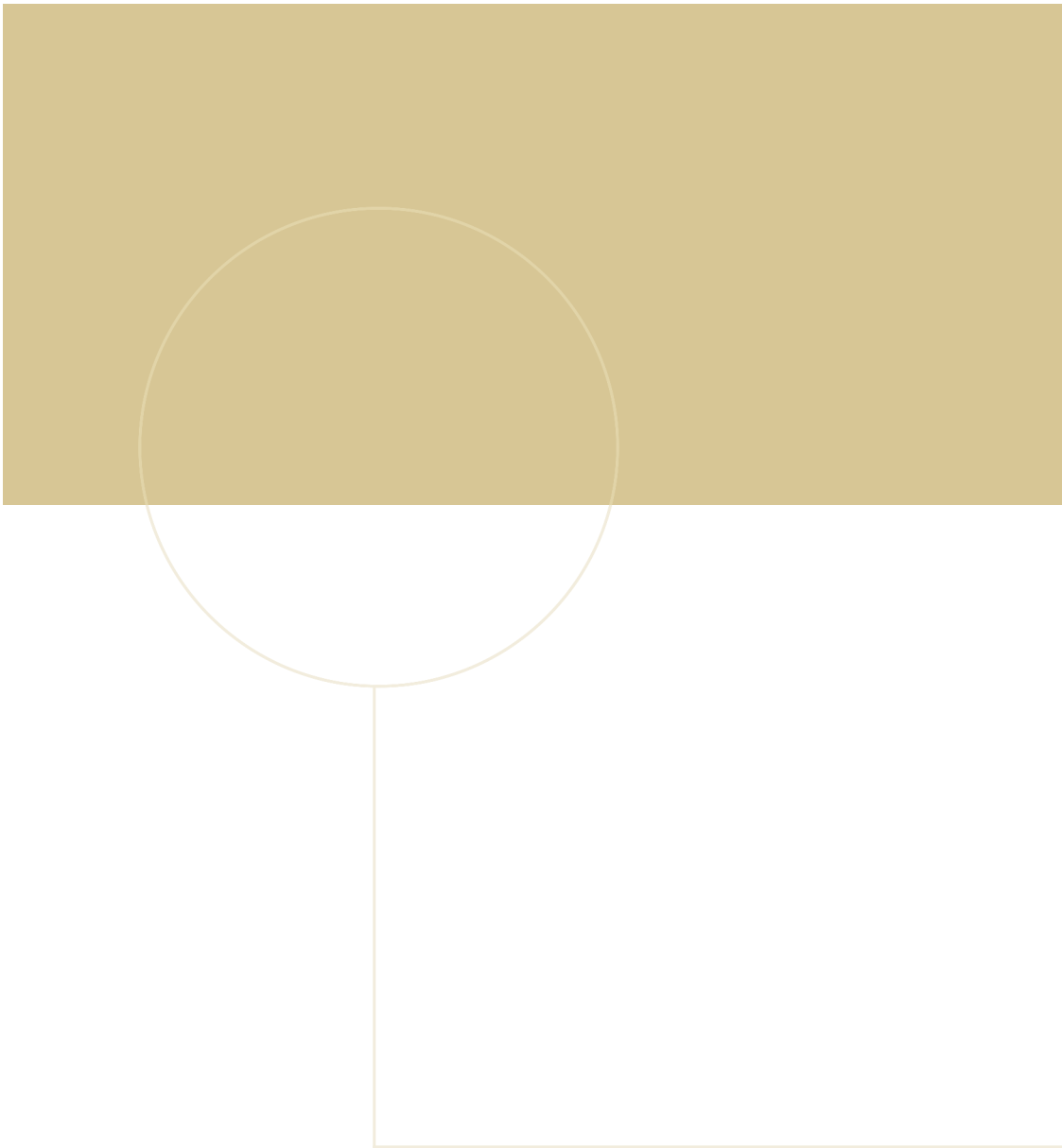

NTNU
Norwegian University of
Science and Technology